FABRICATION OF MULTIFUNCTIONAL NANOCOMPOSITES USING FUNCTIONALIZED CARBON NANOFIBERS

A Dissertation by

Chee Sern Lim

Master of Science, Wichita State University, USA, 2010

Bachelor of Science, Wichita State University, USA, 2007

Submitted to the Department of Mechanical Engineering
and the faculty of the Graduate School of
Wichita State University
in partial fulfillment of
the requirements for the degree of
Doctor of Philosophy

August 2013

FABRICATION OF MULTIFUNCTIONAL NANOCOMPOSITES USING FUNCTIONALIZED CARBON NANOFIBERS

The following faculty have examined the final copy of this dissertation for form and content, and recommend that it be accepted in partial fulfillment of the requirement for the degree of Doctor of Philosophy with a major in Mechanical Engineering.

Bob Minaie, Committee Chair

Ravi Tiruvadi, Committee Member

Hamid Lankarani, Committee Member

Krishna Krishnan, Committee Member

Bin Shuai, Committee Member

Accepted for the College of Engineering

Vishwanath Prasad, Interim Dean

Accepted for the Graduate School

Abu Masud, Interim Dean

DEDICATION

To my wife, my parents, my parent-in-law, my brother, and my dear friends

ACKNOWLEDGMENTS

I would like to express my greatest appreciation to my advisor, Professor Bob Minaie, who offered me the opportunity to join his research group and participate in this research. His endless support, guidance, and encouragement have made this work successful. I would also like to thank Dr. Hamid Lankarani, Dr. T. S. Ravi, Dr. Krishna Krishnan, and Dr. Bin Shuai for serving on my dissertation committee.

I gratefully acknowledge Dr. Alejandro Rodriguez and Joseph Schaefer for their active discussions, as well as their valuable opinions and recommendations. Their professional knowledge and experience have made this work greatly valuable. I also thank my colleague, Mauricio Guzman, for his active participation and experimental support throughout the whole study. Special recognition goes to Rony Das, Ashraf Ahmed, Pooneh Roozbehjavan, Ronald Joven, Tien Vo, Khalil Vora, Mohammad Habibi, Amdadul Islam, Kee Hong Saw, and Nita Yodo for their unconditional friendship, which made this work more enjoyable.

Lastly, I am mostly indebted to my wife, parents, parent-in-law, and my brother for their endless support and comprehension. Words are not enough to express my appreciation for them and thank you for believing in me and my dream.

ABSTRACT

In this work, several novel techniques to fabricate nano-engineered polymeric composites (or nanocomposites) containing functionalized carbon nanofibers (CNFs) were developed. The methodologies address current manufacturing issues of nano-engineered polymeric composites by effectively incorporating functionalized CNFs into polymer matrix and glass fiber layers. For polymeric nanocomposites, optical images of the nanocomposites revealed uniform distribution and alignment of the CNFs in the direction of the electric field. Due to the similarity in the alignment morphology, it was observed that alignment structure of the functionalized CNFs was independent of the functional groups grafted to the CNFs. Test results indicated that mechanical and electrical properties (measured parallel to the direction of the aligned CNFs) of nanocomposites containing aligned CNF network were improved in comparison to nanocomposites containing randomly distributed CNFs and neat epoxy sample. Discussion regarding the contribution of CNF type towards the mechanical and electrical properties is presented. In the first hierarchical composites study, functionalized CNFs were uniformly incorporated into glass fiber layers without inducing significant CNF agglomerate through a simple filtration process. Both in-plane and out-of-plane electrical conductivity of hierarchical composites were comparable to the conductivity of carbon fiber composites due to the formation of conductive path by CNFs. The second study presented the synthesis of functionalized CNF/glass fiber assembly demonstrating that functionalized CNF entangled network can be used to join glass fiber layers in the absence of polymer matrix. Test results showed that the peeling force required to separate the functionalized CNF/glass fiber assembly was significant due to the functionalized CNF entangled network. Possible explanations for both studies are provided in order to investigate the contribution of functionalized CNFs in each form of material.

TABLE OF CONTENTS

TABLE OF CONTENTS (CONTINUED)

Chapter Page

LIST OF TABLES

Table Page

LIST OF FIGURES

Figure Page

LIST OF FIGURES (CONTINUED)

Figure Page

LIST OF FIGURES (CONTINUED)

Figure Page

LIST OF ABBREVIATIONS/NOMENCLATURE

ACNFs	Amine Functionalized-Carbon Nanofibers
AR-CNF	As-Received Carbon Nanofiber
CNF	Carbon Nanofiber
CNT	Carbon Nanotube
CVD	Chemical Vapor Deposition
EPD	Electrophoretic Deposition
FRPCs	Fiber-Reinforced Polymeric Composites
HRTEM	High-resolution Transmission Electron Microscope
MEMS	Microelectromechanical System
MWCNT	Multi-Walled Carbon Nanotube
OCNFs	Carboxylic Acid Functionalized-Carbon Nanofibers
PAN	Polyacrylnitrile
SEM	Scanning Electron Microscope
TEM	Electron Microscope
Tg	Glass Transition Temperature
SWCNT	Single-Walled Carbon Nanotube
VARTM	Vacuum-Assisted Resin Transfer Molding
VGCF	Vapor Grown Carbon Fiber
VGCNF	Vapor Grown Carbon Nanofiber

LIST OF SYMBOLS

Å	Armstrong
°	Degree
µ	Micron
V	Volt
S	Siemen

CHAPTER 1

INTRODUCTION

1.1 Motivation and Scope

As the nanotechnology research rapidly evolves within material science and engineering discipline, carbon nanofibers (CNFs) have attracted considerable research attention in the past two decades. CNFs with unique one-dimensional nanostructures possess an exceptional combination of mechanical, electrical, and thermal properties along with high specific surface area and low density. Previous studies showed that the tensile strength and Young's modulus of a single CNF range from 2.35-2.90 GPa [1] and 6-285 GPa [2], respectively. In addition, several studies reported that the electrical resistivity and thermal conductivity of CNFs are in the range of $4x10^{-5}$ Ω.cm [3] and 2,000 W/m.K [4], respectively. Combining their ease of processing, low cost, and availability, CNFs have been extensively used as an ideal building block for the creation of next generation advanced composites –nano-engineered polymeric composites– with improved properties and multi-functionality. Such advanced composites can be potentially used for aerospace, naval, energy, electromagnetic interference (EMI) shielding, electrostatic dissipation (ESD), automotive industry, electronic, and biological applications [5-10].

Despite of their interesting properties, the use of CNFs in nano-engineered polymeric composites (or simply nanocomposites) is greatly hindered by several issues at material constituent level and processing stage. To effectively exploit the capability of CNFs when manufacturing nano-engineered polymeric composites, several manufacturing challenges must be overcome: (1) uniform CNF dispersion in polymer matrix, (2) orientation of CNFs in composites, (3) homogeneous distribution of CNFs on the reinforcement fabrics, and (4) chemical bonding or compatibility among CNFs, the matrix, and the micro-sized reinforcement

fibers. These challenges, in general, will also be encountered when other carbon nanomaterials such as carbon nanotubes (CNTs) are used to fabricate nano-engineered polymeric composites.

In the context of this dissertation, the inherent manufacturing challenges to incorporate carbon nanomaterials (CNFs or CNTs) into polymeric composites [11, 12] and advanced fiber-reinforced composites [13-17] will be highlighted individually, as illustrated in Figure 1.

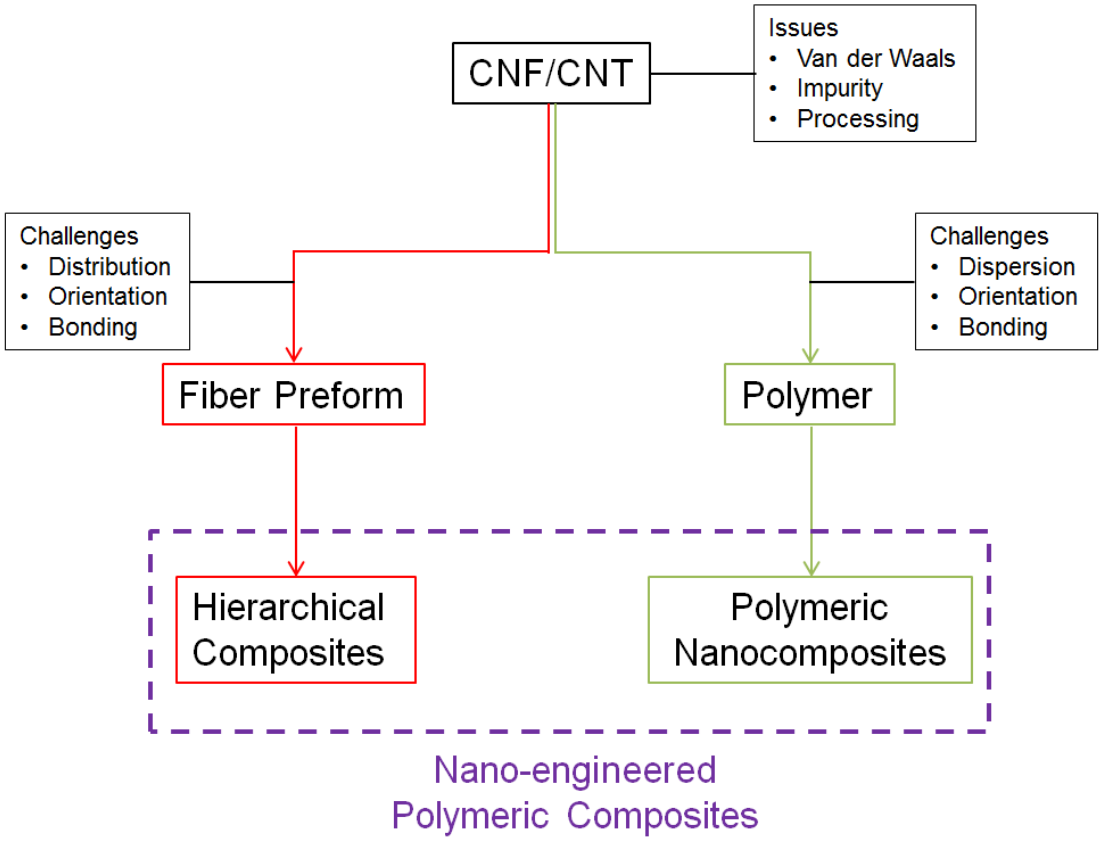

Figure 1. Issues and challenges related to manufacturing of nano-engineered polymeric composites.

When manufacturing polymeric nanocomposites containing carbon nanomaterials, uniform nanomaterial dispersion in polymer matrix is the key prerequisite to fabricating nanocomposites with improved properties. By attaining a uniform dispersion in the polymer matrix, effective load transfer from the matrix to nanomaterials can be achieved when the

nanocomposites are subjected to external load. However, it is difficult to uniformly disperse nanomaterials into polymer matrix due to van der Waals forces and high aspect ratio that cause nanomaterial agglomerates. Even though uniform dispersion is achieved during the mixing process, nanomaterials would re-agglomerate during curing of nanocomposites due to the lack of stability in the polymer matrix. Previous investigations [18, 19] showed that nanomaterial agglomerates are often detrimental to the resulting polymeric nanocomposites because of degradation in mechanical properties. Furthermore, the absence of chemical linkage between nanomaterials and polymer matrix could cause nanomaterial slippage and thus weaken the load carrying capability of nanocomposites [20-22]. Other investigations revealed that mechanical and electrical properties can be further improved when nanomaterials are selectively oriented along a preferential direction [23, 24]. To simultaneously satisfy the abovementioned criteria, various processing techniques such as chemical functionalization, mixing, and alignment methodologies must be adapted in order to manufacture polymeric nanocomposites with promising features.

Another class of composites that will be discussed is advanced fiber-reinforced composites. Fiber-reinforced polymeric composites (FPRCs) are well known for their excellent in-plane strength-to-weight and stiffness-to-weight properties, which are dominated by the 1-D (unidirectional) or 2-D (plain or satin weave) fiber architectures constructed with high performance carbon, glass, or Kevlar fibers. Conversely, FRPCs suffer from poor interlaminar fracture toughness and shear strength due to the presence of weak link between FRPC laminates that is dominated mainly by the properties of polymer matrix. For this reason, scientists and engineers have been actively seeking for an effective strategy to better reinforce the interlaminar region of FRPCs. Some examples of the developed methods to this drawback include through-

the-thickness stitching, z-pinning, and 3D braided fibers [25]. However, FRPCs manufactured following these methods often exhibit weaker in-plane mechanical properties due to fiber displacement/misalignment and low fiber volume fraction. The use of carbon nanomaterials in composites, on the other hand, has led the research of FRPCs to another groundbreaking horizon in terms of property improvement and multi-functionality. Carbon nanomaterials characteristics such as high strength, modulus, and high electrical and thermal conductivity along with low density have triggered tremendous interest within the research community to develop manufacturing techniques that seek the creation of a new class of nano-engineered fiber-reinforced composites –hierarchical composites– with improved and controlled properties. Particularly, numerous studies have shown that the interlaminar shear strength, mode-I fracture toughness, out-of-plane electrical and thermal properties can be significantly enhanced by properly incorporating carbon nanomaterials into traditional FRPCs [15]. Moreover, the conductive network formed by nanomaterials distributed within hierarchical composites can be used for structural health monitoring purpose [26]. To date, there are five main approaches to manufacture hierarchical composites, namely (1) injection of nanomaterial/polymer mixture into the preform [13], (2) direct placement of nanomaterials between laminates [27], (3) growth of nanomaterials on reinforcement layer through chemical vapor deposition (CVD) [28], (4) deposition of nanomaterials onto the reinforcement layer [29], and (5) coating reinforcement fibers with sizing agent containing well-dispersed nanomaterials [30]. While successfully performed at the laboratory scale, some of these methods are not cost-effective and are limited by chemical incompatibility and concentration needed for reinforcement purpose.

1.2 Research Objectives

This research is aimed at obtaining fundamental understanding of processing and characterization of various nano-engineered polymeric composites through different novel processing techniques. These findings are intended to aid in the creation of next generation advanced composites. Based on the motivation and scope of this research, the objectives of this research are as follows:

- Develop a process to fabricate polymeric nanocomposites containing aligned functionalized CNFs and characterize the dispersion, alignment morphology, mechanical and electrical properties of such nanocomposites.
- Develop a scalable process to effectively incorporate functionalized CNFs into glass fiber layer for manufacturing hierarchical composites with enhanced electrical conductivity, as well as to join glass fiber layers using a functionalized CNF entangled network.

Chapter 1 provides an introduction to the subject where the main challenges and issues related to manufacturing nano-engineered polymeric composites are discussed and the research objectives are presented. Chapter 2 presents an extensive review related to CNFs, where the structure, synthesis, and properties of CNFs are examined along with various processing techniques and characterization of the properties of nano-engineered polymeric composites. In Chapter 3, a novel approach to fabricate polymeric nanocomposites containing aligned functionalized CNFs is developed and the dispersion, alignment morphology, and properties of resulting nanocomposites are discussed. Chapter 4 presents the synthesis and characterization of hierarchical composites made of CNF/glass fiber layers, as well as demonstrates the formation of out-of-plane reinforcement in CNF/glass fiber assembly by using solely CNF entangled network. Finally, Chapter 5 presents the conclusions of the work along with recommendations.

CHAPTER 2

LITERATURE REVIEW

2.1 Background of Carbon Nanofibers

The synthesis of carbon filament by Hughes and Chambers in 1889 is regarded as the origin of carbon nanofibers (CNFs) and marked an important milestone for the modern development of CNFs. The true application of CNFs came much later when scientists and engineers realized that excellent material properties can be harvested by incorporating PAN-based and pitch-based carbon fibers into composites in the 1970s and 1980s. At that time, high manufacturing cost of PAN-based and pitch-based carbon fibers had forced researchers to synthesize vapor grown carbon fibers (VGCFs) with size and properties similar to conventional carbon fibers from hydrocarbons at a more affordable cost [31]. The resulting VGCFs were found to possess two types of textures subjected to two different growth processes: core sections with long and straight carbon assemblies caused by catalytic effect and external sections with carbon deposition during the thickening stage [32]. Further studies of VGCF synthesis showed that growing the predecessor of carbon filaments was very encouraging and nanometer sized filaments can be efficiently grown inside the reacting chamber. Eventually, these findings triggered the researchers to modify the synthesis process for continuous production of submicron-sized filaments, known as vapor grown carbon nanofibers (VGCNFs) and later simply CNFs, without unwanted carbon filament thickening effect. Nowadays, CNFs are continuously produced at large scale and are available in large quantity at price range from $100/lb to $500/lb [33].

2.2 Structure, Synthesis, and Properties of Carbon Nanofibers

2.2.1 Structure of Carbon Nanofibers

CNFs are hollow-core cylindrical nanostructures that consist of either a single-layer (left image) [11] or double-layer (right image) [34] graphite planes stacked parallel or at certain angle with respect to its longitudinal axis, as shown in Figure 2. In some cases, CNFs are also known as cup-stacked carbon nanotubes. Depending on the stacking geometry of graphite planes, the structure of CNFs can be categorized into parallel [34], bamboo-like [35], and cup-stacked [36, 37] arrangement. Because of their nano-scale diameter and micron-scale length, CNFs with high aspect ratio, ranges between 250 and 2,000, fill the gap of dimensional hierarchy among commercial carbon fibers, single-walled carbon nanotubes (SWCNTs) and multi-walled carbon nanotubes (MWCNTs), as summarized in Table 1.

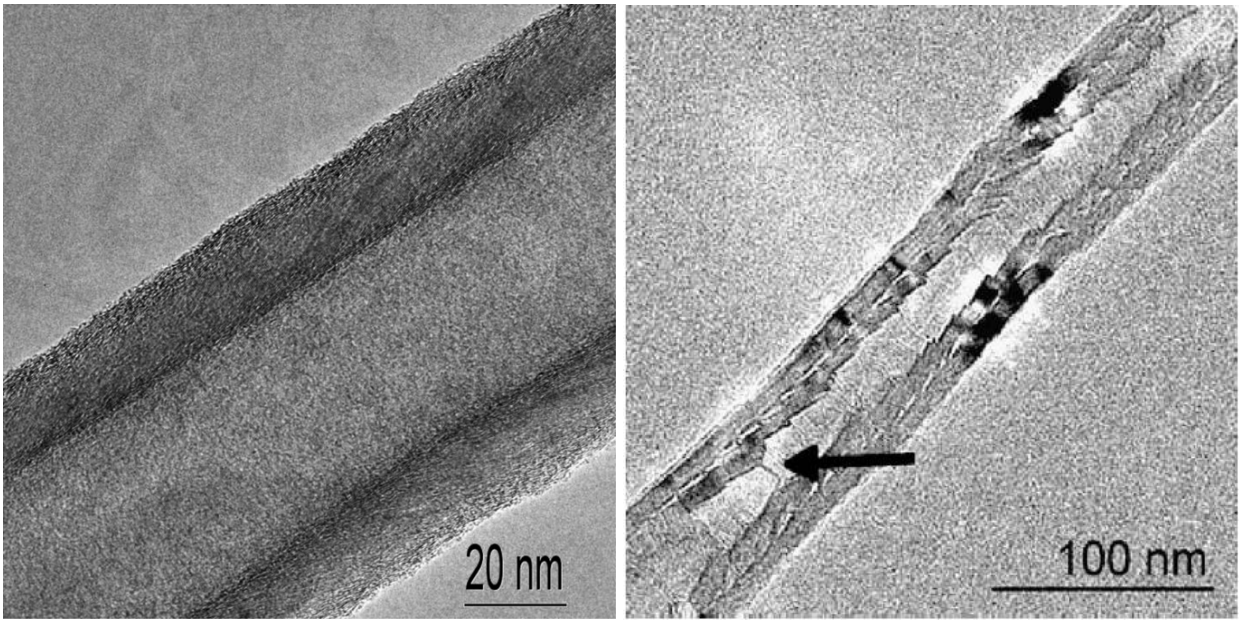

Figure 2. TEM images of individual CNF with single-layer graphite (left) [11] and double-layer graphite (right) [34].

TABLE 1

DIMENSIONS OF COMMERCIAL CARBON FIBERS, CNFS, AND CNTS

Material	Diameter (nm)	Length (μm)	Aspect Ratio
Carbon Fiber [38]	5,000-20,000	3,200	10-50
CNFs [39]	60-200	30-100	250-2,000
SWCNTs [38]	0.6-1.8	0.5-30	100-10,000
MWCNTs [38]	5-50	10-50	100-10,000

By using advanced electron microscopy techniques, numerous researchers have been able to image the interior and exterior configuration of individual CNF. Endo et al. [36] utilized high-resolution transmission electron microscope (HRTEM) to investigate the cross-section of a cup-stacked CNF. Figure 3 clearly showed that the CNF possessed a hollow interior surrounded by concentric cup-stacked graphite planes that lie at an angle between 45˚ and 80˚. The authors also found that the exposed graphite plane edges along the interior and exterior of CNF were covered by amorphous carbon and they can be chemically or thermally treated to facilitate the attachment of chemical functional moiety. Besides revealing the interior and exterior configuration of CNF, an attempt to measure the d-spacing of graphite planes of single layer CNF was performed by Miyagawa and coworkers [40]. Interestingly, the study highlighted that the d-spacing between two adjacent graphite planes is 0.34 nm (3.4 Å) which corresponds to the spacing between the concentric walls of MWCNTs and graphite platelets.

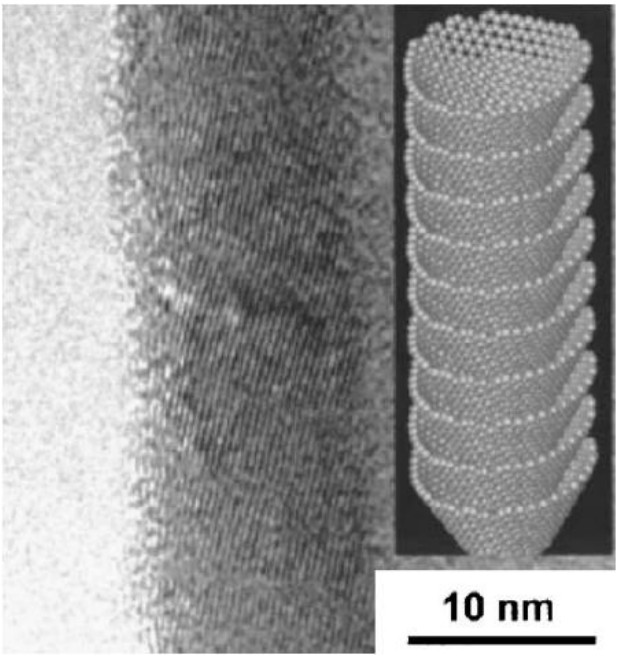

Figure 3. HRTEM image of the side-wall of a CNF with cup-stacked configuration. The inset schematically illustrates the cup-stacked configuration of CNF [36].

2.2.2 Synthesis of Carbon Nanofibers

CNFs are predominantly synthesized through a bottom-up method, which involves chemical vapor deposition (CVD) of decomposed hydrocarbons such as natural gas, propane, acetylene, benzene, ethylene or carbon monoxide over the surface of metal or metal alloy catalyst. The catalyst can be deposited on a substrate or directly fed with the gas phase feedstock before growing CNFs. CVD process is by far the mostly used and cost-effective method to synthesize CNFs and it is usually performed in a reactor operated at a temperature range of 500-1,500 ˚C [3]. The other CNF synthesis method, which involves carbonization of electrospun polyarcylonitrile (PAN) nanofibers at different elevated temperature, was demonstrated by Salman et al [41].

In general, as-synthesized CNFs are covered with layers of amorphous carbon and impurities that may degrade their properties; therefore, as-synthesized CNFs can be further

subjected to graphitization of CNFs exterior layers or recrystallization of the nested graphite planes. The former process results in CNFs with higher mechanical and electrical properties due to alignment of the outer layer parallel to the longitudinal direction; whereas the latter approach results in lower properties due to the formation of discontinuous conical crystallites. Studies have shown that the volumetric electrical resistivity of CNFs after heat treatment is in the range of 10^{-3} Ω.cm to 10^{-5} Ω.cm. The optimum heat treatment temperature for CNFs was investigated by Tibbetts et al. where the authors found that optimum mechanical and electrical properties can be achieved by heat treating the CNFs at 1,500 °C and 1,300 °C, respectively [42].

2.2.3 Properties of Carbon Nanofibers

To better understand the overall properties of nano-engineered polymeric composites, it is imperative to investigate the properties of each material constituent from different aspects. However, the direct measurement of mechanical, electrical, and thermal properties of a single CNF has been practically a tedious task due to the structural complexity of CNF derived from variations in inner and outer wall thickness, cone angle, orientation of graphite planes, and carbon-carbon bonds. Rather, the direct properties measurements of a single CNF can be enabled only with the aid of appropriate assumptions and simplifications other than high-sensitivity instruments. Table 2 summarizes typical physical properties of CNFs, SWCNTs, MWCNTs, commercial carbon fibers, and selected metals.

TABLE 2

MECHANICAL, ELECTRICAL, AND PHYSICAL PROPERTIES OF VARIOUS MATERIALS

Material	Strength [GPa]	Young's Modulus [GPa]	Electrical Conductivity [S/m]	Density [g/cm^3]	Specific Strength [MPa·m^3/Kg]
CNF	2.35-2.9 [1]	6-285 [2]	10^6 [43]	1.95 [43]	1.49
MWCNT	35-82 [44]	590-932 [44]	10^6 [45]	1.3-2.25 [12]	15.5-63.08
SWCNT	97-110 [44]	990-1,105 [44]	10^4 [45]	1.33-1.4 [12]	69.29-82.71
Carbon Fiber (PAN-Based Precursor)	4.65-6.35 [46]	285 [46]	6.66×10^4 [46]	1.78 [46]	2.61-3.57
Aluminum 7075-T6	0.572 [46]	71 [46]	1.91×10^7 [46]	2.80 [46]	0.204
Steel 316 (cold drawn and annealed)	0.620 [46]	193 [46]	1.5×10^6 [46]	8.00 [46]	0.075

2.2.3.1 Mechanical Properties

Tanil et al. [1] performed direct measurements of tensile strength and modulus of three different types of CNFs (PR-24-XT-PS, PR-24-XT-HHT-LD, and PR-24-XT-HHT-LD-OX from Applied Science, Inc.) using a microelectromechanical system (MEMS) based platform, shown in Figure 4. During the course of experiment, the authors estimated the nominal strength of CNFs based only on the CNFs outer diameters because the inner diameter of CNFs could not be accurately assessed. The test results showed that the average tensile strength and modulus of PR-24-XT-PS were 2.9 GPa and 180 GPa, respectively; whereas PR-24-XT-HHT-LD retained average tensile strength and modulus of 2.35 GPa and 245 GPa, respectively. In addition, it was experimentally found that the strength standard deviation of PR-24-XT-HHT-LD decreased in

comparison to PR-24-XT-PS, suggesting a reduction in flaw distribution of CNF as a result of alignment or reorganization of the outer turbostratic layers after heat treatment. Joseph et al. [2] attempted another investigation of CNFs tensile properties through a three-point-bending setup (Figure 5). In that work, CNFs were first mounted on copper grid through the deposition of platinum pads by focused ion beam (FIB), then an AFM probe was used to apply a concentrated transverse force at the midspan of CNFs (middle section of two platinum pads). Test results revealed that the elastic modulus of CNFs ranged from 6 to 207 GPa with improved accuracy and reproducibility. Additionally, the authors claimed that the well-aligned graphite layers at the outer wall that were closest to the inner wall were responsible for the strength of CNFs. Furthermore, the elastic modulus was found to be independent of wall thickness for CNFs with wall thicknesses greater than 80 nm.

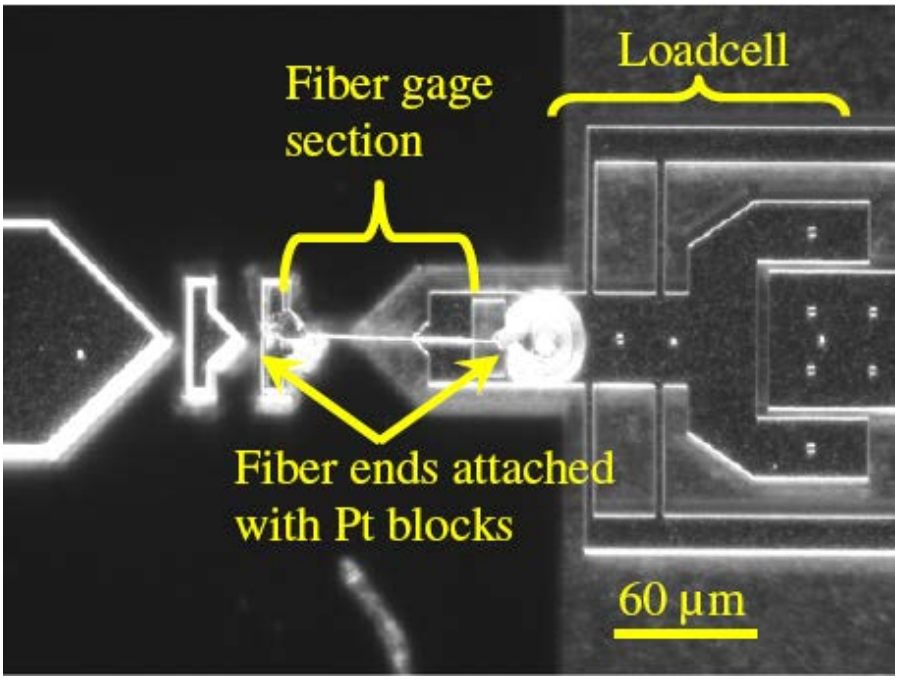

Figure 4. MEMS-based platform for characterizing tensile properties of an individual CNF [1].

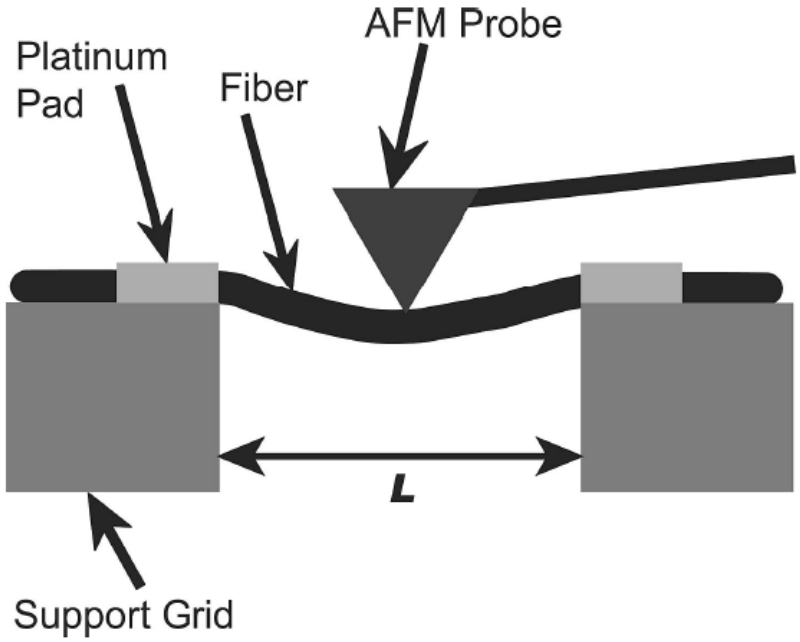

Figure 5. Schematic of the three-point bend test of an individual CNF using the AFM tip [2].

Mechanical testing of long and continuous CNFs was also addressed in a study performed by Salman et al. [41]. The authors synthesized the PAN-based CNFs by first electrospinning PAN-based nanofibers and then carbonizing the electrospun nanofibers at different temperature. Test results showed that the CNFs diameters ranged from 150 nm to 500 nm and tensile strength and modulus of CNFs were dependent on carbonization temperature. Specifically, CNFs carbonized at 1,400 °C attained the highest average tensile strength of 3.5 GPa while CNFs carbonized at 1,700 °C possessed the highest average tensile modulus of 172 GPa. According to the authors, CNF tensile strength reported herein was comparable to tensile strength of commercial T-300 carbon fiber. After subjecting to carbonization, the surfaces of CNFs appeared to be smooth and homogeneous CNF cross sections were observed. By varying the carbonization temperature from 800 °C to 1,700 °C, the average thickness of CNFs

turbostratic carbon crystallites increased from 3 to 8 layers, but the crystallites large size, discontinuous form, and random orientation reduced CNFs tensile strength at carbonization temperature higher than 1,400 °C.

2.2.3.2 Electrical Properties

Although the electrical resistivity of graphite was estimated to be in the range of 10^{-6} Ω.cm, researchers anticipated that the resistivity of CNFs should be slightly higher than graphite due the variations in CNFs structure, wall thickness, and impurities. Typically, as-synthesized CNFs contain amorphous carbon and impurities that degrade their electrical properties; therefore, depending on the application types, post processing is required to increase the crystallinity or eliminate the impurities of CNFs. Heremans et al. [47] measured the electrical resistivity of CNFs as a function of heat-treatment temperature. Test results indicated that the electrical resistivity of CNFs heat-treated at 2,900 °C was as low as 6.8 x 10^{-5} Ω.cm. Endo and coworkers [31] also characterized the electrical resistivity of short-VGCNFs via a four-point-probe method. The authors found that the electrical resistivity of CNFs were in the range of 10^{-3} and 10^{-4} Ω.cm after carbonization and graphitization, respectively.

2.3 Post Processing of Carbon Nanofibers

Pristine CNFs (including other carbon nanomaterials) tend to agglomerate and form clusters, which are difficult to disrupt, due to strong van der Waals forces and high surface area. Previous studies [18, 19] showed that nanomaterial agglomerates are often detrimental to the resulting nano-engineered polymeric composites because of degradation in mechanical properties. To preserve the benefits of adding carbon nanomaterials into polymeric composites, it is imperative to break apart the agglomerates and uniformly disperse nanomaterials within the

matrix in order to allow effective load transfer from the matrix to nanomaterials through proper interaction. A common methodology favored by most researchers to meet this requirement is chemical functionalization of the nanomaterials surfaces, which can be further categorized into non-covalent [48, 49] and covalent functionalization [50-54] schemes. In either case, the ultimate goal is to increase the surface energy of nanomaterials in order to create the repulsive force necessary for individual nanomaterial to remain stable in a medium. Depending on the type of chemical functional groups attached to the nanomaterials, certain level of chemical interaction or bonding between nanomaterials and polymer matrix can be expected for better reinforcement purpose.

In non-covalent functionalization scheme, a combination of surfactant and solvent is usually used to uniformly disperse nanomaterials. Surfactant is an organic compound with bulky molecule that is amphiphilic, which means that it consists of both hydrophobic and hydrophilic groups. When a surfactant is used in the fabrication of polymeric nanocomposites, researchers found that the hydrophobic group can interact with nanomaterials through adsorption mechanism while the hydrophilic group could interact with polymer matrix through hydrogen bonding. Once the surfactant molecules are adsorbed onto the nanomaterials surfaces, they provide steric repulsion among nanomaterials and thus result in individually dispersed nanomaterials. Gong et al. [48] utilized polyoxyethylene-8-lauryl ($C_{12}EO_8$) to disperse CNTs into epoxy resin through magnetic stirring. Test results showed that the resulting nanocomposites containing 1 wt% surfactant-treated CNTs exhibited higher glass transition temperature (T_g) and elastic modulus than neat epoxy counterpart. Geng et al. [49] reported the use of a non-ionic surfactant Triton X-100 to enhance the CNTs dispersion in epoxy resin. The authors found that mechanical and electrical properties of resulting nanocomposites were significantly improved as a result of

"bridging" effect between CNTs and epoxy, which were caused by the hydrophobic and hydrophilic segments of surfactant.

In covalent functionalization scheme, nanomaterials are usually mixed and reacted with various chemical reagents to covalently introduce chemical functional moieties on their surfaces. Such moieties will cause an increase in nanomaterials surface energy, which in turn provides necessary repulsive force to disperse and stabilize nanomaterials in different medium. In terms of chemical compatibility or bonding, researchers have investigated the use of various functional moieties which are compatible with the polymer matrix to achieve better load transfer between material phases. To date, several common functional groups such as carboxylic acid [50, 51], amine [52], hydroxyl [53], and epoxide [54] have been grafted onto carbon nanomaterials with various levels of success. Lachman et al. [55] demonstrated that nanocomposites filled with carboxylic acid- and amine-functionalized MWCNTs exhibited an increase in toughness. The authors attributed such improvement to the enhancement in MWCNTs dispersion quality and interfacial adhesion. Lakshminarayanan et al. [56] oxidized pristine CNFs using 69-71 wt% nitric acid for various treatment time. Results from this work showed that the surface atomic oxygen percentage attained a maximum value of 22.5% in CNFs oxidized for 90 minutes without inducing significant structural damage. The authors also found that the oxidized CNFs were highly soluble in water due to an increase in wettability. Seyhan et al. [57] studied the fracture toughness of an epoxy-based resin reinforced with as-received, acid-treated, and silanized CNFs. Test results showed that addition of 1 wt% silanized CNFs into neat resin led to an increase in fracture toughness of 12%. Prolongo et al. [58] reported a three-stage profile to obtain amine-functionalized CNFs and the effect of incorporating amine-functionalized CNFs on the dispersion and properties of nanocomposites. The authors found that the CNFs dispersion in the

matrix and storage modulus of resulting nanocomposites was enhanced up to a concentration of 1 wt%. The authors also concluded that chemical functionalization coupled with ultrasonic or high shear mixing is needed in order to better disperse CNFs in the epoxy matrix.

Although numerous studies have successfully proven the benefits of using functionalized carbon nanomaterials to reinforce polymeric composites, the controversy of whether pristine or functionalized carbon nanomaterials perform better in nano-engineered polymeric composites continues to escalate. A more comprehensive fundamental understanding of each type of carbon nanomaterials is needed to better establish the structure-property relationship.

2.4 Nano-Engineered Polymeric Composites

2.4.1 Polymeric Nanocomposites

As mentioned earlier, carbon nanomaterials with one-dimensional nanostructure and unique combination of properties have triggered tremendous research interests within the scientific community. They are continuously regarded as an ideal building block for fabricating the next generation advanced composites –polymeric nanocomposites– for a wide spectrum of applications. Much of previous studies successfully showed that the integration of carbon nanomaterials into polymer matrix would result in nanocomposites exhibiting dramatic improvement in mechanical and electrical properties, making them a truly multi-functional advanced material.

Carbon nanomaterials are directly incorporated into polymer matrix through a variety of approaches such as sonication [59], magnetic stirring [60], high-shear homogenization [61], calendering [62], centrifugal mixing [63], and extrusion [64]. The nanomaterial/polymer mixture is then casted into a mold and cured at room temperature or elevated temperature. Typically, the amount of nanomaterials that can be incorporated into polymer matrix through the

abovementioned approaches is limited due to the difficulties in dispersing nanomaterials (the polymer matrix changed from liquid to pasty). Thostenson et al. [62] established a processing protocol to effectively disperse CNTs into epoxy resin through calendering approach. Test results showed that, at low concentration, the fracture toughness of resulting nanocomposites was significantly enhanced in comparison to neat epoxy due to highly-dispersed CNTs. Furthermore, the authors found that the high aspect ratio of CNTs was attained after mixing and the formation of a conductive percolating network was achieved at concentration as low as 0.1 wt%. Lafdi et al. [65] investigated the effect of adding different types of CNFs on mechanical and thermal properties of nanocomposites. At a concentration of 4 wt%, the flexural modulus and yield stress of functionalized CNF-reinforced nanocomposites were improved by 137% and 35%, respectively, while the thermal conductivity of heat treated CNF-filled nanocomposites was enhanced by 80%. The authors also reported that a CNF concentration of 12 wt% was the onset of mechanical properties degradation due to the difficulties in dispersing CNFs. In a separate study, the same authors [66] functionalized as-received CNFs through electrochemical methods with different treatment time and fabricated nanocomposites containing different functionalized CNFs at constant concentration of 12 wt%. Mechanical test results indicated a maximum enhancement in flexural strength and modulus for the nanocomposites filled with functionalized CNFs treated for 12 minutes. However, there was an increase in electrical resistivity for nanocomposites filled with functionalized CNFs treated with longer treatment time, in which case the authors attributed such finding to an increase in oxygen content on CNFs surfaces. Ahn et al. [67] prepared nanocomposites by incorporating amidized CNFs into epoxy resin and assessed the properties of resulting nanocomposites. The authors found that, when compared with neat resin, the maximum improvements in tensile strength and modulus of nanocomposites

occurred at two different concentrations. Specifically, the tensile strength attained a 260 % increase for nanocomposites filled with 12.8 wt% amidized CNFs while the tensile modulus achieved an increase of 136% for nanocomposites filled with 6.4 wt% amidized CNFs. Further failure analysis indicated a robust nanofiber/matrix interface due to the formation of chemical linkage between CNFs and epoxy resin. Despite of CNFs surface modification, the electrical conductivity of nanocomposites filled with 12.8 wt% amidized CNFs reached a value of 3.19 x 10^{-2} S/cm. Prasse et al. [68] performed an alignment study by subjecting the CNF/epoxy mixture to an external AC electric field during curing of nanocompsites. The authors reported electrical resistivity anisotropy (a ratio of resistivity perpendicular to the electric field to resistivity parallel to the electric field) of 10, indicating the formation of aligned CNF network along the direction parallel to applied electric field. Test results showed that the electrical resistivity of nanocomposites containing aligned CNF network decreased to 10^{6} Ω.cm range and the resistivity percolation threshold was identified at approximately 0.75 wt%.

2.4.2 Hierarchical Composites

Hierarchical composites are defined as materials having two or more constituents at nano-scale and micro-scale. While tremendous efforts were spent on researching polymeric nanocomposites, several investigators have worked on developing processes that enable incorporation of carbon nanomaterials into traditional FRPCs to improve the properties that plague material scientists and engineers. To date, there are five main approaches to manufacture hierarchical composites: (1) infusion of nanomaterial/polymer mixture into the preform, (2) direct placement of nanomaterials between laminates, (3) growth of nanomaterials on reinforcement layer through chemical vapor deposition (CVD), (4) deposition of nanomaterials onto the reinforcement fabric, and (5) coating reinforcement fibers with sizing agent containing

well-dispersed nanomaterials. These approaches will be briefly highlighted in the following subsections.

2.4.2.1 Infusion of Nanomaterial/Polymer Mixture into Preform

In this method, the carbon nanomaterials are initially dispersed in the polymer matrix to obtain a nanomaterial/polymer mixture. The mixture is then infused into dry preform by resin transfer molding to manufacture final hierarchical composite part. So far, this method is the most widely used technique to manufacture hierarchical composites due to its practicality and scalability to manufacture large parts. Additionally, the carbon nanomaterials used can be selectively functionalized with desired moieties in order to promote various degree of chemical interaction between nanomaterials and polymer matrix.

Sadeghian et al. [13] manufactured hierarchical composites by injecting a surfactant treated-CNF/polyester mixture into a glass fiber preform. Mechanical test results showed an increase of approximately 100% in mode-I fracture toughness (G_{IC}) for hierarchical composites loaded with 1 wt% surfactant treated-CNFs in polyester resin. Although significant improvement was attained in the final hierarchical composites, the authors identified parts manufacturing difficulties arise due to an increase in viscosity of the CNF/resin mixture as well as void formation in the parts. Gojny et al. [69] prepared CNT/epoxy mixture by incorporating amidized CNTs into epoxy resin through a calendering approach. The mixture was then infused into a mold cavity containing glass fiber preform and cured at elevated temperature. The interlaminar shear strength of hierarchical composites containing 0.3 wt% amidized CNTs was found to be 20% higher than the base panel while no significant difference was observed in tensile properties of hierarchical composites and base panel since they were dominated by the fiber properties. The author also found that, for hierarchical composites containing 0.3 wt% amidized CNTs, the in-

plane electrical conductivity was one order of magnitude higher than the out-of-plane electrical conductivity.

Despite of interesting results, the shortcomings (include uniform nanomaterial dispersion, nanomaterial filtration by micron-scale reinforcement fibers, high viscosity of matrix, and void formation) of this method greatly limit the scalability of manufacturing large hierarchical composite parts.

2.4.2.2 Direct Placement of Nanomaterials Between Laminates

Due to the difficulties associated with manufacturing hierarchical composites, researchers employed a direct placement method to alleviate some of the shortcomings encountered in the infusion method. In this method, carbon nanomaterials are directly placed between laminates before curing at elevated temperature. Through this protocol, the challenges to obtain uniform nanomaterial dispersion in polymer matrix and to prevent filtration of nanomaterials by reinforcement fibers can be better addressed and, in some cases, orientation of nanomaterials can be controlled.

Several researchers have used this technique to manufacture hierarchical composites yielding different levels of success. Li et al. [27] employed a “powder method” to introduce CNF interlayer at the mid-plane of commercial prepreg laminates before curing (Figure 6 left). A sifter was used to help uniformly disperse CNFs onto the laminates during the process. Test results revealed a simultaneous improvement in the mode-I fracture toughness and bending strength and modulus of resulting hierarchical composites. Garcia et al. [70] developed a “transfer-printing” approach to incorporate aligned CNT arrays onto commercial carbon fiber prepregs (Figure 6 right). By taking advantage over the tackiness of prepreg, vertically aligned CNT arrays pre-grown on a substrate were “transfer-printed” onto the laminates by a

combination of rolling and pressing processes and then cured in an autoclave at elevated temperature. Results from this work showed that the mode-I and mode-II fracture toughness of final hierarchical composites increased by 1.5-2.5 times and 3 times, respectively, in comparison to base panel. In a study by Rojas et al. [71], both CNTs and CNFs were sprayed onto the carbon fiber layers before preform layup and infusion of polymer matrix. The authors concluded that even though a significant improvement in interlaminar shear strength of hierarchical composites was not achieved, the change in failure mode from delamination to tensile fracture was considered the evidence of reinforcement in the mid-plane of test sample.

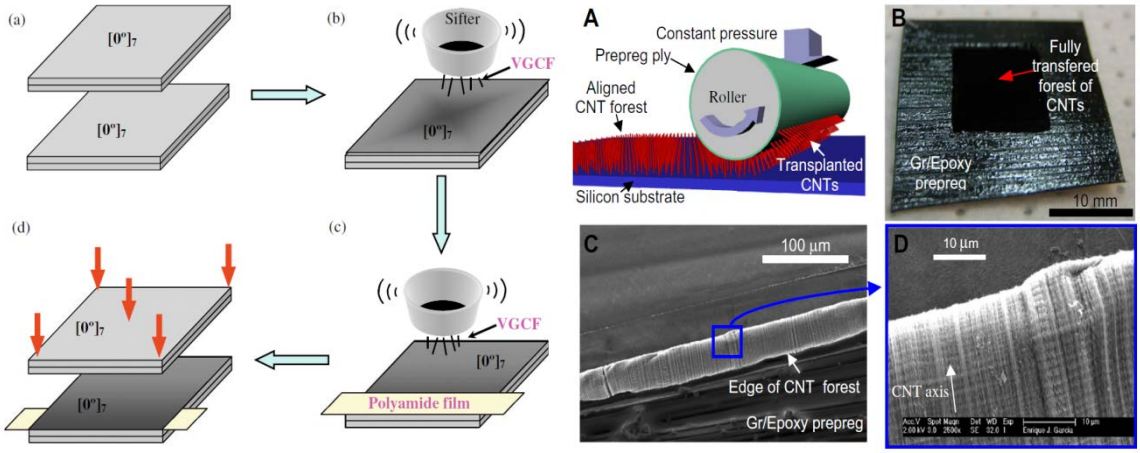

Figure 6. Direct placement route through "powder-method" (left) [27] and "transfer-printing" technique (right) [70].

The main setbacks of this approach lie on the thickness increase and variation of final hierarchical composite parts as well as size limitation in growing large volume of nanomaterials on a substrate (for "transfer-printing" technique).

2.4.2.3 Growth of Nanomaterials on Reinforcement Layer

Another innovative approach that was developed in the last decade is by directly growing nanomaterials on the surface of micro-scale reinforcement fibers through chemical vapor deposition. Several multiscale reinforcement layers are then assembled and cured with polymer matrix at room temperature or elevated temperature. This method offers several advantages, with the most important ones being the ability to effectively control distribution and orientation of nanomaterials grown on the fibers.

Several researchers successfully developed various conditions to directly grow nanomaterials on alumina fibers [28], silica fibers [72], quartz fibers [73], and carbon fibers [74-78]. Garcia et al. [28] employed a modified CVD protocol to grow radially aligned CNT forests on the surfaces of alumina fibers (Figure 7). Several hybrid layers were infiltrated with epoxy resin, assembled, and cured through wet layup technique. According to this study, the wetting behavior of hybrid layers by epoxy resin was governed by capillary effect and the alumina fiber and CNT volume fraction of resulting hierarchical composites were approximately 60% and 0.6-2.9%, respectively. Interestingly, the authors observed an increase of 69% in interlaminar shear strength for hierarchical composites over the base panel, while further electrical properties measurements showed that both in-plane and out-of-plane electrical conductivity of hierarchical composites were improved by several orders of magnitude. These results confirmed that proper incorporation of nanomaterials would indeed transform traditional FRPCs into a multifunctional composite. Sager et al. [75] attempted a similar approach to grow CNTs on the surfaces of carbon fibers. The sizing layer of as-received carbon fibers was removed prior to the growing process. The authors reported that an increase of up to 71% in interfacial shear strength can be expected when comparing the shear strength of hybrid fiber to the unsized fiber. Although higher interfacial shear strength was attained, the authors also found that extreme growing conditions

necessary for a typical CVD process could significantly decrease the tensile strength of carbon fiber by up to 37%.

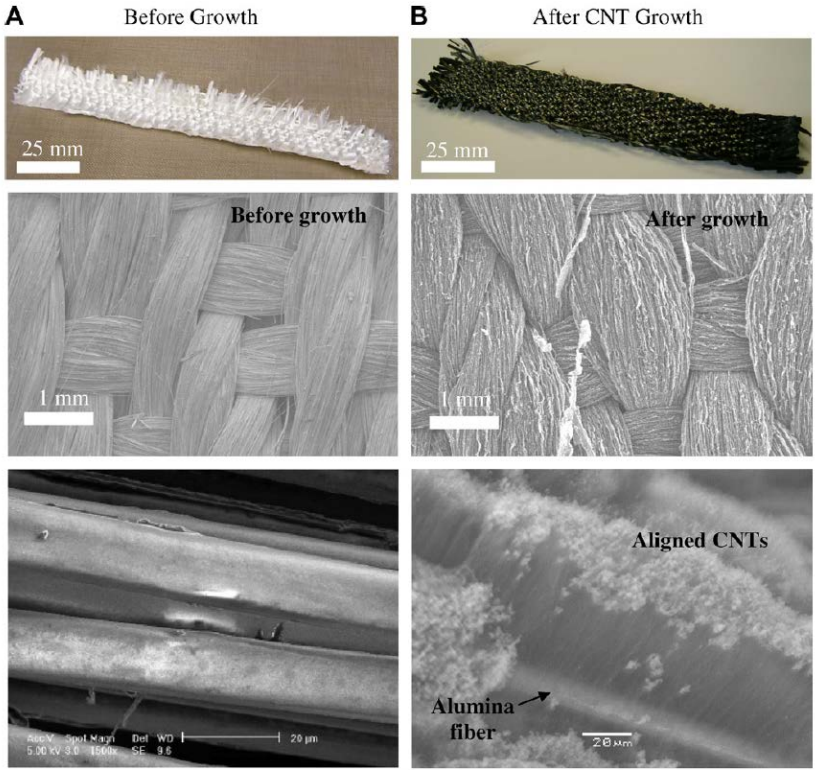

Figure 7. Radially aligned CNT forest grown on alumina fiber through CVD process [28].

The growth method is by far the most promising technique to fabricate hierarchical composites in terms of uniform distribution and orientation of nanomaterials and, most importantly, highest improvement in properties. However, the main disadvantages of this approach include the lack of practicality due to the limitations in growing nanomaterials in large size, presence of catalysts (act as impurity), lack of chemical compatibility between nanomaterials and polymer matrix, and degradation of fiber properties due to aggressive processing conditions.

2.4.2.4 Deposition of Nanomaterials onto Reinforcement Fabric

Deposition (especially electrophoretic deposition (EPD)) of nanomaterials onto the surface of reinforcement fabric is a promising method that shows the highest advantages in terms of scalability, practicality, cost-effectiveness, and capability to manufacture hierarchical composites with various types of functionalized nanomaterials. In this process, the nanomaterials are initially modified with desired chemical functional groups. Then, the functionalized nanomaterials are dispersed in a solvent and the nanomaterials will travel and deposit onto a targeted substrate when subjected to an electric field.

Several researchers have proven the applicability of this method to manufacture hierarchical composites with different levels of achievements. Bekyarova et al. [79] utilized EPD to deposit carboxylic acid-functionalized CNTs onto the surfaces of carbon fiber layers that were then used to manufacture hierarchical composites. Results from this study showed an increase in interlaminar shear strength and through-plane electrical conductivity of approximately 27% and 30%, respectively. When EPD was used to synthesize multiscale fabrics containing carboxylic acid-functionalized CNTs, the authors found that the in-plane tensile strength of resulting hierarchical composites was not compromised. This indicates that the EPD process does not affect the intrinsic properties of fibers, which is a great advantage over other method such as CVD growth that tends to weaken the fiber tensile strength as a result of aggressive processing conditions. Rodriguez et al. [16, 29] prepared multiscale fabrics by depositing amine functionalized CNFs onto the surfaces of carbon fiber layers through a two-stage EPD process and used the multiscale fabrics to manufacture hierarchical composites. Mechanical test results revealed that both interlaminar shear strength and compressive strength of hierarchical composites were improved by approximately 12% and 13%, respectively, with respect to base composites (not containing CNFs). An interesting finding from this work is that the compliance

(as evidenced by the change in slope of loading nose force vs. displacement graph) of the matrix and fiber/matrix interface changed from ductile to more brittle behavior possibly due to the formation of covalent bond between the epoxide groups of the matrix and the amine groups of the CNFs. Zhang et al. [80] successfully deposited functionalized CNTs onto electrically insulating glass fibers through EPD. Single-fiber fragmentation test showed that the interfacial shear strength of CNT/glass fiber composites increased significantly in comparison to the as-received glass fiber composites. In addition, the semi-conductive CNT/glass fiber interface was highly sensitive to the tensile strain of single-fiber composites making this behavior a feasible feature for damage sensing purpose.

The main disadvantages of this technique lie on the lack of nanomaterial alignment on the fabrics and the short length of nanomaterials after functionalization (it is well know that nanomaterials with high aspect ratio provide better reinforcement efficiency).

2.4.2.5 Coating Reinforcement Fibers with Nanomaterial/Sizing Agent

In recent years, carbon nanomaterials are also incorporated into FRPCs through "sizing" approach. In this process, carbon nanomaterials are initially dispersed in polymer-based sizing agent (commercially available) and then reinforcement fibers or fabrics are coated with the modified sizing agent before being used to manufacture hierarchical composites. Godara et al. [81] coated the virgin glass fibers with CNTs by drawing the fibers through a diluted phenoxy-based sizing agent containing 0.5 wt% CNTs and fabricated hierarchical composites using such modified glass fibers. When compared to base composites made of virgin glass fibers, single-fiber fragmentation test showed an increase of 92% in interfacial shear strength of hierarchical composites by solely introducing CNTs onto the surfaces of glass fibers. Such improvement indicated that the interfacial adhesion of fiber/matrix interface can be enhanced and thus increase

the overall mechanical properties of hierarchical composites. Gao et al. [30] manufactured CNT/glass fiber hierarchical composites by infusing a diluted CNT/sizing agent into dry glass fiber preform through VARTM process, volatizing the solvent, and injecting neat epoxy resin into the modified preform. For comparison, the authors fabricated another CNT/glass fiber hierarchical composite by curing the glass fiber layers with CNT/epoxy mixture prepared through calendering process. Results from this work revealed that the electrical conductivity of hierarchical composites manufactured through "sizing" approach is 2 to 3 orders of magnitude higher than the one by calendering. The authors attributed such improvement in electrical conductivity to controlled CNT agglomerations on the glass fibers surfaces and concluded that the CNT conductive network can be potentially used for damage sensing and EMI shielding of composites.

Although promising results are achievable, this method requires multiple processing stages and conditions, which make it a complex approach. Furthermore, the CNT/sizing layer (usually nanometers thick) added to the surfaces of reinforcement fibers complicate the composites interface among the original sizing on fibers, additional CNT/sizing coating, and matrix, which inevitably causing the interface characterization a challenging and tedious task.

2.5 Summary

In this chapter, the morphology, synthesis, properties of CNFs have been reviewed. Special emphasis was placed in the mechanical and electrical properties of CNFs due to the promise that they hold as nano-scale building block for enhancing the macro-scale properties of nano-engineered polymeric composites.

Processing requirements to effectively incorporate carbon nanomaterials into polymer matrices have been addressed and discussed. Current techniques for manufacturing hierarchical

composites have been reviewed and introduced in this chapter. Several researchers have worked on the development of processes that allow incorporation of carbon nanomaterials into traditional FRPCs to improve the properties of such materials having different levels of success. To date, there are five different approaches to manufacture hierarchical composites: (1) infusion of nanomaterial/polymer mixture into the preform, (2) direct placement of nanomaterials between laminates, (3) growth of nanomaterials on reinforcement layer through chemical vapor deposition (CVD), (4) deposition of nanomaterials onto the reinforcement fabric, and (5) coating reinforcement fibers with sizing agent containing well-dispersed nanomaterials. These methodologies are discussed to emphasize the main advantages and disadvantages of these approaches in terms of manufacturability, scalability, and final properties of the hierarchical composites.

CHAPTER 3

FABRICATION AND CHARACTERIZATION OF POLYMERIC NANOCOMPOSITES CONTAINING ALIGNED FUNCTIONALIZED CARBON NANOFIBERS

3.1 Introduction

In the last two decades, carbon nanofibers (CNFs) and carbon nanotubes (CNTs) have been extensively investigated and considered as an effective building block in polymeric composites due to their low density, high aspect ratio, and unique combination of mechanical and electrical properties. To date, CNFs and CNTs continue to excel as primary choice of nano-fillers for constructing the next generation multi-functional polymeric composites to facilitate a wide range of applications. A closer comparison, however, indicates that CNFs are more favorable than CNTs in the fabrication of polymeric nanocomposites due to their lower cost, availability, and ease of processing. Although this study focuses only on CNFs, the following sections also partially discuss fabrication challenges of CNT-based polymeric nanocomposites.

As mentioned earlier, several key prerequisites must be fulfilled in order to manufacture carbon nanomaterial/polymer composites with promising properties, these include (1) carbon nanomaterials must be uniformly dispersed in the matrix so that the external load can be equivalently transferred to the nanofibers, (2) the formation of chemical linkage between carbon nanomaterials and matrix for better load transfer as well as preventing carbon nanomaterials from slipping relative to the matrix when sustaining external load, and (3) carbon nanomaterials alignment in composites for better properties enhancement. Ever since the use of carbon nanomaterials in polymeric composites became increasingly popular, a wide variety of processing techniques were developed to uniformly disperse carbon nanomaterials into the matrix and attach chemical functional groups onto carbon nanomaterials for the first two requirements. Through these processing techniques, researchers successfully demonstrated that

mechanical and electrical properties of resulting carbon nanomaterial/polymer composites were dramatically improved in comparison to neat polymer counterpart.

Interestingly, the orientation of carbon nanomaterials was found to inflict additional positive effects on properties of carbon nanomaterial/polymer composites. In recent years, studies have shown that carbon nanomaterial/polymer composites with outstanding mechanical and electrical properties can be fabricated at lower amount of nanomaterials by selectively orienting them into a preferential direction through AC electric field [23, 68, 82-84], magnetic field [85, 86], flow induction [87, 88], in-situ growth [89, 90], and mechanical stretching [91]. Among these methodologies, the use of AC electric field is one of the promising methods since it has proven to be effective in promoting alignment of carbon nanomaterials in organic solvent or polymer matrix. Experiments aimed at aligning CNFs using AC electric field in polymer resins have so far been limited to pristine CNFs and none have reported the study of composites with aligned functionalized CNFs. Since functionalized CNFs, especially amine-functionalized CNFs, have previously been shown to disperse uniformly in polymer resins and are capable of chemically interact with the matrix, it is of great interest to pursue the study of the alignment effect of functionalized CNFs on the mechanical and electrical properties of composites. Furthermore, no study has reported the mechanical properties of composites with aligned functionalized CNFs tailored by AC electric field.

In this chapter, the effect of functionalized CNFs aligned in the direction of electric field on the mechanical and electrical properties of final nanocomposites was investigated. An external AC electric field was used to align functionalized CNFs in the polymer matrix. Incorporation of functionalized CNFs into the resin was carried out through a novel process involving a combination of high-speed shear mixing, calendaring, and centrifugal mixing. The

resulting nanocomposites were characterized for dispersion and alignment, electrical resistivity, and compressive strength and modulus parallel to the direction of the aligned CNFs.

3.2 Experimental Section

3.2.1 Materials

As-received CNFs (AR-CNFs) used in this study were Pyrograf PR-24-XT-PS from Applied Sciences, Inc. According to the vendor, the CNFs' average diameter and length were in the range of 60-150 nm and 30-100 μm, respectively, and iron content is approximately 14,000 ppm. The two-part epoxy system used were diglycidyl ether of bisphenol F epoxy resin (EPON 862) and diethyl toluene diamine curing agent (EPIKURE-W) from HEXION Specialty Chemicals. The components were mixed in a ratio of 100 parts resin to 26.4 parts curing agent by weight. A two-part silicon rubber and a Teflon block (McMaster Carr) were used as molds for curing the nanocomposites due to their high electrical and temperature resistance. All chemicals were obtained from Fisher Scientific and used as-received.

3.2.2 Functionalization of Carbon Nanofibers

Both carboxylic acid- and amine-functionalization methodologies employed herein were obtained elsewhere [92, 93] and is illustrated in Figure 8. To obtain carboxylic acid-functionalized CNFs (OCNFs), 2.5 g of AR-CNFs were first mixed with 500 mL of nitric acid in a round bottom flask and sonicated in a water bath for 20 minutes at high power (170 W). The solution was then refluxed and stirred at 260 °C for 4 hours. After that, the OCNFs were filtered out using 0.45 μm pore size nylon membrane, rinsed continuously with reverse osmosis water, acetone, and ultrapure deionized water until chemically neutral and dried in an oven at 100 °C

with vacuum overnight. The OCNFs were then hand grinded and kept in a desiccator until further use.

The amine-functionalization of CNFs consisted of three steps. The first step involved the abovementioned 4-hour carboxylic acid functionalization. The second and third step encompassed acylation and amidation of OCNFs, respectively. In the second step, 5 g of OCNFs were mixed with 80 mL of thionyl chloride ($SOCl_2$) and 4 mL of dimethylformamide (DMF) and sonicated in a water bath at medium power (80 W) for 20 minutes. The mixture was then stirred and heated to 65 °C for 24 hours. After that, the mixture was distilled to remove excess $SOCl_2$. In the third step, the remaining CNFs after distillation were mixed with 100 mL of ethylenediamine and 5 mL of DMF followed by heating and stirring for 48 hours at 100 °C. The mixture was then allowed to cool to room temperature, diluted in ultrapure water, filtered with a 0.45 µm pore size membrane, and dried in vacuum at 60 °C overnight. After drying, the amine-functionalized CNFs (ACNFs) were also hand grinded and kept in a desiccator until further processing.

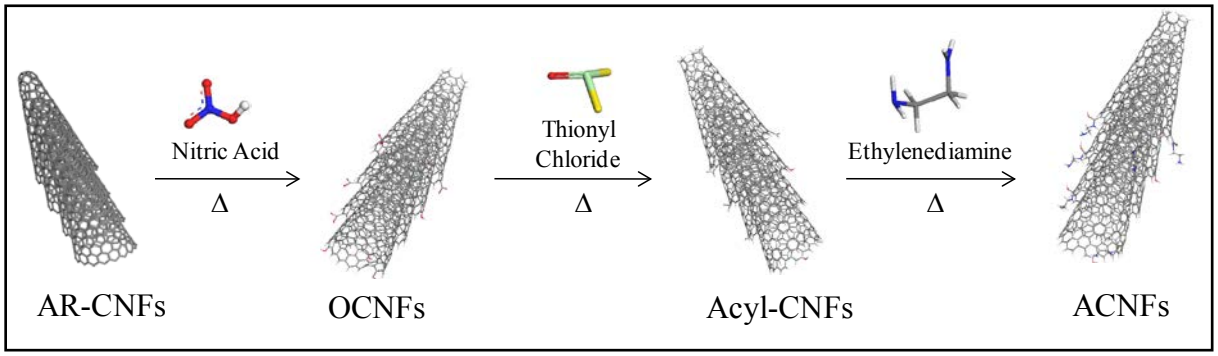

Figure 8. Chemical functionalization scheme of OCNFs and ACNFs [94].

3.2.3 Fabrication of Nanocomposites

In this study, nanocomposites with six different concentrations of functionalized CNFs were studied: 0.25, 0.5, 0.75, 1.5, 3 and 4.5 wt%. Functionalized CNFs were dispersed in the epoxy resin through a novel methodology involving four main steps: sonication, high-speed homogenization, calendering, and planetary centrifugal mixing (Figure 9). To prepare OCNF/epoxy mixture, OCNFs were first sonicated with 150 mL acetone in a water bath for 10 minutes at high power followed by evaporation of acetone in a convective oven. When the mixture became pasty, 185.92 g of epoxy resin was added to the mixture and hand-stirred to saturate the OCNFs with resin. Then, the mixture was homogenized in a water bath using a high-speed homogenizer at three different speeds for 15 minutes and then calendered by passing the mixture through a three-roll-mill set at three different combinations of gap size and speed. Finally, 49.08 g of curing agent was added to the mixture and centrifugally mixed for four repetitions at 2,000 rpm (each repetition consisted of 5 minutes of mixing with vacuum and 5 minutes of cooling at room temperature). For ACNF/epoxy mixture, ACNFs were first sonicated with 150 mL of ethanol in a water bath for 3 minutes at medium power. Then, 118.7 g of preheated epoxy resin (preheated to reduce its viscosity) was added to the mixture and sonicated for additional 10 minutes followed by evaporation of ethanol through mechanical stirring on a hot plate. Afterward, the blend was cooled in a freezer to drastically increase the viscosity of the blend. The blend was then homogenized, calendered, and centrifugally mixed using the same profile for preparing OCNF/epoxy mixture. The amount of curing agent for the ACNF/epoxy mixture was 31.3 g.

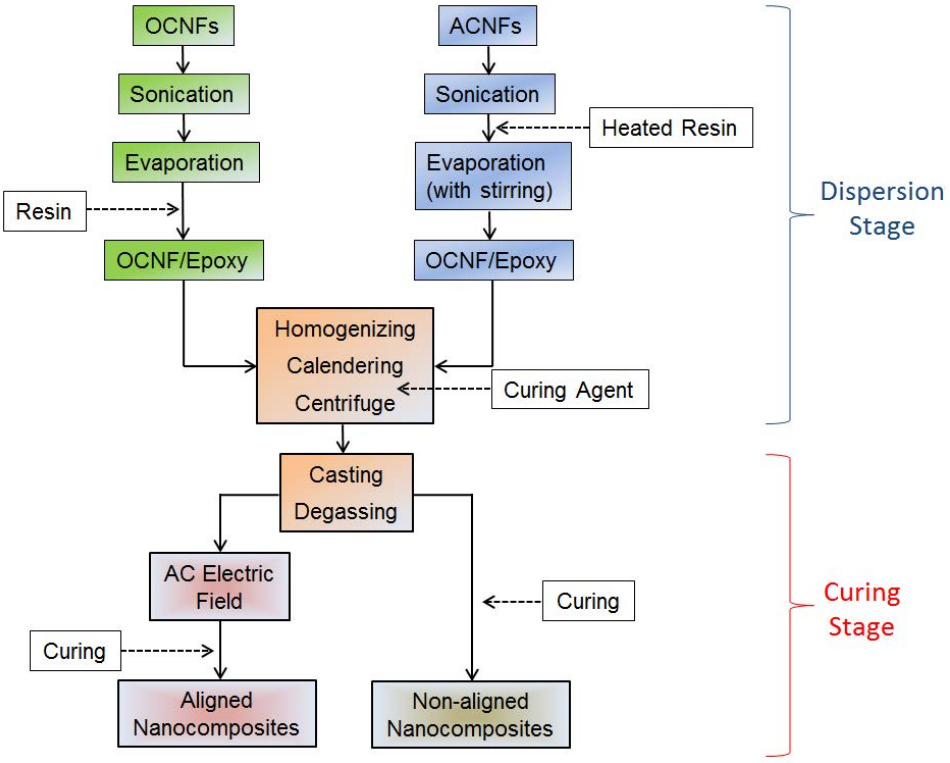

Figure 9. Protocol for dispersing functionalized CNFs into epoxy resin using a combination of sonication, high-speed shear mixing, calendering, and planetary centrifugal mixing.

When aligning functionalized CNFs suspended in the resin, two stainless steel plates, which were 31.75 mm apart, were used as electrodes to apply AC electric field. The sinusoidal AC electric field used was 630 $V_{peak\text{-}to\text{-}peak}$/cm at 2 kHz and was generated using a combination of function generator (GW Instek) and high voltage amplifier (Trek Inc.), as shown in Figure 10. This electric field was calculated by taking the division of applied peak-to-peak voltage by the separation of electrodes. This level of electric field was chosen because it was experimentally found that this level of electric field would yield the optimum alignment structure of functionalized CNFs. The electric field was applied while maintaining the oven temperature at 100 °C for 20 minutes followed by constant temperature ramp (3 °C/min) to 177 °C. Upon reaching 177 °C, the electric field was kept for an additional 20 minutes to ensure that the resin

gelled before the electric field was removed. Subsequently, the resin was allowed to cure at 177 °C for 160 minutes. For electrical test samples, the mixture was casted into a Teflon mold and degassed in a vacuum oven for 15 minutes. Two aluminum plates, which were 12.7 mm apart, were used as electrodes to apply the same electric field strength and frequency. Subsequent procedures to manufacture electrical test samples with electric field was identical to the one followed for mechanical test samples. The resulting dimensions of electrical test samples were approximately 25.4 mm × 8 mm × 12.7 mm.

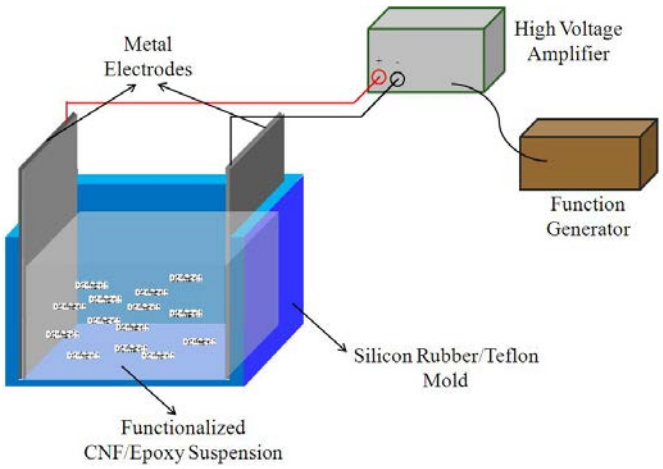

Figure 10. Illustration of experimental setup to align functionalized CNFs suspended in the resin [24].

3.2.4 Preparation and Characterization of Test Samples

All test specimens were machined using a precision cutting machine. The samples were carefully machined according to a layer-by-layer trimming method to ensure the flatness of each specimen. The dimensions of compression and electrical test specimens were 12.7 mm × 12.7 mm × 25.4 mm and 6.45 mm × 6.45 mm × 2 mm, respectively. The two larger surfaces of the electrical test specimens (perpendicular to the CNF alignment direction) were

coated with silver paint to provide better electrical contact between electrodes and surfaces of the specimens.

Optical microscopy images of the composites were obtained to qualitatively characterize the dispersion and alignment structure of functionalized CNFs. Compression test was performed according to ASTM D695-02 using a MTS testing machine. Electrical resistivity test was conducted based on two-probe method with a high-precision Keithley Digital Multimeter. For nanocomposites that were subjected to electric field, both compression and electrical resistivity were measured in the direction parallel to the aligned CNFs. Four specimens were tested for compressive strength and modulus and three specimens were tested for electrical resistivity at room temperature. Electrical resistance of each specimen was recorded after allowing the resistance value to stabilize for at least one minute. The electrical resistivity was then calculated based on the following equation,

$$\rho = \frac{RA}{t} \tag{1}$$

where R, A, and t are resistance, area of electrodes, and thickness specimen ,respectively.

3.3 Results and Discussion

3.3.1 Dispersion of Functionalized CNFs Before and After Curing

Before investigating the morphology of alignment, it is necessary to inspect the dispersion quality of functionalized CNFs in nanocomposites before and after curing. Figure 11 contains a set of optical images showing the dispersion of 0.5 wt% and 1.5 wt% OCNFs in the resin before (Figure 11 (a) and (c)) and after (Figure 11 (b) and (d)) curing of nanocomposites. Clearly, the OCNFs seem to be uniformly dispersed into the resin and no significant agglomerate is observed after curing. A similar dispersion quality can also be attained in the nanocomposites

containing 0.5 wt% and 1.5 wt% ACNFs before and after curing, as shown in Figure 12. Even though the amount of OCNFs and ACNFs that were incorporated into the resin increased by three times (from 0.5 wt% to 1.5 wt%), evidence of individual OCNFs and ACNFs confirms that uniform OCNF and ACNF dispersion in the resin is achieved before curing and after curing of nanocomposites. This finding is highly interesting since such dispersion quality can be attributed to the novel mixing method and also the carboxylic acid and amine functional groups grafted on the surfaces of OCNFs and ACNFs, respectively. It is believed that the steric repulsion caused by the functional groups among adjacent OCNFs and ACNFs is the primary factor to achieve uniform dispersion.

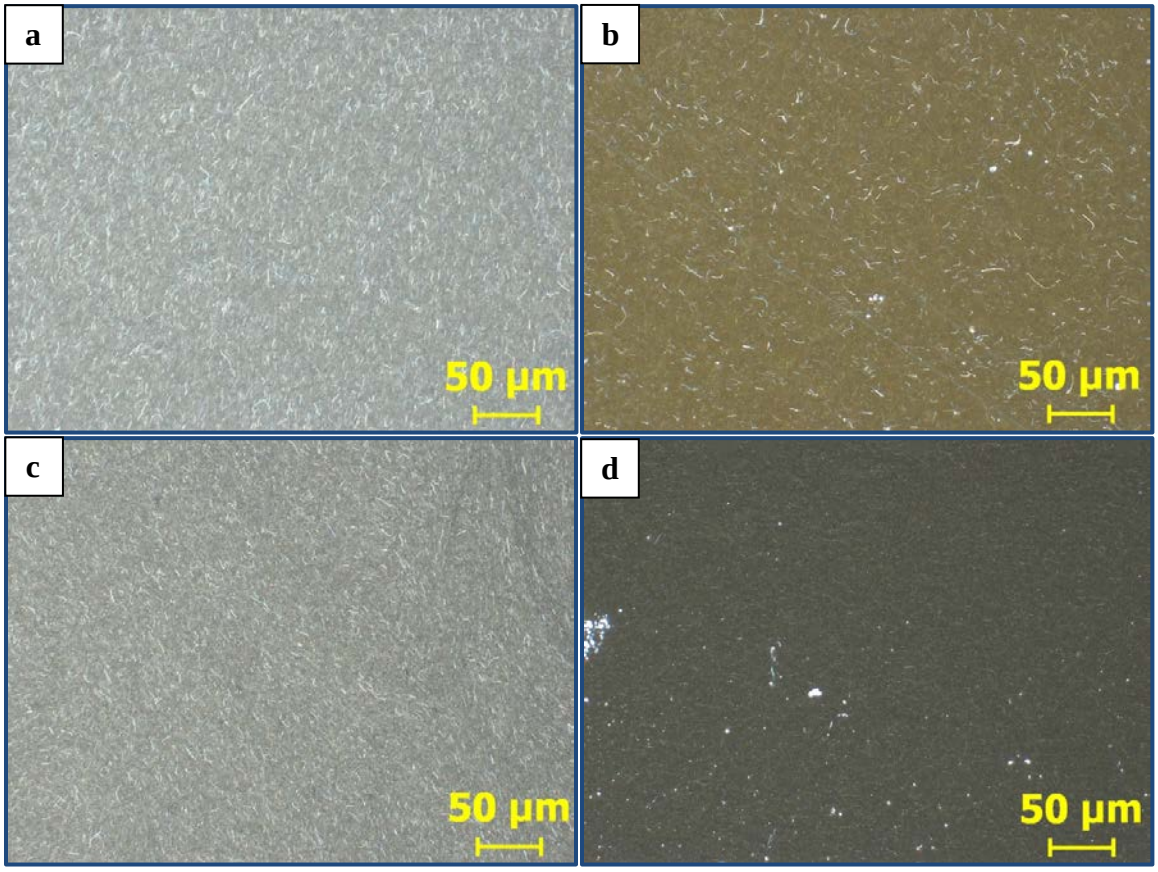

Figure 11. Optical images showing the dispersion of 0.5 wt% OCNFs a) before, b) after curing; and 1.5 wt% OCNFs c) before, d) after curing of nanocomposites. Images were published in [24].

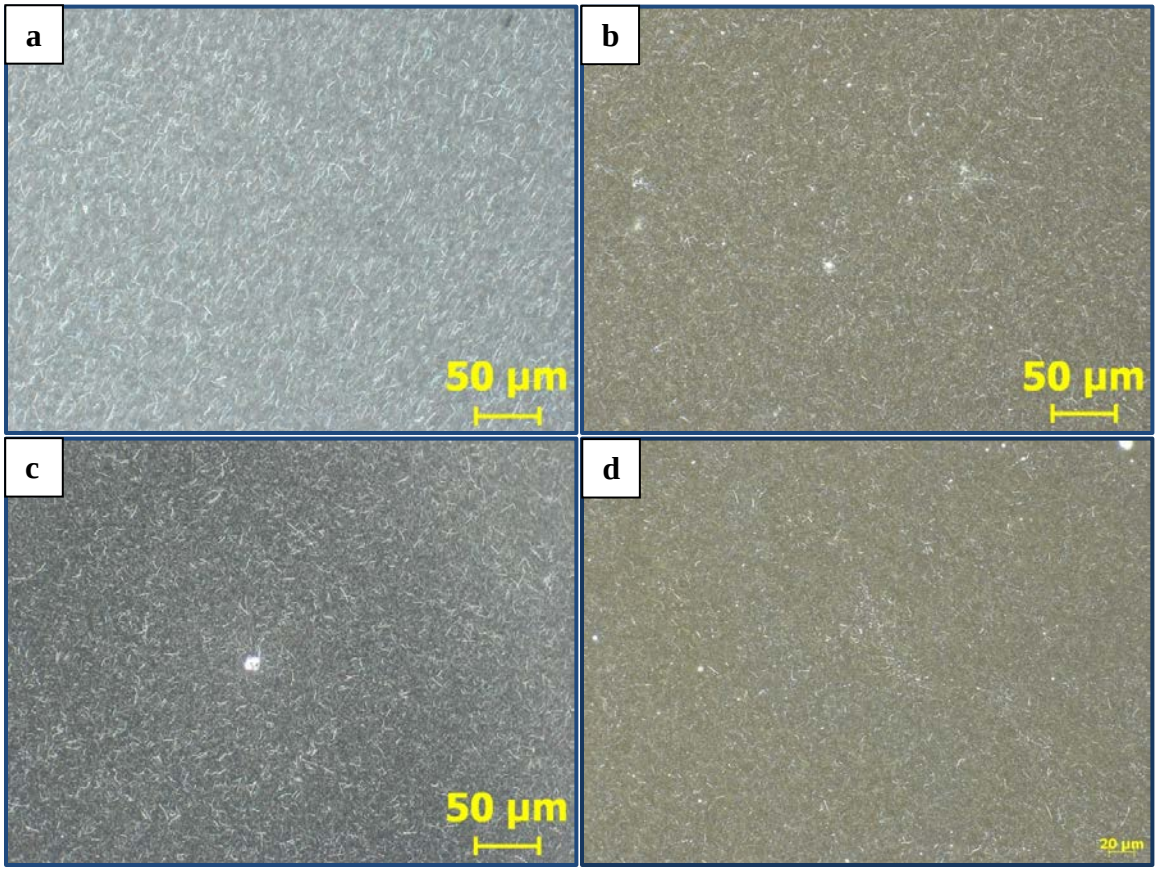

Figure 12. Optical images showing the dispersion of 0.5 wt% ACNFs a) before, b) after curing; and 1.5 wt% ACNFs c) before, d) after curing of nanocomposites. Images were published in [24].

Under optical microscope, the average length of functionalized CNFs is estimated to reduce from 100 µm (length of AR-CNFs provided by vendor) to approximately 10-20 µm due to the chemical functionalization and rigorous mixing processes. Based on this length, the aspect ratio of functionalized CNFs is estimated to be 100-200. In addition, Figure 11 and 12 do not show any significant OCNF and ACNF clusters, which can be attributed to repeated micro-gap shear mixing during homogenization and calendering process.

During the course of the experiments, it is experimentally found that the mixing process involving calendering of resin and functionalized CNFs at concentrations higher than 1.5 wt%

became difficult because the resulting mixture changed from liquid to pasty state. Therefore, the use of three-roll-mill to disperse functionalized CNFs into resin is speculated to be effective until a concentration of approximately 1.5 wt%.

3.3.2 Morphology of Alignment

Figure 13 presents a set of optical images showing the alignment structures of nanocomposites containing 0.5 and 1.5 wt% OCNFs and ACNFs, respectively. From these images which were captured roughly at the mid-section of mechanical test samples, it is clear that the functionalized CNFs aligned in the direction parallel to the electric field and that the alignment morphology varied with respect to the concentration of functionalized CNFs. At a concentration of 0.5 wt%, the formation of thick individual aligned OCNF and ACNF bundles is identified when the samples were subjected to the electric field. When the concentration of functionalized CNFs reached 1.5 wt%, the alignment structure changed to a dense web-like network along with thin aligned OCNF and ACNF bundles. However, the alignment structure at a fixed concentration did not change regardless of the type of functionalized CNFs used, suggesting that the alignment morphology of functionalized CNFs is independent of the functional groups grafted to the CNFs. Since Figure 13 shows only the CNF alignment structure at the mid-section of the samples, it is imperative to investigate the alignment structure at other locations so that continuous aligned functionalized CNF network can be revealed. Therefore, the alignment structure of nanocomposites containing 0.5 wt% OCNFs at five different locations was investigated and is shown in Figure 14. From the optical images in Figure 14, it can be seen that the aligned OCNF network was formed continuously between electrodes and each magnified fragment appears to attain similar alignment morphology.

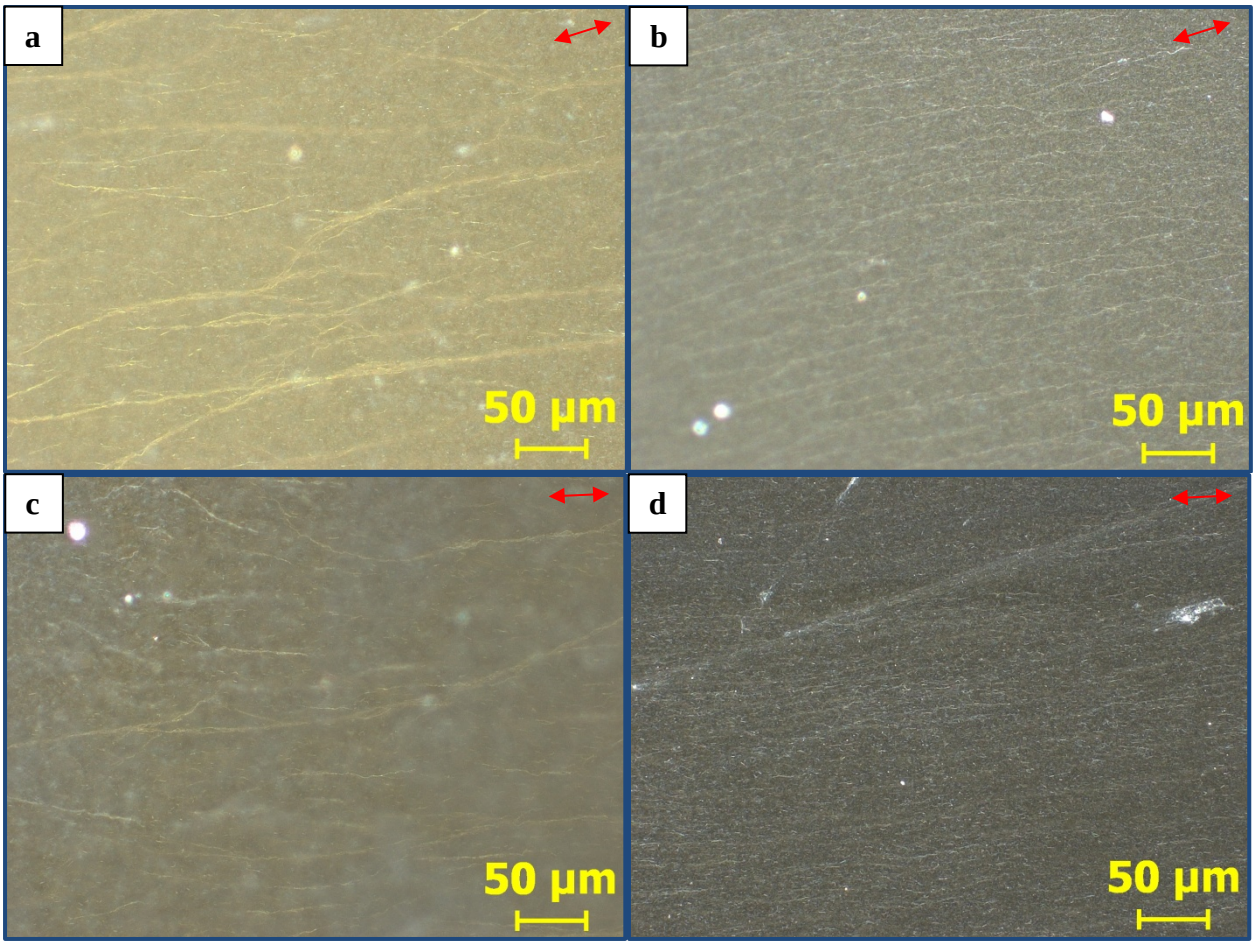

Figure 13. Optical images showing the alignment structure of nanocomposites containing a) 0.5 wt% and b) 1.5 wt% OCNFs; and c) 0.5 wt% and d) 1.5 wt% ACNFs. The red two-headed arrows indicate the direction of applied electric field. Images were published in [24].

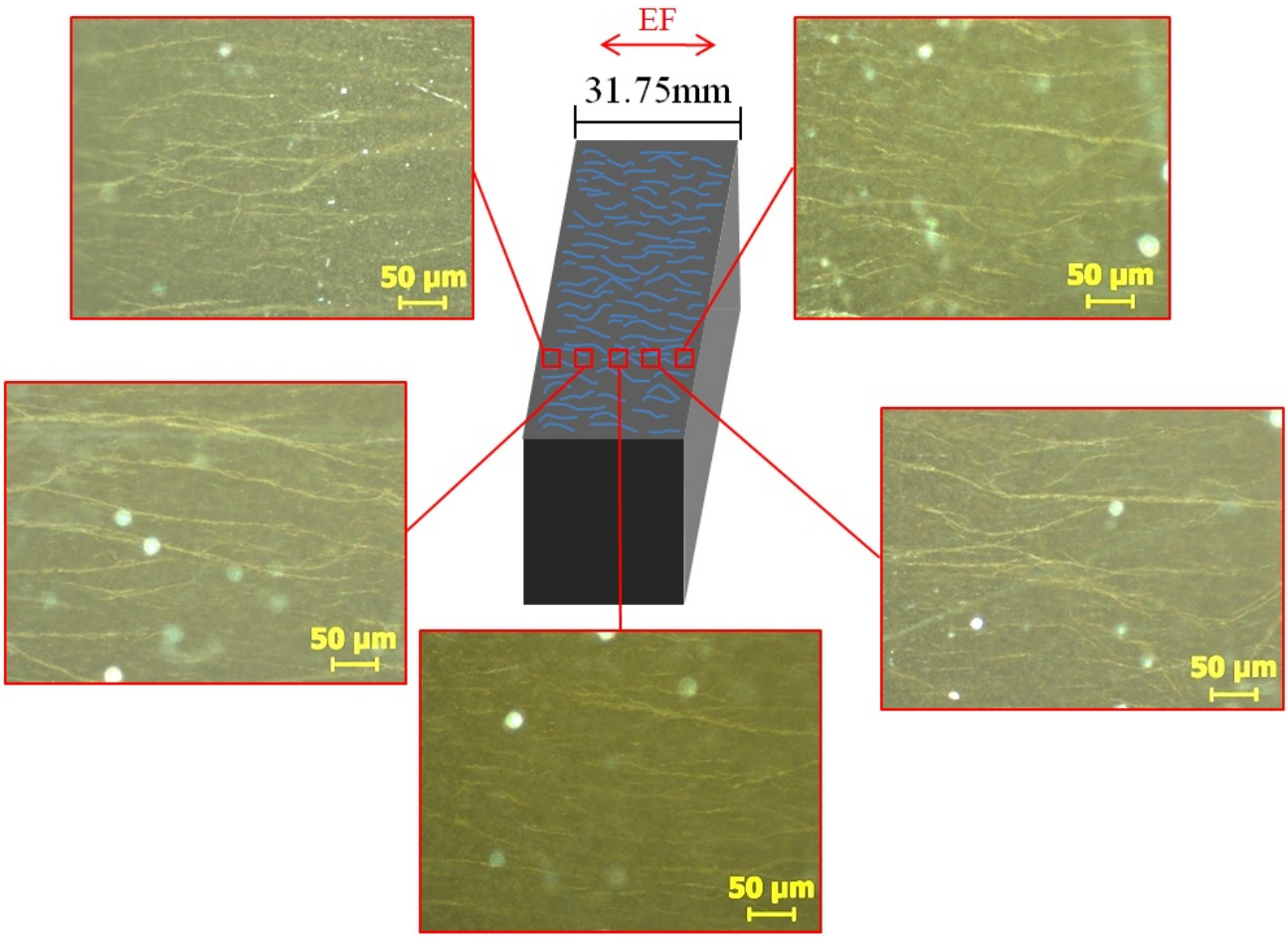

Figure 14. A set of optical images showing the alignment structure of nanocomposites containing 0.5 wt% OCNFs at five different locations. The red two-headed arrow indicates the direction of applied electric field. Images were published in [24].

From the findings shown in Figure 13 and 14, it seems like the applied electric field not just aligned the functionalized CNFs, but also induced certain interaction among OCNFs and ACNFs that caused lateral agglomeration in the aligned bundles. A similar phenomenon was previously observed by Zhu et al. [23] when the authors fabricated nanocomposites containing aligned amine-functionalized CNTs through electric field. Hence, the explanation employed by the authors is referred herein to explain the mechanism of lateral agglomeration in the aligned functionalized CNF bundles. A schematic illustrating the evolution of lateral agglomeration of

functionalized CNFs is presented in Figure 15. When exposed to external electric field, the functionalized CNFs, which can be visualized as micro-size rods, are polarized and experienced electric charge redistribution near the ends of the CNFs. This effect produces dipole moments on the CNFs, which subsequently causes rotary motions and force the CNFs to align in the direction of applied electric field. At the meantime, the redistribution of electric charge near the ends of CNFs also generates new interaction among adjacent CNFs. Because of this new interaction, opposite electric charges that are congregated at the ends of adjacent CNFs attract each other and force the CNFs to close in and laterally agglomerate into micro-scale bundles, which resemble the findings in Figure 13 and 14. In the bundles, it is believed that the CNFs are maintaining certain distance to attain force equilibrium (e.g. electric force and van der Waals force) rather than chemically connected to each other.

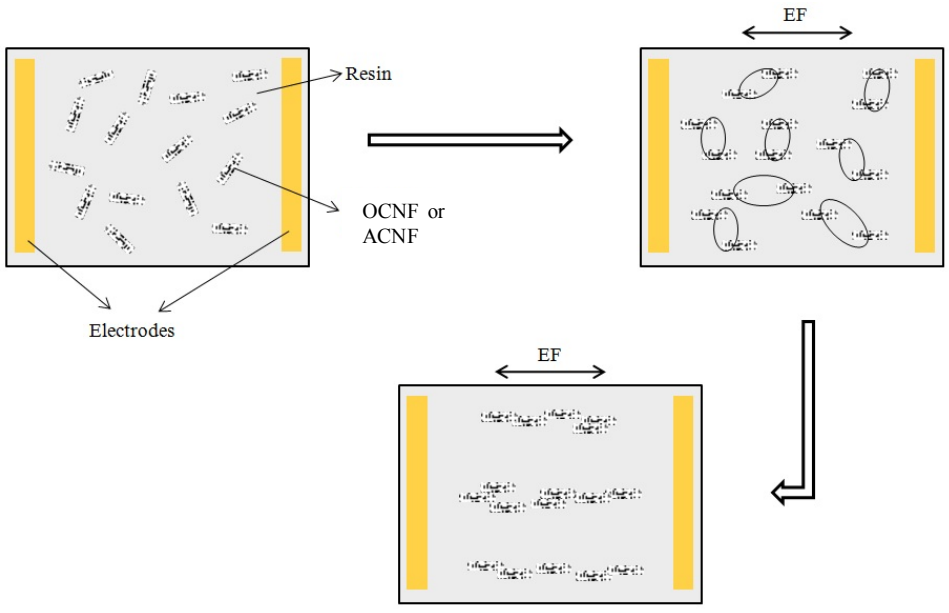

Figure 15. A schematic illustrating the evolution of OCNF or ACNF lateral agglomeration in the aligned bundles when subjected to electric field. The "ellipses" in the top right diagram show the possible interaction between opposite electric charges of adjacent CNF at both ends. The schematic was published in [24].

For the nanocomposites with lower CNF amount per unit volume (e.g. 0.5 wt%), lesser CNF aligned bundles are seen due to limited local interaction among adjacent CNFs that caused lateral agglomeration. As the CNF amount per unit volume of nanocomposites increases (e.g. 1.5 wt%), the local interaction among adjacent CNFs intensifies and thus, more aligned CNF bundles are identified. Furthermore, the explanation for lateral agglomeration in the aligned CNF bundles used herein complements with the earlier hypothesis that suggested the dependency of nanocomposites alignment morphology on the concentration rather than the type of functionalized CNFs used.

3.3.3 Mechanical Properties

Figure 16 and 17 summarize the compressive strength and percentage change of compressive strength, respectively, of nanocomposites fabricated for this study: OCNF/epoxy without electric field (OCNF-NF), OCNF/epoxy with electric field (OCNF-EF), ACNF/epoxy without electric field (ACNF-NF), and ACNF/epoxy with electric field (ACNF-EF). In general, it is clear that the compressive strength of nanocomposites containing OCNFs or ACNFs (regardless of whether or not the nanocomposite was subjected to electric field) is improved with respect to neat resin sample.

When considering the nanocomposites made of only OCNFs, the compressive strength of OCNF-NF and OCNF-EF increased exponentially as a function of OCNF concentration. At a concentration of 0.25 wt%, no significant change in compressive strength is observed between OCNF-EF and OCNF-NF, suggesting that the amount of OCNFs was insufficient to attain reinforcement purpose in spite of the presence of aligned network. Beyond 0.25 wt%, the difference in strength between the two becomes more pronounced for each corresponding concentration. Upon reaching a concentration of 4.5 wt%, a maximum improvement of 6.09%

and 8.36% in compressive strength of OCNF-NF and OCNF-EF, respectively, was achieved in comparison to neat resin sample. A closer comparison between OCNF-NF and OCNF-EF indicates that the strength of OCNF-EF was higher than OCNF-NF throughout the entire range of concentration studied. Due to the presence of aligned network shown earlier, it is valid to presume that OCNF-EF capability of sustaining the compressive load (parallel to the direction of aligned network) is better than OCNF-NF.

In the case of nanocomposites made of only ACNFs, the compressive strength of ACNF-NF and ACNF-EF is found to behave differently in comparison to OCNF-NF and OCNF-EF. Although the compressive strength is higher than neat resin sample, the change in strength of ACNF-NF is rather less obvious as the concentration increased. On the contrary, a gradual increase in compressive strength is observed for ACNF-EF until a concentration of 1.5 wt% and then the change in strength becomes more prominent at higher ACNF concentration. At a concentration of 4.5 wt%, a maximum improvement of 5.09% and 8.76% in compressive strength of ACNF-NF and ACNF-EF, respectively, was achieved in comparison to neat resin sample. Like the trend observed in nanocomposites containing OCNFs, the strength of ACNF-EF is higher than ACNF-NF for all concentration, confirming the positive effect of aligned network parallel to the direction of electric field on the strength of nanocomposites.

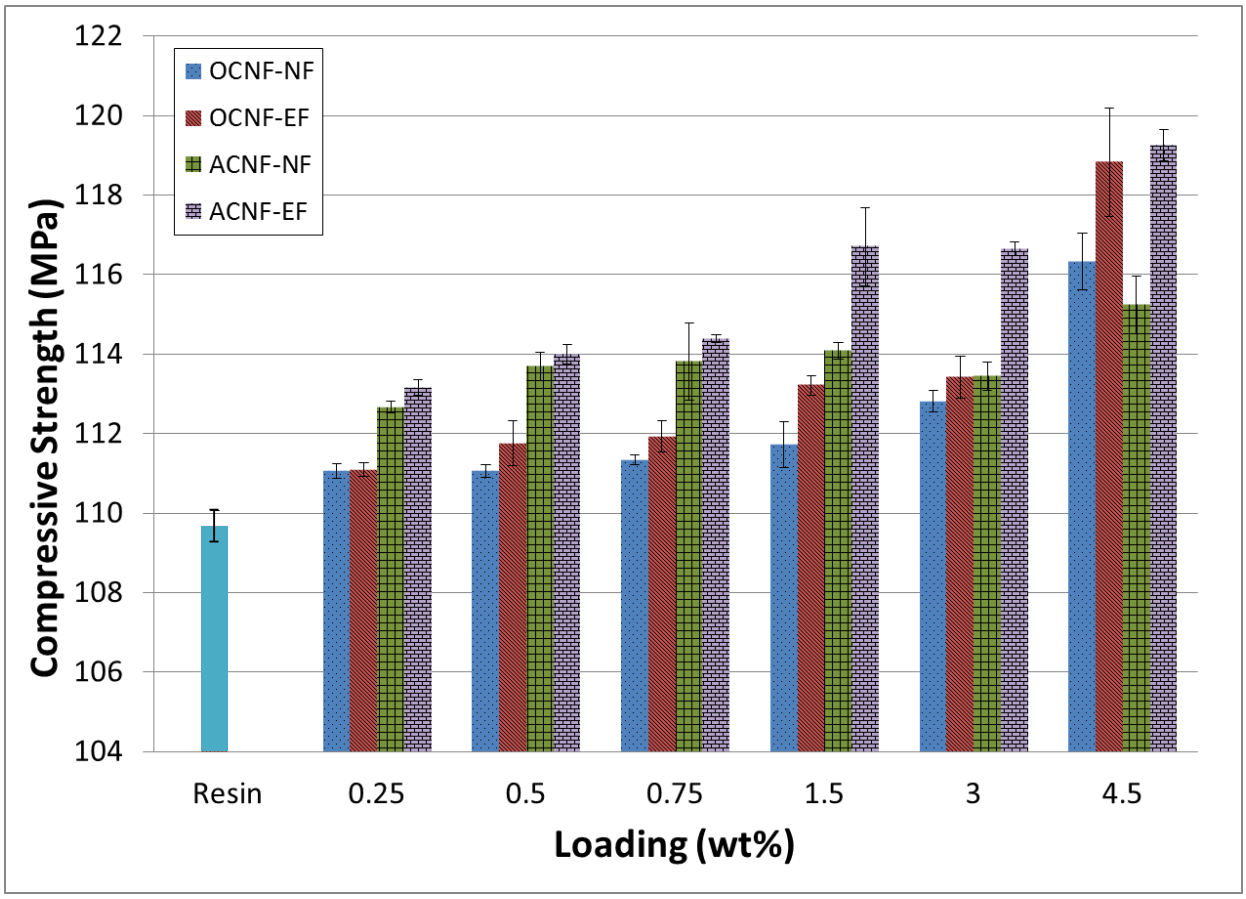

Figure 16. Compressive strength of nanocomposites designated OCNF-NF, OCNF-EF, ACNF-NF, and ACNF-EF. The error bars denote the standard deviation. Results were published in [24].

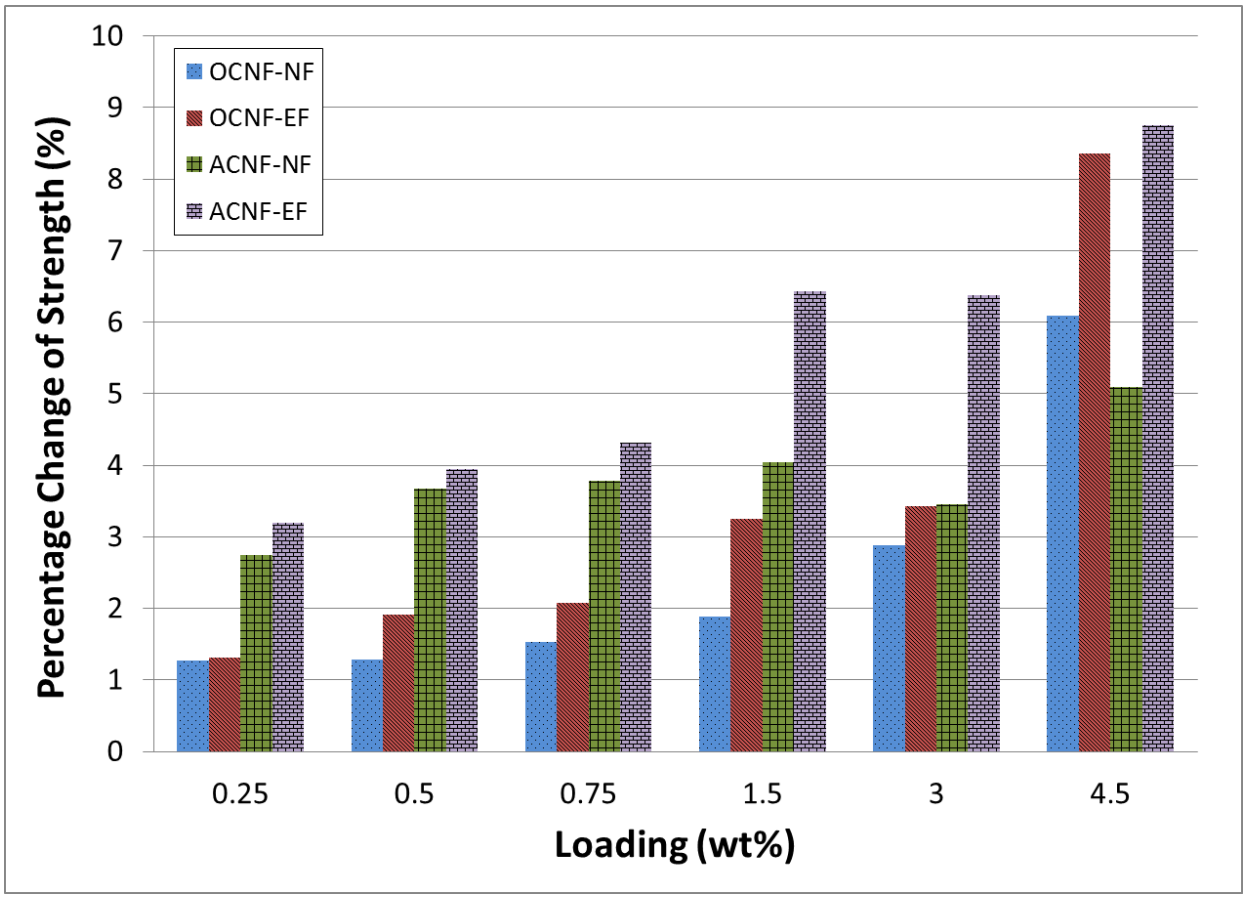

Figure 17. Percentage change of compressive strength of nanocomposites designated OCNF-NF, OCNF-EF, ACNF-NF, and ACNF-EF with respect to neat resin sample. Results were published in [24].

Figure 18 and 19 summarize the compressive modulus and percentage change of compressive modulus, respectively, of nanocomposites containing OCNFs and ACNFs fabricated for this study. Like compressive strength, the compressive modulus of nanocomposites containing OCNFs or ACNFs (regardless of whether the nanocomposite was subjected to electric field) is improved with respect to neat resin sample except for OCNF-NF loaded at 0.25 wt% which shows a negligible change.

Looking at the nanocomposites made of only OCNFs, the compressive modulus of OCNF-NF and OCNF-EF increases approximately linearly as the OCNF concentration increases,

but the linear trend is applicable for OCNF-EF up to 3 wt%. Under this condition, the maximum improvement in compressive modulus of OCNF-NF (+9.04%) and OCNF-EF (+11.37%) occurred at a concentration of 4.5 wt% and 3 wt%, respectively. Nevertheless, the modulus of OCNF-EF is higher than OCNF-NF for all concentrations mainly due to the presence of aligned network. Another interesting finding is that the change in modulus of OCNF-EF is more pronounced than OCNF-NF at 0.25 wt%. This indicates that the aligned network imposed a more influential effect to the enhancement of modulus at such concentration, even though the strength of OCNF-NF and OCNF-EF remained approximately unchanged.

For the nanocomposites containing ACNFs, the compressive modulus of ACNF-NF and ACNF-EF increases at a non-linear trend with respect to ACNF concentration. In contrast to OCNF-NF and OCNF-EF, the maximum improvement in compressive modulus of ACNF-NF (+12.43%) and ACNF-EF (+19%) occurred at a concentration of 3 wt% and 4.5 wt%, respectively. In addition, an interesting observation can be drawn when comparing the percentage change of modulus of ACNF-EF and ACNF-NF at each concentration. From Figure 18, it can be seen that the percentage change of modulus of ACNF-EF is two to three times greater than ACNF-NF, which can be attributed to the combination of enhanced compatibility between ACNFs and the resin and the presence of aligned network in the nanocomposites.

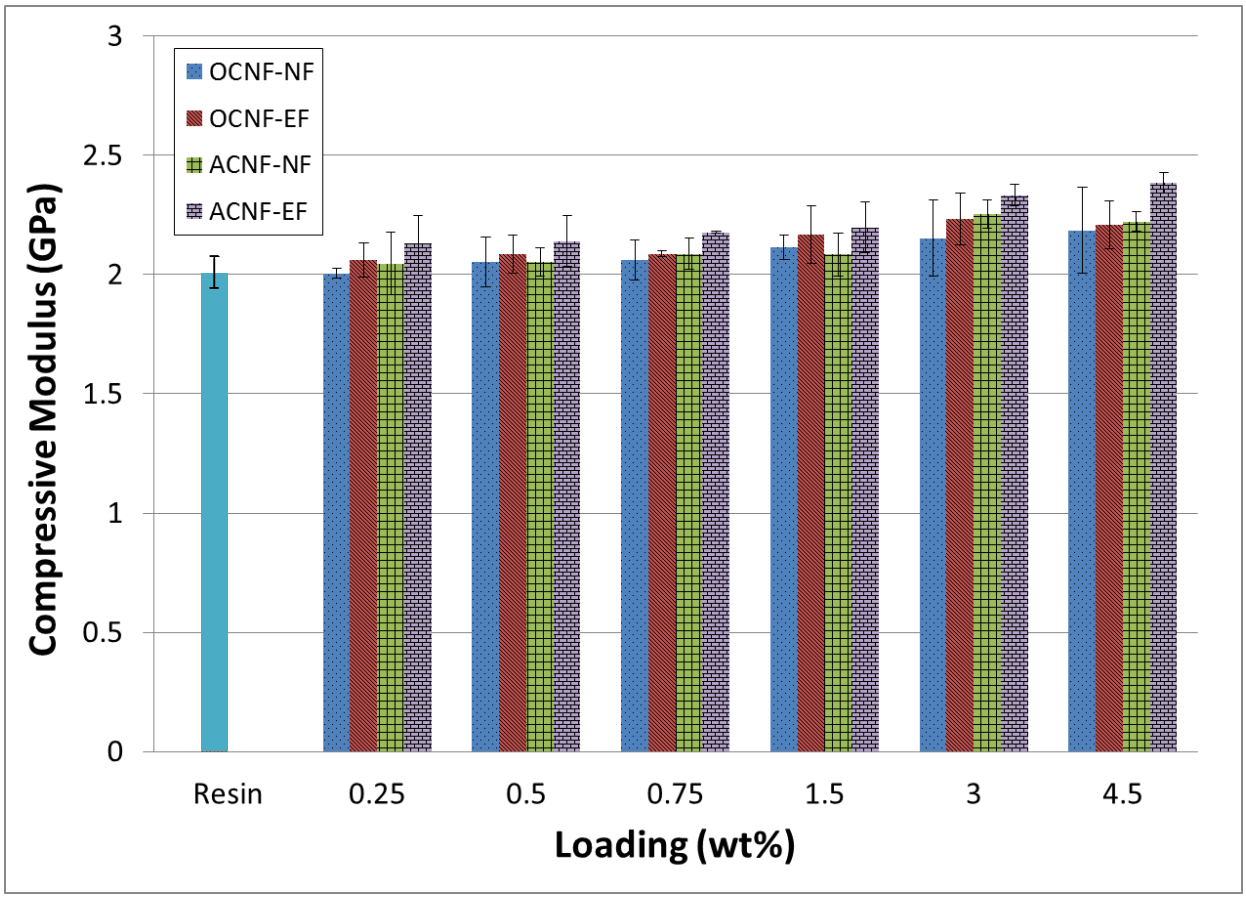

Figure 18. Compressive modulus of nanocomposites designated OCNF-NF, OCNF-EF, ACNF-NF, and ACNF-EF. The error bars denote the standard deviation. Results were published in [24].

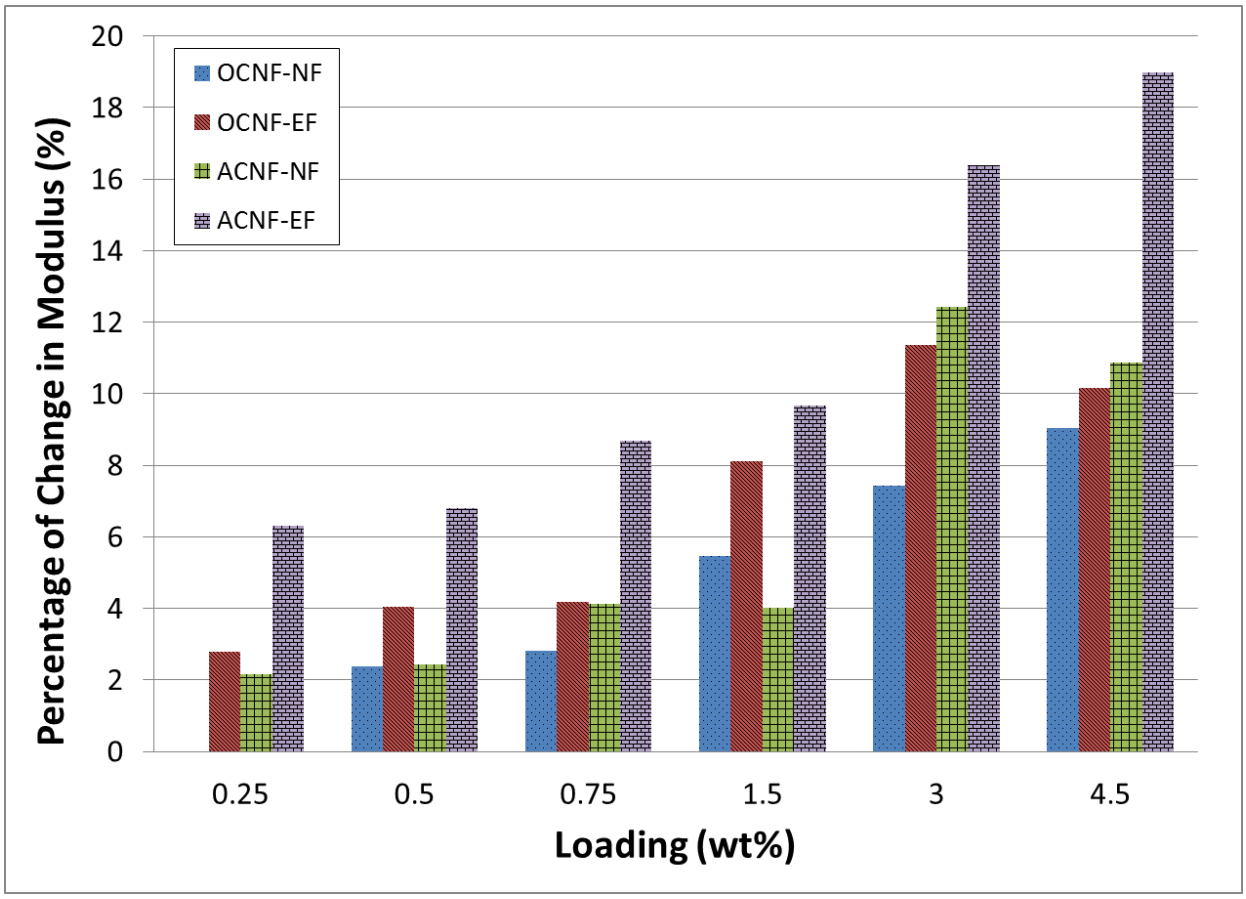

Figure 19. Percentage change of compressive modulus of nanocomposites designated OCNF-NF, OCNF-EF, ACNF-NF, and ACNF-EF with respect to neat resin sample. Results were published in [24].

As mentioned previously, the attachment of amine functional groups on the surface of pristine carbon nanomaterials will help to improve the chemical compatibility between nanomaterials and polymer matrix, thus resulting in better load transfer from polymer matrix to nanomaterials. To validate this hypothesis, both compressive strength and modulus of nanocomposites containing OCNFs and ACNFs are compared. Note that only nanocomposites loaded at 4.5 wt% are considered since the best improvement in compressive strength and modulus occurred at this concentration. Figure 20 shows the comparison of percentage change of compressive strength among OCNF-NF, OCNF-EF, ACNF-NF, and ACNF-EF. Clearly, no

significant difference can be obtained when comparing the strength of OCNF-NF to ACNF-NF and OCNF-EF to ACNF-EF, respectively. Through this comparison, it seems like the strength of nanocomposites does not depend on the type of functionalized CNFs used for the concentrations studied. Figure 21 shows the comparison of percentage change of compressive modulus among OCNF-NF, OCNF-EF, ACNF-NF, and ACNF-EF. On the contrary to strength, the difference is more pronounced when comparing the modulus of OCNF-NF to ACNF-NF and OCNF-EF to ACNF-EF, respectively, especially in the latter comparison. It is believed that the combination of amine functional group and aligned network is the key factor for such difference in modulus, causing a 9% difference between OCNF-EF and ACNF-EF. This finding also indicates that the modulus of nanocomposites is dependent on the type of functionalized CNFs used.

Based on these comparisons, one can satisfactorily presume that the coupling of amine functional group grafted on ACNFs and aligned network will result in nanocomposite with better modulus and hence better load transfer from the matrix to CNFs. As such, it is possible that if higher concentration of functionalized CNFs can be incorporated and selectively aligned using other methods, nanocomposites with higher strength and modulus along the aligned direction can be achieved provided that uniform dispersion of CNFs is preserved.

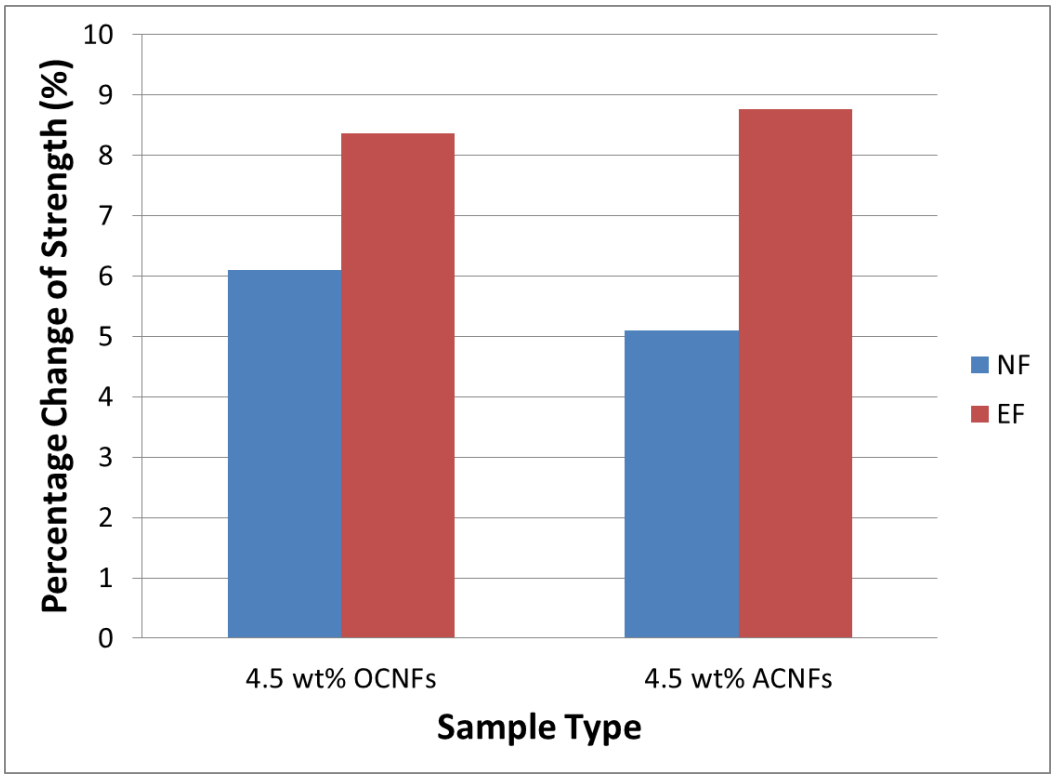

Figure 20. Comparison in percentage change of compressive strength between OCNF- and ACNF-enhanced nanocomposites at 4.5 wt% with respect to neat resin sample. Results were published in [24].

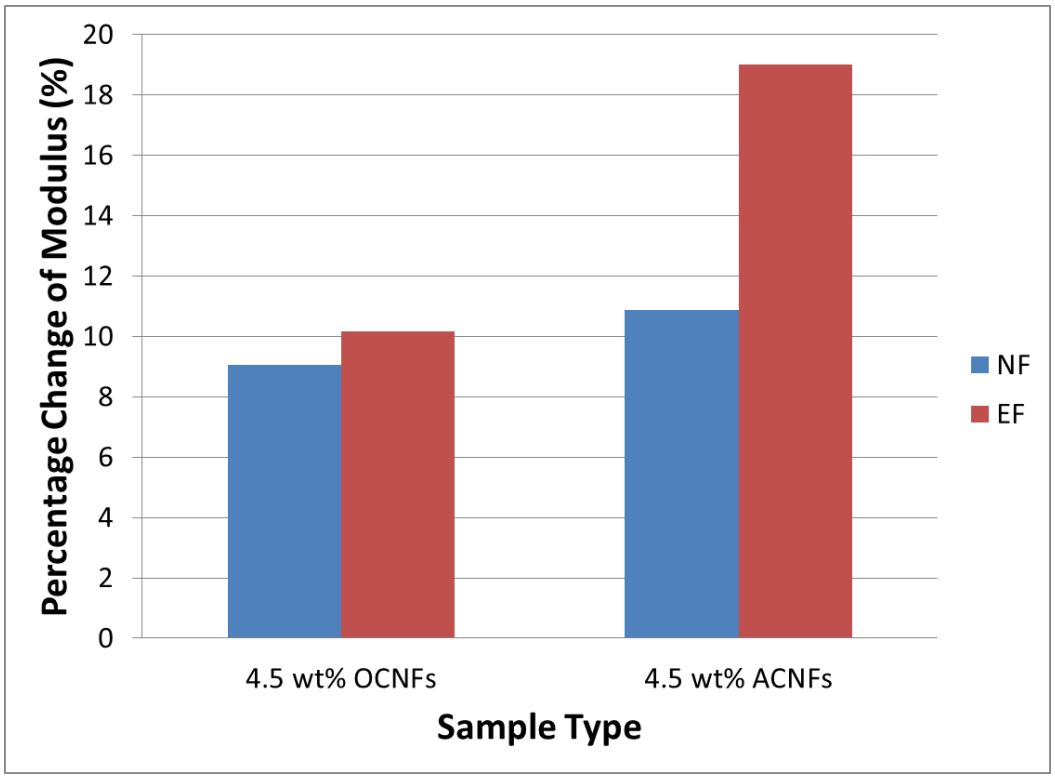

Figure 21. Comparison in percentage change of compressive modulus between OCNF- and ACNF-enhanced nanocomposites at 4.5 wt% with respect to neat resin sample. Results were published in [24].

3.3.4 Electrical Properties

Figure 22 shows the electrical resistivity of OCNF-NF and OCNF-EF. Note that the electrical resistivity of neat epoxy resin was obtained from literature [66]. In the case of OCNF-NF, the addition of 0.25 wt% OCNFs reduced the electrical resistivity of nanocomposites to 10^9 Ω.cm range; however, further increase in OCNF concentration did not impose a significant change in electrical resistivity. This can be possibly due to the failure of OCNF-NF in reaching electrical resistivity percolation threshold upon the addition of 4.5 wt% OCNFs to the neat resin. In fact, Prasse et al. [68] reported that the electrical resistivity percolation threshold would not take place unless 6 wt% of CNFs is incorporated into the nanocomposites without the application of electric field. Furthermore, studies performed by Ahn et al. [67] and Lafdi et al. [66]

demonstrated that the aspect ratio and oxygen content of functionalized CNFs are the main factors affecting the electrical conductivity percolation threshold. In particular, the lower the CNF aspect ratio, the higher the amount of functionalized CNFs is required to reach percolation threshold; the higher the oxygen content, the higher the electrical resistivity of functionalized CNFs. Based on these findings, it is believed that the resistivity percolation threshold of OCNF-NF would occur at a concentration higher than 6 wt% because of the low aspect ratio and increased oxygen content of OCNFs as a result of chemical functionalization.

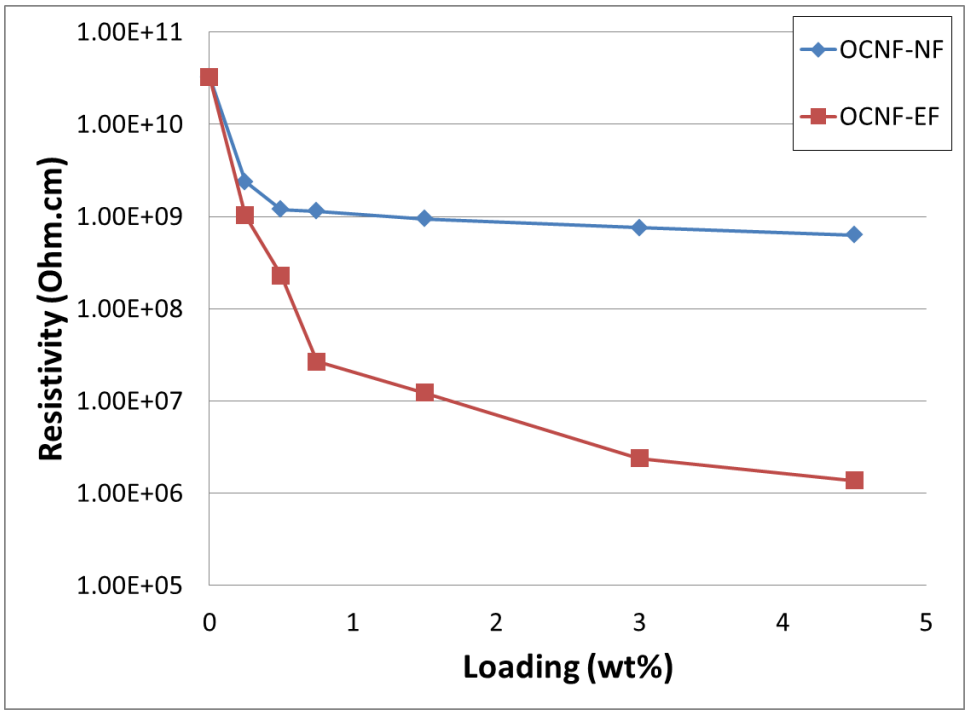

Figure 22. Electrical resistivity of OCNF-NF and OCNF-EF as a function of OCNF concentration. Results were published in [24].

Considering OCNF-EF, the electrical resistivity (measured parallel to the direction of electric field) also reduced to 10^9 Ω.cm range at a concentration of 0.25 wt% but with slightly lower value. As the OCNF concentration increased, the reduction in electrical resistivity became apparent and percolation threshold was observed to occur at around 0.75 wt%. Subsequently, the

resistivity of nanocomposites loaded at 1.5 wt% reduced to 10^7 Ω.cm range and continued to decrease to 10^6 Ω.cm range at a concentration of 4.5 wt%. Even though the concentration increased by three fold from 1.5 wt% to 4.5 wt%, the change of resistivity was not significant, indicating that further increase in OCNF concentration will not significantly alter the resistivity of OCNF-EF. Overall, a reduction of four orders of magnitude in electrical resistivity is achieved by fabricating nanocomposites with 4.5 wt% OCNFs aligned in the direction of electric field.

Figure 23 reports the electrical resistivity of ACNF-NF and ACNF-EF. For ACNF-NF, the addition of 0.25 wt% ACNFs also reduced the electrical resistivity of nanocomposites to 10^9 Ω.cm range. Like the trend of OCNF-NF, further increase in ACNF concentration did not alter the electrical resistivity of ACNF-NF considerably. By taking a closer look at the resistivity values of OCNF-NF and ACNF-NF at each concentration, it is found that ACNF-NF was slightly less resistive than OCNF-NF. Nevertheless, because of the low aspect ratio and increased oxygen content of ACNFs as a result of chemical functionalization, it is also believed that the resistivity percolation threshold of ACNF-NF would occur at a concentration greater than 6 wt%. On the other hand, the electrical resistivity (measured parallel to the direction of electric field) of ACNF-EF decreased to a value slightly below10^9 Ω.cm at a concentration of 0.25 wt%. Then, the resistivity of nanocomposites loaded at 1.5 wt% dropped to 10^6 Ω.cm range and continued to decrease to a value slightly lower than 10^6 Ω.cm at a concentration of 4.5 wt%. Coincidentally, the percolation threshold for ACNF-EF is also found to occur at approximately 0.75 wt% and further increase in ACNF concentration (from 1.5 wt% to 4.5 wt%) did not cause a significant change in resistivity. Although ACNFs were used to fabricate nanocomposites, the electrical test results showed that a reduction of four orders of magnitude in resistivity was also achievable by aligning ACNFs with electric field.

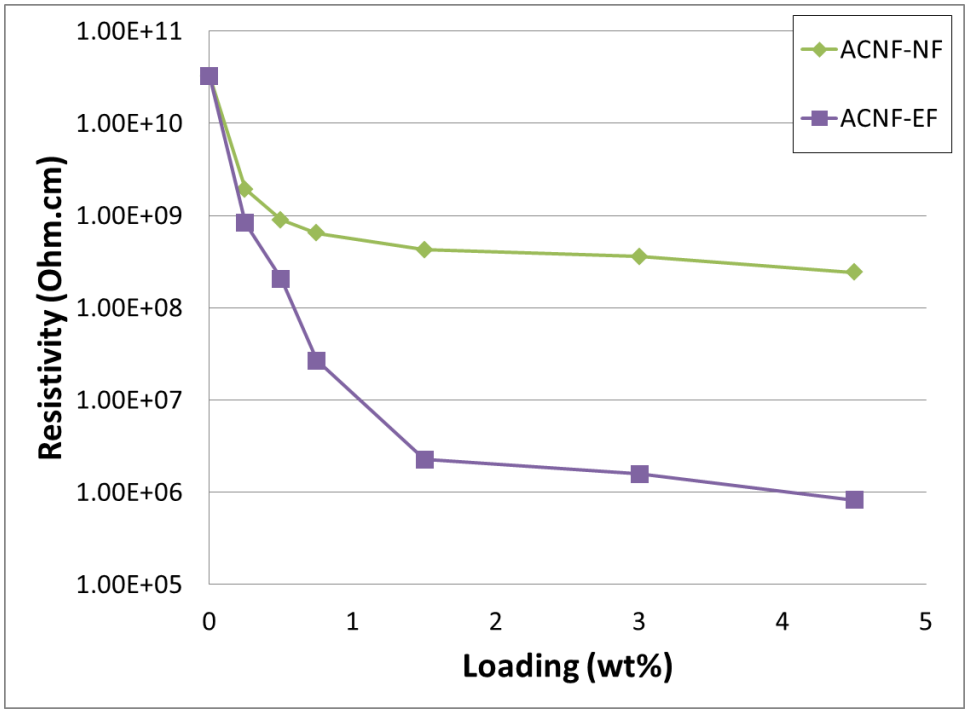

Figure 23. Electrical resistivity of ACNF-NF and ACNF-EF as a function of ACNF concentration. Results were published in [24].

The resistivity trend of OCNF-EF and ACNF-EF shown in this study is similar to the results (the electrical resistivity of nanocomposites that was measured parallel to the direction of electric field) reported by Prasse et al. [68] except with higher resistivity values at each concentration, which can be attributed to difference in CNF type, lower aspect ratio, and increased oxygen content of functionalized CNFs. Although the resistivity of ACNF-EF loaded at 1.5 wt% was approximately half an order of magnitude lower than OCNF-EF loaded at 1.5 wt%, both nanocompsites saturated at similar resistivity value at a concentration of 4.5 wt%. Additionally, it is found that the use of electric field to prepare OCNF-EF and ACNF-EF with aligned network parallel to the direction of electric field was beneficial until 1.5 wt%. Beyond this concentration, no apparent benefit in resistivity can be expected for such nanocomposites.

3.4 Summary and Conclusions

In this chapter, processing and characterization of nanocomposites with improved mechanical and electrical properties in a preferential direction —containing aligned functionalized CNF network— was presented. All properties of nanocomposites with aligned CNF network were measured parallel to the CNF alignment direction. Optical images revealed the evidence of uniform distribution and alignment of functionalized CNFs in the direction of electric field. Even though different chemical functional groups were grafted to the CNFs, it was found that the alignment morphology of the functionalized CNFs was independent of the functional groups studied.

At a concentration of 4.5 wt%, compressive strength of the nanocomposites with aligned OCNF and ACNF network attained similar values, which were 8.36% and 8.76% higher than neat resin sample, respectively. In contrast to strength, compressive modulus of the nanocomposite with aligned ACNFs was 9% higher than the nanocomposite with aligned OCNFs at the same concentration (4.5 wt%), resulting in an overall increase of 19% with respect to neat resin sample. These results suggest that the strength of nanocomposites is independent of the type of functionalized CNFs whereas the modulus of nanocomposites is dependent on the type of functionalized CNFs. Compatibility between amine functional groups grafted to the CNFs and the epoxy matrix provided better load transfer from the matrix to CNFs, resulting in a better improvement in modulus. When compared to neat resin sample, a reduction of four orders of magnitude in electrical resistivity was observed for the nanocomposites containing aligned OCNFs and ACNFs.

Due to their unique properties, cost effectiveness, and ease of processing, CNFs are attractive candidates for manufacturing hierarchical composites with improved properties and multi-functionality. Therefore, understanding the fundamental alignment behavior of

functionalized CNFs in the polymer matrix and properties of final nanocomposites provides a thoughtful insight before alignment of nanomaterials can be featured to manufacture hierarchical composites.

CHAPTER 4

PROCESSING AND CHARACTERIZATION OF HIERARCHICAL COMPOSITES USING FUNCTIONALIZED CARBON NANOFIBERS

4.1 Introduction

Fiber-reinforced polymeric composites (FPRCs) are well known for their excellent in-plane strength-to-weight and stiffness-to-weight properties, which are dominated by the 1-D (unidirectional) or 2-D (plain or satin weave) fiber architectures with high strength and modulus. Nevertheless, FRPCs suffer from poor interlaminar fracture toughness and shear strength due to the presence of weak link between FRPC plies that is dominated mainly by polymer matrix properties. For this reason, scientists and engineers have been desperately seeking for a feasible solution to address this shortcoming. Several possible solutions to this problem include the development of through-the-thickness stitching, z-pinning, and 3D braided fibers [25]. These approaches, however, yield composite parts exhibiting weaker in-plane strength and stiffness due to fiber displacement/misalignment and low fiber volume fraction.

As nanotechnology research rapidly evolves within material science and engineering, carbon nanomaterials possessing fascinating features such low density, high strength and modulus, and high electrical and thermal conductivity arise as a potential candidate to better enhance FRPCs performance. Such materials have undoubtedly triggered tremendous interest within the research community to develop feasible manufacturing processes that enable the creation of new class nano-engineered fiber-reinforced composites –hierarchical composites– with improved properties and multi-functionality. By prevailing over the aforementioned manufacturing challenges, researchers have shown that the interlaminar shear strength, mode-I fracture toughness, out-of-plane electrical and thermal properties of hierarchical composites can be significantly improved with respect to traditional FRPCs [15]. In addition, the conductive

network formed by the nanomaterials within hierarchical composites can be used to detect micro-cracks or flaws unseen by naked eyes [26]. To date, there are five main approaches to manufacture hierarchical composites: (1) injection of nanomaterial-polymer mixture into the preform, (2) direct placement of nanomaterials between laminates, (3) growth of nanomaterials on reinforcement layer through chemical vapor deposition (CVD), (4) deposition of nanomaterials onto the reinforcement layer, and (5) coating reinforcement fibers with sizing agent containing well-dispersed nanomaterials. While successfully performed at the laboratory scale, some of these methods are not cost-effective and are limited by chemical incompatibility and concentration needed for reinforcement purpose.

In this chapter, two separate studies will be presented. The first study focuses on fabrication and electrical properties of hierarchical composites made of functionalized CNF/glass fiber layers. The hybrid layers were fabricated by a simple filtration process, assembled, and cured with epoxy resin at elevated temperature. The second study addresses the synthesis and characterization of functionalized CNF/glass fiber assembly demonstrating that functionalized CNF entangled network can be used to join glass fiber layers in the absence of polymer matrix.

4.2 Experimental Section

4.2.1 Materials

As-received CNFs (AR-CNFs) used in this study were Pyrograf PR-24-XT-PS from Applied Sciences, Inc. According to the vendor, the CNFs' average diameter and length were in the range of 60-150 nm and 30-100 μm, respectively, and iron content is approximately 14,000 ppm. Commercially available plain-weave glass fiber layers (Composites One LLC) were used as the base material to synthesize functionalized CNF/glass fiber layers and assembly. The two-part epoxy system used were diglycidyl ether of bisphenol F epoxy resin (EPON 862) and

diethyl toluene diamine curing agent (EPIKURE-W) from HEXION Specialty Chemicals. The components were mixed in a ratio of 100 parts resin to 26.4 parts curing agent by weight. All chemicals were obtained from Fisher Scientific and used as-received.

4.2.2 Functionalization of Carbon Nanofibers

To obtain carboxylic acid-functionalized CNFs (OCNFs), 2.5 g of AR-CNFs were first mixed with 500 mL of nitric acid in a round bottom flask and sonicated in a water bath for 20 minutes at high power (170 W). The solution was then refluxed and stirred at 260 °C for 2 hours. After that, the OCNFs were filtered out using 0.45 μm pore size nylon membrane, rinsed continuously with reverse osmosis water, acetone, and ultrapure deionized water until chemically neutral and dried in an oven at 100 °C with vacuum overnight. The OCNFs were then hand grinded and kept in a desiccator until further use. Note that the OCNFs were functionalized for only 2 hours in order to preserve the length of CNFs and minimize CNF structural damage [95].

4.2.3 Hierarchical Composites Made of CNF/Glass Fiber Layers

4.2.3.1 Synthesis of CNF/Glass Fiber Layers

The OCNFs were incorporated onto the glass fiber layers (5.08 cm x 5.08 cm) through simple vacuum filtration method (Figure 24). The weight of glass fiber layer was measured before subjecting to filtration process. The OCNFs were initially mixed with ultrapure water at concentration of 0.35 mg/mL and tip-sonicated in a water bath for 10 minutes at medium power. The OCNF aqueous solution (200 mL) was added to the glass fiber layer drop-wise using a pipette. Note that each side of the glass fiber layer was filtered with half portion of the prepared OCNF aqueous solution. The layer was then dried in the air for 12 hours after completing the addition of OCNF solution on each side of the glass fiber layer. After completing the filtration

and drying processes, the weight of the OCNF-coated glass fiber layer was measured to estimate the amount of OCNFs added to the layer. Optical microscope was used to qualitatively characterize the distribution of OCNFs on the OCNF/glass fiber layer.

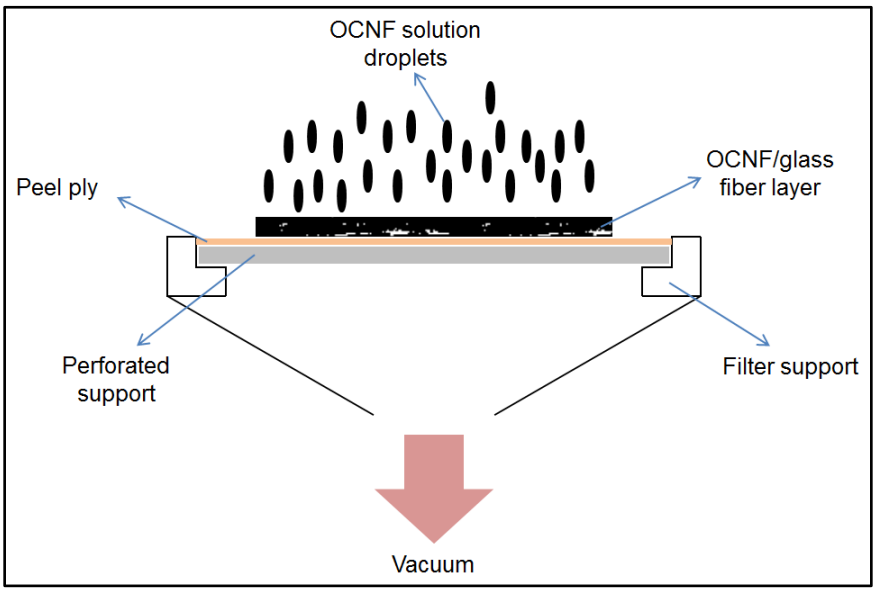

Figure 24. A schematic illustrating the incorporation OCNFs onto glass fiber layer through vacuum filtration method.

4.2.3.2 Hierarchical Composites Manufacturing

In this study, three types of panels with stacking sequence of $[0]_{12}$ were manufactured, shown in Table 3. The first panel (labeled as CNF-GF/EP) was made by curing OCNF/glass fiber layers with neat epoxy resin while the second panel (labeled as CNF-GF/CNF-EP) was manufactured by curing OCNF/glass fiber layers with OCNF-toughened epoxy resin. The third panel (labeled as CFP) was manufactured using as-received carbon fiber layers (Hexcel PAN-based IM7 6K) and neat epoxy resin for comparison purpose. All panels were manufacture through vacuum assisted resin transfer molding (VARTM) process (Figure 25) and cured at 121 °C for 8 hours. To prepare OCNF-toughened epoxy resin for manufacturing CNF-GF/CNF-EP, OCNFs (1 wt% with respect to epoxy resin) were first tip-sonicated with acetone for 15 minutes.

Then, diluted epoxy resin (EPON 862 and acetone) was slowly added to the OCNF/acetone mixture and the whole blend was continuously sonicated for additional 15 minutes. The blend was placed on a hot plate at 110°C to evaporate the acetone. Subsequently, the OCNF/epoxy mixture was cooled to room temperature and subjected to a calendering process using a three-roll-mill. Afterward, adequate amount of curing agent (EPICURE W) was added to the OCNF/epoxy mixture at weight ratio of 100:26.4 and the whole mixture was mixed using a centrifugal mixer.

TABLE 3

DESCRIPTION OF PANELS MANUFACTURED AND CHARACTERIZED

	Layer Type	**OCNFs in Resin**	**Designation**
1	OCNF/Glass Fiber	-	CNF-GF/EP
2	OCNF/Glass Fiber	1 wt%	CNF-GF/CNF-EP
3	Carbon Fiber	-	CFP

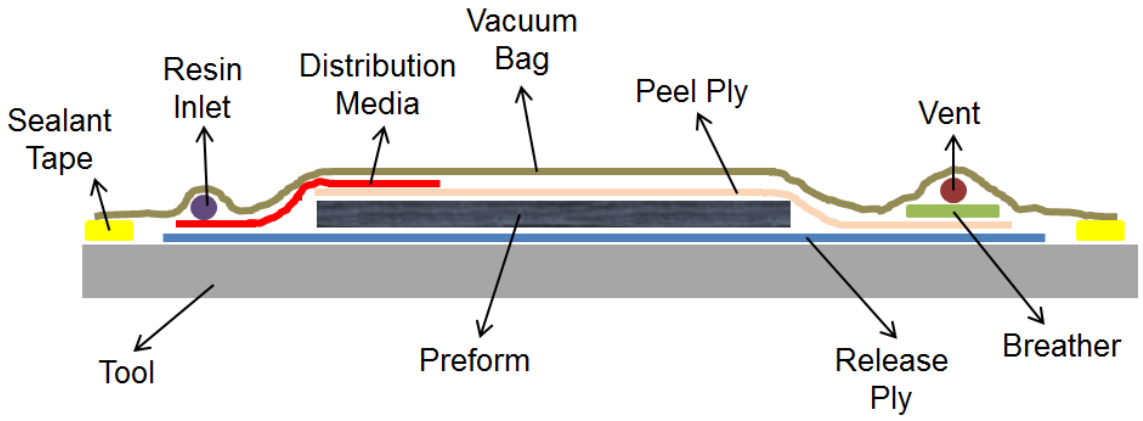

Figure 25. Schematic of Vacuum-Assisted Resin Transfer Molding (VARTM) setup.

4.2.3.3 Preparation and Characterization of Test Specimens

All test specimens were machined using a precision cutting machine. A continuous coolant supply was used during cutting to prevent overheating of the samples. Three 12.7 mm x 12.7 mm specimens were machined and polished from each panel for in-plane and out-of-plane electrical conductivity test. Each specimen was coated with silver paint to ensure good contact and the test was performed according to a two-probe method. The in-plane electrical conductivity of each sample was calculated by:

$$\sigma_{in} = \frac{L}{RA} \tag{2}$$

where R, A, and L are resistance, area (thickness × width) of electrodes, and length of each specimen, respectively. The out-of-plane electrical conductivity of each was calculated using:

$$\sigma_{out} = \frac{t}{RA} \tag{3}$$

where R, A, and L are resistance, area (length × width) of electrodes, and thickness of each specimen, respectively.

4.2.4 CNF/Glass Fiber Assembly

A solution filtration setup was used to join two as-received plain-weave glass fiber layers (5.08 cm x 5.08 cm) with OCNFs, as illustrated in the top schematic Figure 26. The OCNF aqueous solution (0.35 mg/mL) was prepared by tip-sonicating OCNFs with ultrapure deionized water at medium power for 10 minutes. To prepare OCNF/glass fiber assembly, a nylon membrane (0.45 μm pore size) was first coated with 50 mL of OCNF solution (over an area of the dimensions of glass fiber layers). Afterward, the first glass fiber layer was placed on the OCNF-coated area and half of the layer was covered with aluminum foil to prevent OCNF coating. Then, additional 250 mL of OCNF solution was slowly added to the first glass fiber

layer. Subsequently, the second glass fiber layer was placed on top of the first glass fiber layer and filtered with additional 300 mL of OCNF solution. Note that the OCNF solution was added to membrane and glass fiber layers drop-wise using a pipette. Upon completing the filtration, the OCNF/glass fiber assembly was rinsed with acetone and dried in air with vacuum overnight.

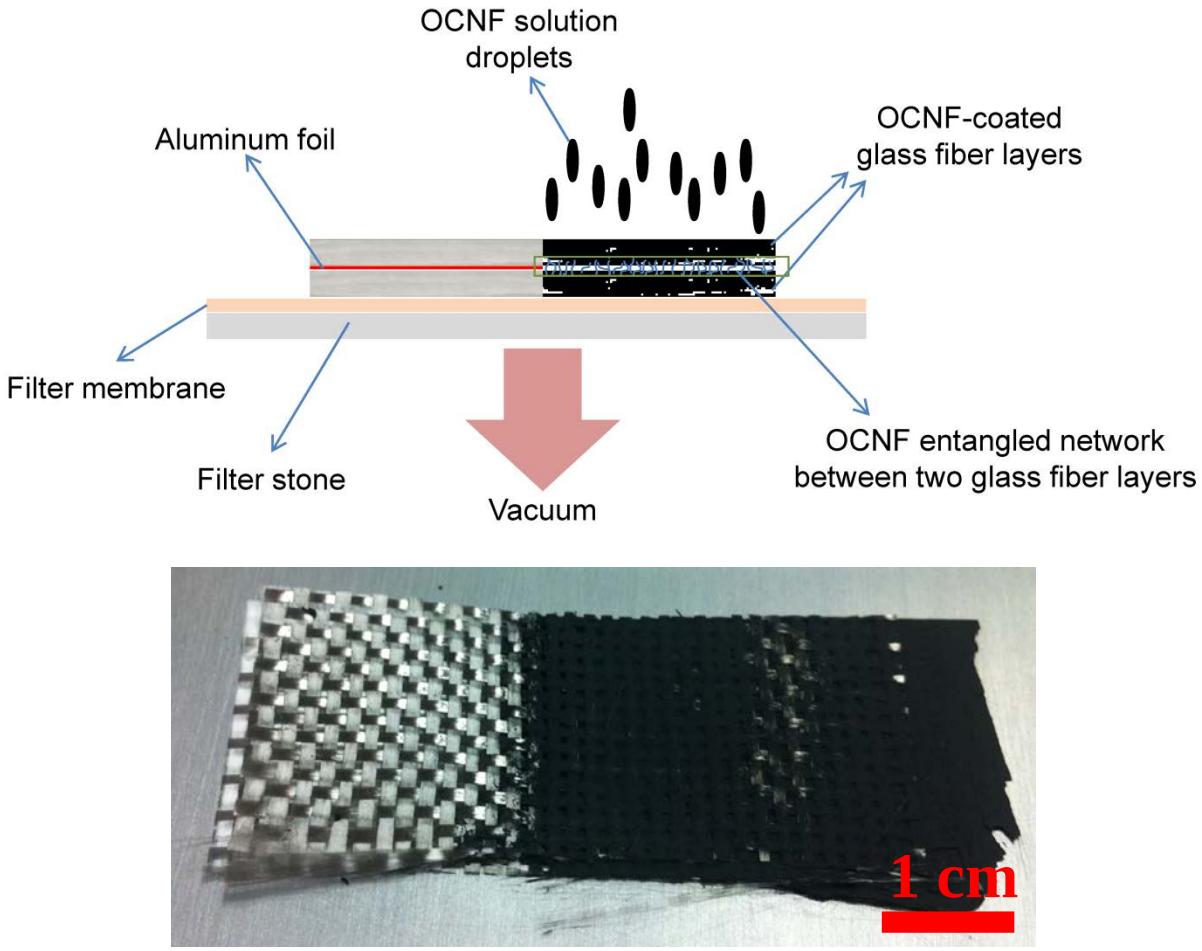

Figure 26. Experimental setup for preparing sample (top) and actual photograph (bottom) of OCNF/glass fiber assembly. Images were published in [95].

The amount of OCNFs added to the OCNF/glass fiber assembly was approximately 154 mg and an actual photograph of OCNF/glass fiber assembly is presented at the bottom of Figure 26. After removing the aluminum foil, the OCNF/glass fiber assembly was cut to obtain a thin

strip of approximately 9 mm x 50.8 mm. The specimen was then tested using a tensile test instrument. The cross-section of the specimen was imaged using optical microscope and field emission scanning electron microscope before and after testing.

4.3 Results and Discussions

4.3.1 Hierarchical Composites with CNF/Glass Fiber Layers

Figure 27 shows the photograph of as-received glass fiber layer and glass fiber layer coated with OCNFs. This image clearly shows that OCNFs were successfully incorporated onto the glass fiber layer through simple vacuum filtration process and the distribution of OCNFs seems to be uniform macroscopically. The OCNF/glass fiber layer was further characterized using optical microscope to investigate the distribution of OCNFs at fiber tow level. From Figure 28(a), it can be observed that the OCNFs are uniformly distributed within a single fiber tow without inducing significant OCNF agglomerate. Intriguingly, such finding was not seen when OCNFs were deposited onto carbon fiber layer (Figure 28(b)). Previously, Rodriguez [94] successfully incorporated OCNFs onto carbon fiber layer through electrophoretic deposition and reported that the distribution of OCNFs on carbon fiber layer was not uniform. Instead, spot-wise OCNF distribution was observed within a single carbon fiber tow and some areas appeared to be free of OCNF deposition. It is believed that the distribution of OCNFs on glass and carbon fiber layer, respectively, is affected by several possible factors including the methodology used to incorporate OCNFs onto each layer, OCNF functionalization time, preparation of OCNF aqueous solution, flatness of the layer during processing, and the layer's sizing chemistry.

Another interesting finding is the amount of OCNFs added to glass and carbon fiber layer, respectively. When OCNFs were deposited onto carbon fiber layer through EPD, the amount of OCNFs added to the layer was 31.61 mg, which was equivalent to an aerial weight of

0.744 g/m^2. In contrast, the amount of OCNFs incorporated to the glass fiber layer through vacuum filtration method is 23.61 mg, which is equivalent to an aerial weight 9.15 g/m^2. Clearly, the amount of OCNFs per unit area added to glass fiber layer is much higher compared to carbon fiber layer without inducing significant OCNF agglomerate, suggesting that vacuum filtration is a viable method to fabricate hybrid glass fiber layer with high nanomaterial concentration. If multiple OCNF/glass fiber layers are used to manufacture hierarchical composite, both in-plane and out-of-plane electrical conductivity of resulting composite are expected to dramatically improve. Such improvement in composite electrical conductivity can be used to detect damage or flaw in composites as well as to dissipate electrostatic charges.

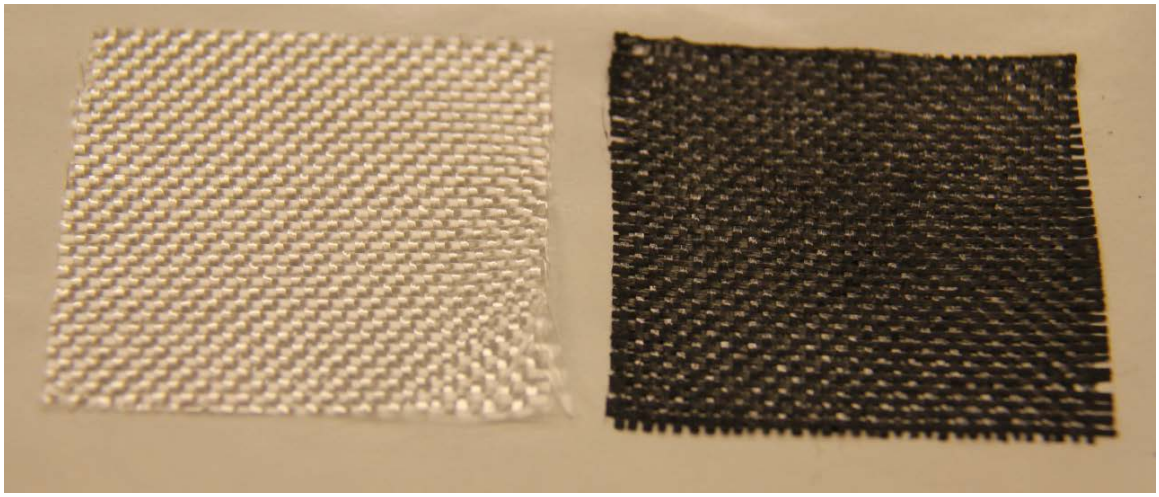

Figure 27. Photograph of as-received glass fiber layer (left) and OCNF/glass fiber layer (right).

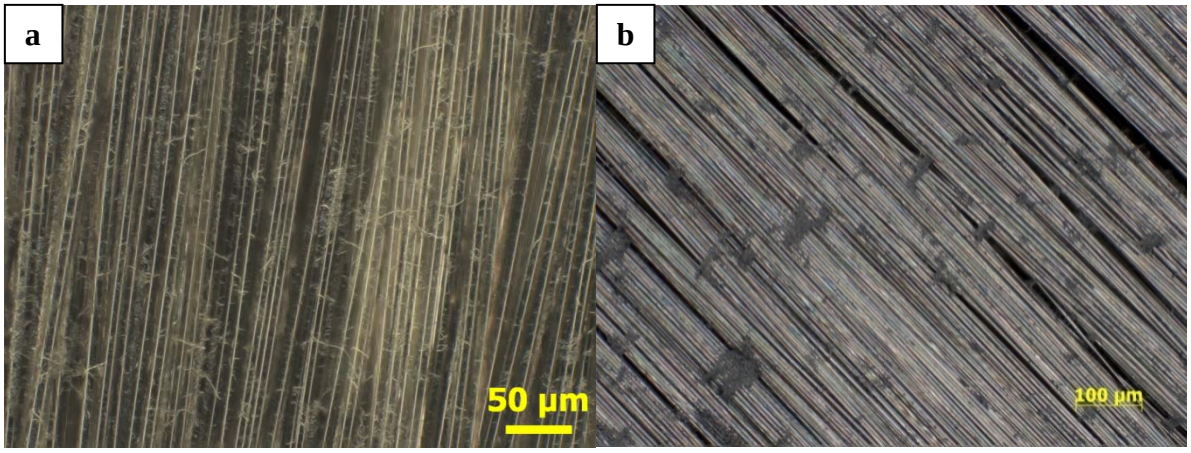

Figure 28. Optical images of (a) OCNF/glass fiber layer at 200x magnification and (b) OCNF/carbon fiber layer at 100x magnification [94].

Figure 29 summarizes both in-plane and out-of-plane electrical conductivity of CNF-GF/EP, CNF-GF/CNF-EP, and CFP, respectively. Clearly, the addition of OCNFs onto glass fiber layers transformed insulating glass fiber composites into conductive hierarchical composites. In general, the in-plane electrical conductivity of all three panels is 2 to 3 orders of magnitude higher than their out-of-plane electrical conductivity. This can be explained by the formation of continuous conductive path by OCNFs that were deposited onto the surfaces of glass fibers which acted as "guiding channels". When comparing the in-plane electrical conductivity of CNF-GF/EP (6.3 S/m) and CNF-GF/CNF-EP (8 S/m), no significant difference is observed between these panels even though additional 1 wt% of OCNFs was added to the resin used to manufacture CNF-GF/CNF-EP because the in-plane electrical conductivity is dominated by the afore-mentioned OCNF continuous conductive path. Although the in-plane electrical conductivity of CFP (1,559 S/m) is approximately 3 orders of magnitude higher than CNF-GF/EP and CNF-GF/CNF-EP, the improvement in in-plane electrical conductivity ascertains the benefit of using OCNFs to transform insulating glass fiber composites into a conductive material.

Unlike in-plane electrical conductivity, the out-of-plane electrical conductivity of CNF-GF/CNF-EP (0.1702 S/m) is found to be approximately 310 % higher than CNF-GF/EP (0.0415 S/m) in spite an insignificant difference in in-plane electrical conductivity between these panels. It is well known that the out-of-plane electrical conductivity of FRPCs is lower than in-plane electrical conductivity due to poor electrical properties of the matrix. Therefore, a change in the matrix properties will influence the out-of-plane electrical conductivity of FRPCs. In this case, it is believed that the OCNF-toughened epoxy resin used to fabricate CNF-GF/CNF-EP is the primary factor governing the difference in out-of-plane electrical conductivity. A schematic illustrating such difference is shown in Figure 30 and is discussed in the following section. Before adding OCNFs into the matrix, the out-of-plane conductive path is formed by the OCNFs deposited onto the surfaces of glass fibers. Under this scenario, the electrons can only travel along the path where OCNFs are in contact with each other thus lowering the overall out-of-plane electrical conductivity. After adding OCNFs into the matrix, additional conductive path is formed by OCNFs distributed within the matrix phase. The two-prong conductive path allows more electrons to travel and thus increases the overall out-of-plane electrical conductivity of CNF-GF/CNF-EP. Interestingly, the out-of-plane electrical conductivity of CFP (2 S/m) is only an order of magnitude higher than CNF-GF/CNF-EP, suggesting that the addition of OCNFs to glass fiber and polymer matrix is a feasible strategy to enhance the out-of-plane electrical conductivity of hierarchical composites.

As mentioned earlier, such improvement in electrical conductivity of hierarchical composites can be used for structural health monitoring purpose. Although investigation is not pursued in this study, the rationale of using OCNFs as in-situ sensors to detect damage is described below. Based on the results and illustration presented, the damage sensing mechanism

can take place at two different regions in composites: fiber/matrix interface and matrix phase. In the first region, since OCNFs are directly incorporated onto the surfaces of glass fibers, the conductive OCNFs can act as sensors to detect fiber/matrix interface debonding, which is a failure mode often encountered in composites subjected to compression or interlaminar shear test. In the second region, OCNFs distributed with the matrix phase can also act as sensors to detect matrix micro-crack and ply delamination, which are failure modes often encountered in composites subjected to mode-I or mode-II fracture toughness test.

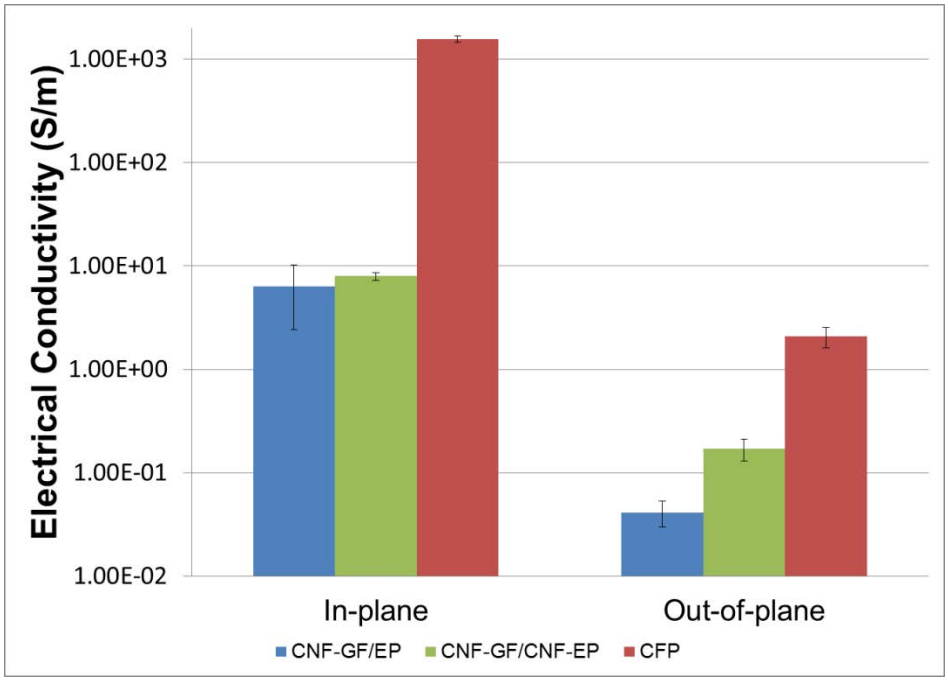

Figure 29. In-plane and out-of-plane electrical conductivity of CNF-GF/EP, CNF-GF/CNF-EP, and CFP. Error bar denotes standard deviation.

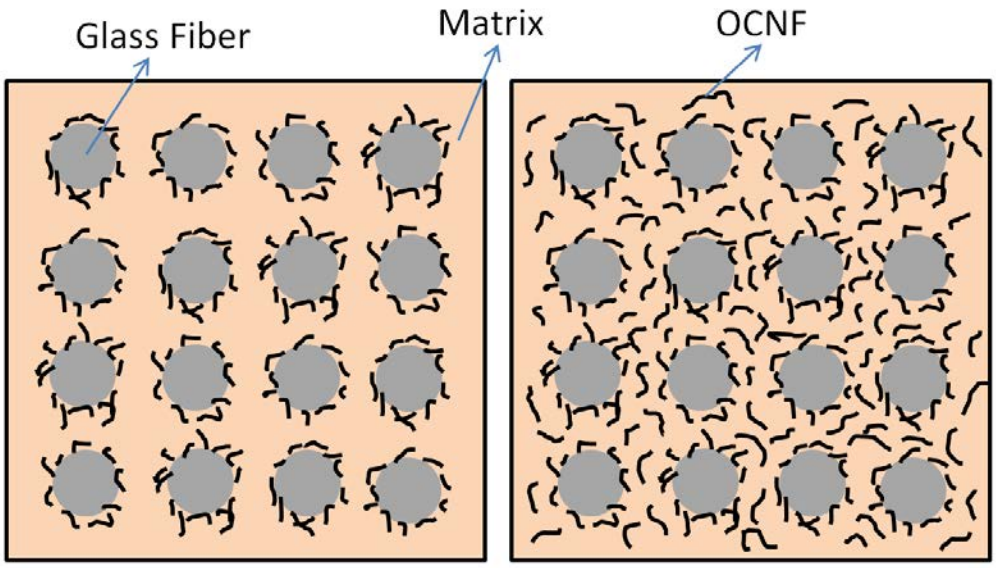

Figure 30. A schematic illustrating the difference in out-of-plane electrical conductivity of OCNF-GF/EP and OCNF-GF/OCNF/EP.

4.3.2 OCNF/Glass Fiber Assembly

The cross-section of OCNF/glass fiber assembly was characterized using optical and SEM imaging before conducting the peel test. Figure 31(a) shows the optical cross-sectional image of the OCNF/glass fiber assembly. The image clearly indicates that the OCNFs were successfully incorporated into the glass fiber layers and the layers seemed to be joined by the OCNF entangled network after filtering.

To gain better insight into the hierarchical structure, three different sections across the cross-section of the OCNF/glass fiber assembly were further analyzed using SEM. An SEM image taken at the mid-section of the OCNF/glass fiber assembly (Figure 31(b)) reveals that the OCNFs were tightly packed and interconnected with each other at the region between the glass fiber layers, a morphology that is similar to CNF entangled network in a buckypaper. When inspecting the structure inside the glass fiber layer, Figure 31(c) shows that the OCNFs penetrated into the fiber tows and connected individual filaments (indicated by the small yellow

arrows), resulting in fiber-bridging effect that could benefit the load transfer. Another interesting finding (Figure 31(d)) that can be obtained from the cross-section of OCNF/glass fiber assembly is the continuity of OCNF network at the interface (defined by the yellow curve) between the glass fiber layer and OCNF entangled network.

Combining the observations shown in Figure 31, it is clearly shown that the OCNFs continuously extended from the first to the second glass fiber layer, creating a stitched architecture based solely on OCNFs. From macroscopic point of view, the OCNF network formed in the OCNF/glass fiber assembly can be viewed as the out-of-plane mechanical reinforcement. As such, it is suggested that the peeling force required for separating OCNF/glass fiber assembly can be substantially higher than two as-received glass fiber layers (practically zero force since nothing holds the layers together) in the absence of polymer matrix. It is worth mentioning that the stitched architecture created through this method is unlike the commercial stitched laminate produced using through-the-thickness stitching, z-pinning, and 3-D braided fibers due to the elimination of fiber displacement/misalignment. Since no additional handling was applied to the as-received glass fiber layers after their placement, the OCNFs would penetrate into and in between the fiber tows without inducing a force that would displace or misalign the fibers.

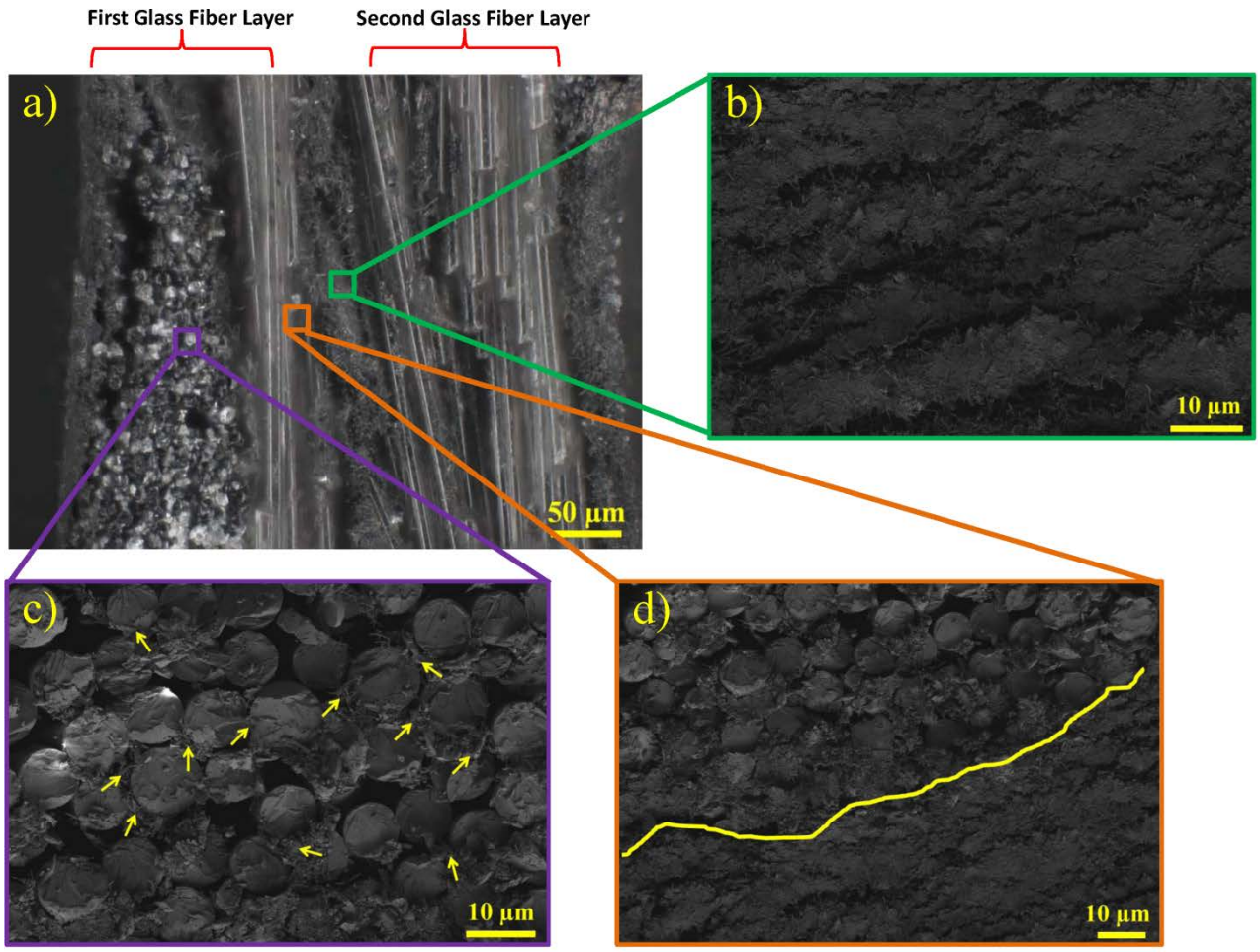

Figure 31. (a) Optical image of the cross-section of OCNF/glass fiber assembly and SEM images of (b) OCNF entangled network between the glass fiber layers, (c) fiber-bridging by OCNFs, and (d) the interface between the glass fiber layer (above the yellow curve) and OCNF entangled network (below the yellow curve). Images were published in [95].

To validate the above statement speculated based on the findings shown in Figure 31, a peel test was conducted (illustrated in the inset of Figure 32) at a speed 20 µm/min. The peeling force was recorded with respect to the crosshead displacement during the test, as shown in Figure 32. As the test progressed, the test specimen underwent repetitive loading and unloading behavior. The initial and maximum peeling force for causing the separation of OCNF/glass fiber assembly were approximately 170 mN and 250 mN, respectively. These findings can be

attributed to the sequential detachment of OCNF entangled network as possible reinforcement mechanism. To investigate this, the crack cross-section of the test specimen was carefully examined using SEM. As shown in Figure 33, significant OCNF pull-out effect at the interface between glass fiber layer and OCNF entangled network was observed. It is believed that the pull-out effect was caused by the interlocking mechanism within the OCNF entangled network, which is directly responsible for the elevated peeling force to separate the OCNF/glass fiber assembly. In addition, evidence of OCNF alignment perpendicular to the glass fiber layer was observed after the test, suggesting that the pronounced pull-out effect could promote alignment as the OCNFs slide with respect to each other during the test.

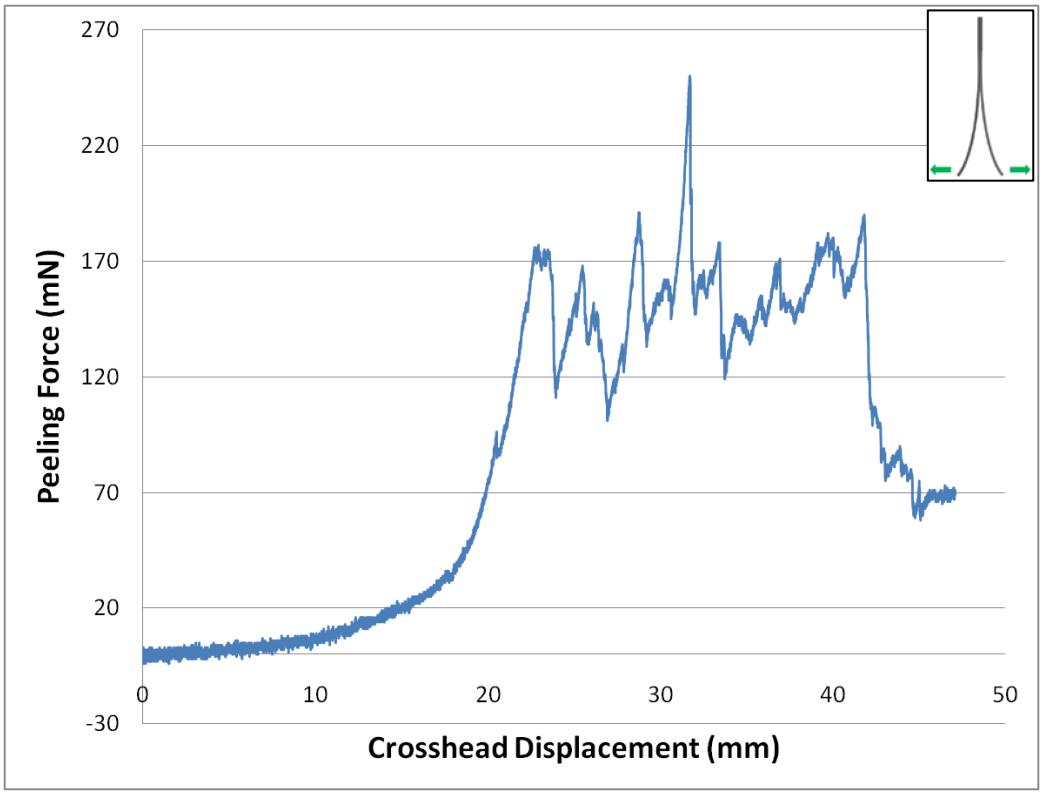

Figure 32. Peeling force for separating the OCNF/glass fiber assembly as a function of stage crosshead displacement. The inset illustrates the schematic of the peel test (Figure B1). Results were published in [95].

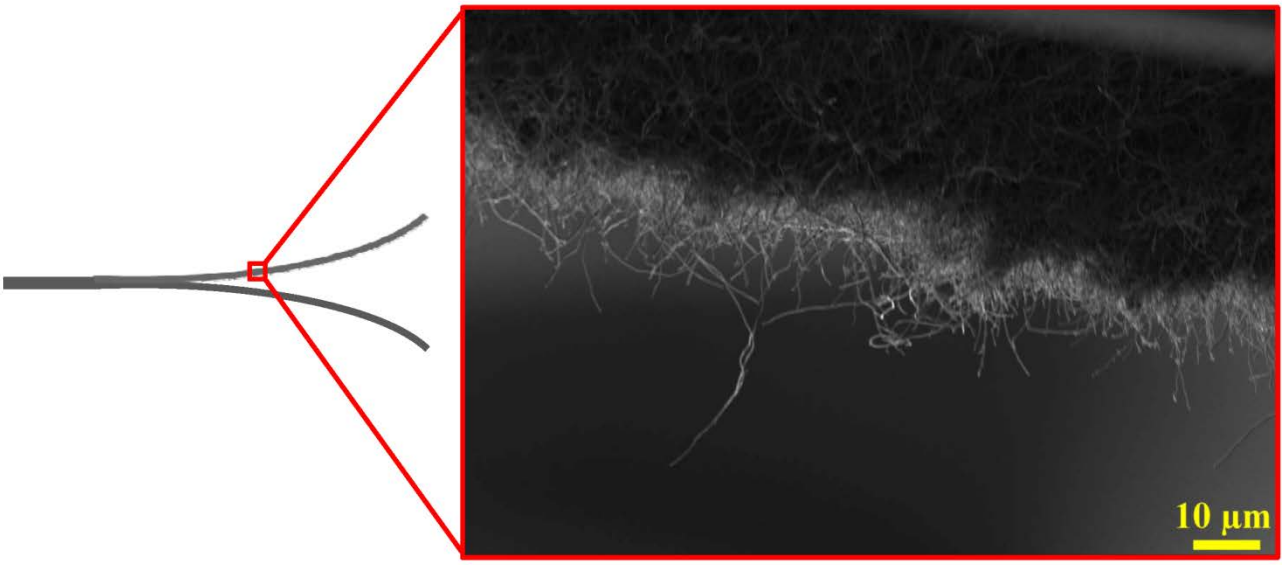

Figure 33. SEM image of tested specimen's cross-section indicating OCNF pull-out effect and alignment perpendicular to the glass fiber layer along the crack. Image was published in [95].

4.4 Summary and Conclusions

In summary, two independent studies were pursued to demonstrate the feasibility of utilizing functionalized CNFs to fabricate hierarchical composites with multi-functionality. By filtering OCNF aqueous solution through the glass fiber layer, optical image indicated that the OCNFs were uniformly incorporated to the glass fiber layer and no significant OCNF agglomerate was observed even though the amount of OCNF per unit area was high. Test results showed that both in-plane and out-of-plane electrical conductivity of glass fiber hierarchical composites were comparable to the conductivity of carbon fiber composites. Further comparison of composites out-of-plane electrical conductivity revealed that the addition of OCNFs into both glass fiber layers and epoxy resin was more effective than adding OCNFs solely into glass fiber layers, since the former approach enabled the formation of a two-prong conductive path leading to a higher overall out-of-plane electrical conductivity. Although not pursued in this

investigation, it is suggested that the conductive network embedded in hierarchical composites can be used to detect a variety of failure modes occur at fiber/matrix interface or matrix phase.

In the second study, joining of glass fiber layers using solely OCNF entangled network through a solution filtering process was demonstrated. Cross-sectional view, characterized using optical and SEM microscopy, of the OCNF/glass fiber assembly showed evidence of continuous OCNF entangled network extending from the first to the second glass fiber layer and fiber-bridging effect, which is beneficial to the load transfer. As a result of the filtering process, the peeling force required to separate the OCNF/glass fiber assembly was significant due to the presence of OCNF entangled network. Further failure analysis revealed significant OCNF pull-out effect and alignment perpendicular to the glass fiber layer along the crack, which could be explained by the sequential detachment of OCNF entangled network as possible reinforcement mechanism. Based on the results presented, it is believed that the mechanical properties, especially interlaminar shear strength and mode-I fracture toughness, of hierarchical composites can be significantly improved if OCNF/glass fiber assembly is used.

CHAPTER 5

CONCLUSIONS AND RECOMMENDATIONS

Carbon nanofibers (CNFs) have a unique combination of mechanical, electrical, and physical properties that makes them promising candidates to be used as reinforcing nanomaterials in nano-engineered polymeric composites. To take full advantage of these properties, several manufacturing challenges must be overcome. In this research, several types of nano-engineered polymeric composites were successfully fabricated by prevailing over the afore-mentioned manufacturing challenges. Particularly, functionalized CNFs were directly incorporated into epoxy resin or dry glass fiber layers prior to post-processing and final curing at elevated temperature.

In the study of polymeric nanocomposites, several optical images revealed that the functionalized CNFs were uniformly incorporated into epoxy resin and that the functionalized CNFs were aligned in the direction parallel to the applied electric field. Although different functionalized CNFs were used to fabricate nanocomposites, it was qualitatively found that the alignment morphology of the functionalized CNFs was independent of the functional groups grafted onto CNFs. Both mechanical and electrical properties measured parallel to the CNF alignment direction were improved with respect to neat epoxy sample. At a concentration of 4.5 wt%, compressive strength of the nanocomposites containing aligned OCNF and ACNF network was similar to each other, showing an improvement of 8.36% and 8.76% higher than neat resin sample, respectively. Unlike compressive strength, compressive modulus of the nanocomposites with aligned ACNF network showed a better increase in comparison to the nanocomposite with aligned OCNF network at the same concentration, which was 19% higher than neat resin sample. These results suggest that the type of functional groups grafted to the CNFs would influence the

compressive modulus of nanocomposites, in which case it is believed that the compatibility between amine functional groups grafted to the CNFs and the epoxy matrix facilitated a more efficient load transfer from the matrix to CNFs, thus leading to a better improvement in modulus. When compared to neat resin sample, a reduction of four orders of magnitude in electrical resistivity was observed for the nanocomposites containing aligned OCNF and ACNF network and the resistivity percolation threshold for both types of nanocomposites was estimated to be 0.75 wt%. Interestingly, the trend of electrical resistivity shown herein was similar to the one reported by other researchers but with different resistivity values due to the differences in CNF type, lower aspect ratio, and increased oxygen content of functionalized CNFs.

As for hierarchical composites, two independent studies were performed to demonstrate the feasibility of utilizing functionalized CNFs to manufacture multifunctional hierarchical composites. By filtering OCNF aqueous solution through the glass fiber layer, the OCNFs were observed to be uniformly distributed within the glass fiber layer without creating significant OCNF agglomerate even though the amount of OCNF per unit area was high. Test results showed that both in-plane and out-of-plane electrical conductivity of glass fiber hierarchical composites were dramatically improved and were comparable to the conductivity of carbon fiber-epoxy composites. By comparing the out-of-plane electrical conductivity of hierarchical composites, it was experimentally found that the addition of OCNFs into both glass fiber layers and epoxy resin was more effective than adding OCNFs solely into glass fiber layers, since the former strategy enabled the creation of more conductive paths leading to a higher overall out-of-plane electrical conductivity. Although not investigated in this research, it is suggested that the conductive network embedded in hierarchical composites can be used as an in-situ sensor to detect a variety of failure modes occur at fiber/matrix interface or matrix phase. Additionally,

experiment aiming at joining of glass fiber layers using solely OCNF entangled network through a solution filtering process was performed. By carefully examining the cross-section of the OCNF/glass fiber assembly, evidences of continuous OCNF entangled network extending from the first to the second glass fiber layer and fiber-bridging effect were found. Through the filtering process, the peeling force required to separate the OCNF/glass fiber assembly was significant due to the presence of OCNF entangled network. Further failure analysis revealed significant OCNF pull-out effect and alignment perpendicular to the glass fiber layer along the crack, which could be explained by the sequential detachment of OCNF entangled network as possible reinforcement mechanism. Based on the results presented, it is suggested that the mechanical properties of hierarchical composites can be significantly improved if OCNF/glass fiber assembly is used.

Although exceptional properties of CNFs have been routinely reported in literatures, it is not certain whether these properties were completely harnessed. From the results reported in this study, it was observed that both mechanical and electrical properties of nano-engineered polymeric composites were far below the properties of CNFs most likely due to structural defects, lower aspect ratio, discontinuity among CNFs, and the concentration needed to attain reinforcement purpose. It is, however, believed that the properties of nano-engineered polymeric composites can be further improved if these deficiencies are satisfactorily resolved. One potential solution is by using CNFs that are much longer than current commercially available CNFs to overcome issues in aspect ratio and optimum concentration. Other alternative includes promoting chemical bonding between nanomaterials and matrix (for polymeric nanocomposites) and among reinforcement-fiber/nanomaterial/matrix interface (for hierarchical composites) to enable better load transfer. Nevertheless, the investigations performed in this research can be

extended to the use of CNTs, a mixture of CNFs and CNTs, and graphene in order to establish a more comprehensive understanding of nano-engineered polymeric composites.

REFERENCES

LIST OF REFERENCES

1. Ozkan, T., M. Naraghi, and I. Chasiotis, *Mechanical properties of vapor grown carbon nanofibers.* Carbon, 2010. **48**(1): p. 239-244.

2. Lawrence, J.G., L.M. Berhan, and A. Nadarajah, *Elastic properties and morphology of individual carbon nanofibers.* ACS Nano, 2008. **2**(6): p. 1230-1236.

3. Al-Saleh, M.H. and U. Sundararaj, *A review of vapor grown carbon nanofiber/polymer conductive composites.* Carbon, 2009. **47**(1): p. 2-22.

4. Heremans, J. and C.P. Beetz, Jr., *Thermal conductivity and thermopower of vapor-grown graphite fibers.* Physical Review B, 1985. **32**(4): p. 1981-1986.

5. Hossain, M.K., M.E. Hossain, M.V. Hosur, and S. Jeelani, *Flexural and compression response of woven E-glass/polyester–CNF nanophased composites.* Composites Part A: Applied Science and Manufacturing, 2011. **42**(11): p. 1774-1782.

6. Bortz, D.R., C. Merino, and I. Martin-Gullon, *Augmented fatigue performance and constant life diagrams of hierarchical carbon fiber/nanofiber epoxy composites.* Composites Science and Technology, 2012. **72**(3): p. 446-452.

7. Shuying, Y., K. Lozano, A. Lomeli, H.D. Foltz, and R. Jones, *Electromagnetic interference shielding effectiveness of carbon nanofiber/LCP composites.* Composites Part A (Applied Science and Manufacturing), 2005. **36**(5): p. 691-7.

8. Lozano, K., *Vapor-grown carbon fiber composites: processing and electrostatic dissipative applications.* JOM, 2000. **52**(11): p. 34-6.

9. Pelsoci, T.M., *Composites Manufacturing Technologies: Applications in Automotive, Petroleum, and Civil Infrastructure Industries*, 2004.

10. Shim, B.S., J. Starkovich, and N. Kotov, *Multilayer composites from vapor-grown carbon nano-fibers.* Composites Science and Technology, 2006. **66**(9): p. 1171-1178.

11. Tibbetts, G.G., M.L. Lake, K.L. Strong, and B.P. Rice, *A review of the fabrication and properties of vapor-grown carbon nanofiber/polymer composites.* Composites Science and Technology, 2007. **67**(7-8): p. 1709-18.

12. Thostenson, E.T., C. Li, and T.-W. Chou, *Nanocomposites in context.* Composites Science and Technology, 2005. **65**(3-4): p. 491-516.

13. Sadeghian, R., S. Gangireddy, B. Minaie, and K.-T. Hsiao, *Manufacturing carbon nanofibers toughened polyester/glass fiber composites using vacuum assisted resin transfer molding for enhancing the mode-I delamination resistance.* Composites Part A: Applied Science and Manufacturing, 2006. **37**(10): p. 1787-1795.

14. Iwahori, Y., S. Ishiwata, T. Sumizawa, and T. Ishikawa, *Mechanical properties improvements in two-phase and three-phase composites using carbon nano-fiber dispersed resin.* Composites Part A (Applied Science and Manufacturing), 2005. **36**: p. 1430-9.

15. Qian, H., E.S. Greenhalgh, M.S.P. Shaffer, and A. Bismarck, *Carbon nanotube-based hierarchical composites: a review.* Journal of Materials Chemistry, 2010. **20**(23).

16. Rodriguez, A.J., M.E. Guzman, C.-S. Lim, and B. Minaie, *Mechanical properties of carbon nanofiber/fiber-reinforced hierarchical polymer composites manufactured with multiscale-reinforcement fabrics.* Carbon, 2011. **49**(3): p. 937-948.

17. Kelkar, A.D., R. Mohan, R. Bolick, and S. Shendokar, *Effect of nanoparticles and nanofibers on Mode I fracture toughness of fiber glass reinforced polymeric matrix composites.* Materials Science & Engineering: B (Advanced Functional Solid-State Materials), 2010. **168**: p. 85-9.

18. Martone, A., C. Formicola, M. Giordano, and M. Zarrelli, *Reinforcement efficiency of multi-walled carbon nanotube/epoxy nano composites.* Composites Science and Technology, 2010. **70**(7): p. 1154-1160.

19. Ma, P.-C., S.-Y. Mo, B.-Z. Tang, and J.-K. Kim, *Dispersion, interfacial interaction and re-agglomeration of functionalized carbon nanotubes in epoxy composites.* Carbon, 2010. **48**(6): p. 1824-1834.

20. Wang, S., R. Liang, B. Wang, and C. Zhang, *Load-transfer in functionalized carbon nanotubes/polymer composites.* Chemical Physics Letters, 2008. **457**(4–6): p. 371-375.

21. Shen, J., W. Huang, L. Wu, Y. Hu, and M. Ye, *Thermo-physical properties of epoxy nanocomposites reinforced with amino-functionalized multi-walled carbon nanotubes.* Composites Part A: Applied Science and Manufacturing, 2007. **38**(5): p. 1331-1336.

22. Li, X. and M.R. Coleman, *Functionalization of carbon nanofibers with diamine and polyimide oligmer.* Carbon, 2008. **46**(8): p. 1115-1125.

23. Zhu, Y.-F., C. Ma, W. Zhang, R.-P. Zhang, N. Koratkar, and J. Liang, *Alignment of multiwalled carbon nanotubes in bulk epoxy composites via electric field.* Journal of Applied Physics, 2009. **105**(5).

24. Lim, C.-S., A.J. Rodriguez, M.E. Guzman, J.D. Schaefer, and B. Minaie, *Processing and properties of polymer composites containing aligned functionalized carbon nanofibers.* Carbon, 2011. **49**(6): p. 1873-1883.

25. Marvin B. Dow, H.B.D., *Development of Stitched, Braided and Woven Composite Structures in the ACT Program and at Langley Research Center*, 1997: Hampton, Virginia.

26. Thostenson, E.T. and T.W. Chou, *Carbon Nanotube Networks: Sensing of Distributed Strain and Damage for Life Prediction and Self Healing.* Advanced Materials, 2006. **18**(21): p. 2837-2841.

27. Li, Y., N. Hori, M. Arai, N. Hu, Y. Liu, and H. Fukunaga, *Improvement of interlaminar mechanical properties of CFRP laminates using VGCF.* Composites Part A: Applied Science and Manufacturing, 2009. **40**(12): p. 2004-2012.

28. Garcia, E.J., B.L. Wardle, A. John Hart, and N. Yamamoto, *Fabrication and multifunctional properties of a hybrid laminate with aligned carbon nanotubes grown In Situ.* Composites Science and Technology, 2008. **68**(9): p. 2034-2041.

29. Rodriguez, A.J., M.E. Guzman, C.-S. Lim, and B. Minaie, *Synthesis of multiscale reinforcement fabric by electrophoretic deposition of amine-functionalized carbon nanofibers onto carbon fiber layers.* Carbon, 2010. **48**(11): p. 3256-3259.

30. Gao, L., T.-W. Chou, E.T. Thostenson, A. Godara, Z. Zhang, and L. Mezzo, *Highly conductive polymer composites based on controlled agglomeration of carbon nanotubes.* Carbon, 2010. **48**(9): p. 2649-2651.

31. Endo, M., Y.A. Kim, T. Hayashi, K. Nishimura, T. Matusita, K. Miyashita, and M.S. Dresselhaus, *Vapor-grown carbon fibers (VGCFs). Basic properties and their battery applications.* Carbon, 2001. **39**: p. 1287-97.

32. Oberlin, A., M. Endo, and T. Koyama, *Filamentous growth of carbon through benzene decomposition.* Journal of Crystal Growth, 1976. **32**(3): p. 335-349.

33. *Pyrograf Products, Inc.; [cited 2013 March 10]. Available from: <http://www.pyrografproducts.com>.*

34. Uchida, T., D.P. Anderson, M.L. Minus, and S. Kumar, *Morphology and modulus of vapor grown carbon nano fibers.* Journal of Materials Science, 2006. **41**: p. 5851-6.

35. Merkulov, V.I., D.H. Lowndes, Y.Y. Wei, G. Eres, and E. Voelkl, *Patterned growth of individual and multiple vertically aligned carbon nanofibers.* Applied Physics Letters, 2000. **76**: p. 3555-7.

36. Endo, M., Y.A. Kim, T. Hayashi, Y. Fukai, K. Oshida, M. Terrones, et al., *Structural characterization of cup-stacked-type nanofibers with an entirely hollow core.* Applied Physics Letters, 2002. **80**: p. 1267-9.

37. Young-Kuk, C., Y. Gotoh, K. Sugimoto, S. Sung-Moo, T. Yanagisawa, and M. Endo, *Processing and characterization of epoxy nanocomposites reinforced by cup-stacked carbon nanotubes.* Polymer, 2005. **46**: p. 11489-98.

38. Karen I. Winey, R.A.V., *Polymer Nanocomposites.* MRS Bulletin, 2007. **32**(4): p. 314-322.

39. *Applied Sciences, Inc., Pyrograf® III; [cited 2013 March 10]. Available from: < http://www.apsci.com/ppi-pyro3.html>.*

40. Miyagawa, H., M.J. Rich, and L.T. Drzal, *Thermo-physical properties of epoxy nanocomposites reinforced by carbon nanotubes and vapor grown carbon fibers.* Thermochimica Acta, 2006. **442**: p. 67-73.

41. Arshad, S.N., M. Naraghi, and I. Chasiotis, *Strong carbon nanofibers from electrospun polyacrylonitrile.* Carbon, 2011. **49**(5): p. 1710-1719.

42. Tibbetts, G.G., C. Kwag, J.Y. Howe, and M.L. Lake. *Heat treating carbon nanofibers for optimal composite performance*. in *Advancing Materials in the Global Economy - Applications, Emerging Markets and Evolving Technologies, May 11, 2003 - May 15, 2003*. 2003. Long Beach, CA, United states: Soc. for the Advancement of Material and Process Engineering.

43. Jana, S.C. and G.A. Jimenez, *Electrically conductive polymer nanocomposites of polymethylmethacrylate and carbon nanofibers prepared by chaotic mixing.* Composites Part A (Applied Science and Manufacturing), 2007. **38**: p. 983-93.

44. Peng, B., Locascio, M., Zapol, P., Li, S., Mielke, S. L., Schatz G. C., Espinosa, H. D., *Measurements of near-ultimate strength for multiwalled carbon nanotubes and irradiation-induced crosslinking improvements.* Nature Nanotechnology, 2008. **3**(10): p. 626-631.

45. Terrones, M., *Science and technology of the twenty-first century: synthesis, properties, and applications of carbon nanotubes.* Annual Review of Materials Research, 2003. **33**(1): p. 419-501.

46. Callister, W., *Materials science and engineering an introduction*. 6th Edition ed, ed. N.J.W.S. New York 2003.

47. Heremans, J., *Electrical conductivity of vapor-grown carbon fibers.* Carbon, 1985. **23**: p. 431-6.

48. Gong, X., J. Liu, S. Baskaran, R.D. Voise, and J.S. Young, *Surfactant-Assisted Processing of Carbon Nanotube/Polymer Composites.* Chemistry of Materials, 2000. **12**(4): p. 1049-1052.

49. Geng, Y., M.Y. Liu, J. Li, X.M. Shi, and J.K. Kim, *Effects of surfactant treatment on mechanical and electrical properties of CNT/epoxy nanocomposites.* Composites Part A: Applied Science and Manufacturing, 2008. **39**(12): p. 1876-1883.

50. Marques, R.R.N., B.F. Machado, J.L. Faria, and A.M.T. Silva, *Controlled generation of oxygen functionalities on the surface of Single-Walled Carbon Nanotubes by HNO3 hydrothermal oxidation.* Carbon, 2010. **48**(5): p. 1515-1523.

51. Hu, H., P. Bhowmik, B. Zhao, M.A. Hamon, M.E. Itkis, and R.C. Haddon, *Determination of the acidic sites of purified single-walled carbon nanotubes by acid–base titration.* Chemical Physics Letters, 2001. **345**(1–2): p. 25-28.

52. Chen, C., B. Liang, D. Lu, A. Ogino, X. Wang, and M. Nagatsu, *Amino group introduction onto multiwall carbon nanotubes by NH3/Ar plasma treatment.* Carbon, 2010. **48**(4): p. 939-948.

53. Buffa, F., G.A. Abraham, B.P. Grady, and D. Resasco, *Effect of nanotube functionalization on the properties of single-walled carbon nanotube/polyurethane composites.* Journal of Polymer Science Part B: Polymer Physics, 2007. **45**(4): p. 490-501.

54. Miller, S.G., J.L. Bauer, M.J. Maryanski, P.J. Heimann, J.P. Barlow, J.-M. Gosau, and R.E. Allred, *Characterization of epoxy functionalized graphite nanoparticles and the physical properties of epoxy matrix nanocomposites.* Composites Science and Technology, 2010. **70**(7): p. 1120-1125.

55. Lachman, N. and H. Daniel Wagner, *Correlation between interfacial molecular structure and mechanics in CNT/epoxy nano-composites.* Composites Part A: Applied Science and Manufacturing, 2010. **41**(9): p. 1093-1098.

56. Lakshminarayanan, P.V., H. Toghiani, and C.U. Pittman, Jr., *Nitric acid oxidation of vapor grown carbon nanofibers.* Carbon, 2004. **42**(12-13): p. 2433-42.

57. Seyhan, A.T., Z. Sun, J. Deitzel, M. Tanoglu, and D. Heider, *Cure kinetics of vapor grown carbon nanofiber (VGCNF) modified epoxy resin suspensions and fracture toughness of their resulting nanocomposites.* Materials Chemistry and Physics, 2009. **118**(1): p. 234-242.

58. Prolongo, S.G., M. Burón, M.R. Gude, R. Chaos-Morán, M. Campo, and A. Ureña, *Effects of dispersion techniques of carbon nanofibers on the thermo-physical properties of epoxy nanocomposites.* Composites Science and Technology, 2008. **68**(13): p. 2722-2730.

59. Safadi, B., R. Andrews, and E.A. Grulke, *Multiwalled carbon nanotube polymer composites: Synthesis and characterization of thin films.* Journal of Applied Polymer Science, 2002. **84**(14): p. 2660-2669.

60. Ruan, S.L., P. Gao, X.G. Yang, and T.X. Yu, *Toughening high performance ultrahigh molecular weight polyethylene using multiwalled carbon nanotubes.* Polymer, 2003. **44**(19): p. 5643-5654.

61. Zhou, B., Y. Lin, D.E. Hill, W. Wang, L.M. Veca, L. Qu, et al., *Polymeric nanocomposite films from functionalized vs suspended single-walled carbon nanotubes.* Polymer, 2006. **47**(15): p. 5323-5329.

62. Thostenson, E.T. and T.-W. Chou, *Processing-structure-multi-functional property relationship in carbon nanotube/epoxy composites.* Carbon, 2006. **44**(14): p. 3022-3029.

63. Tsuchiya, K., A. Sakai, T. Nagaoka, K. Uchida, T. Furukawa, and H. Yajima, *High electrical performance of carbon nanotubes/rubber composites with low percolation threshold prepared with a rotation–revolution mixing technique.* Composites Science and Technology, 2011. **71**(8): p. 1098-1104.

64. Meincke, O., D. Kaempfer, H. Weickmann, C. Friedrich, M. Vathauer, and H. Warth, *Mechanical properties and electrical conductivity of carbon-nanotube filled polyamide-6 and its blends with acrylonitrile/butadiene/styrene.* Polymer, 2004. **45**(3): p. 739-748.

65. Khalid, L. and M. Matthew. *Carbon Nanofibers As A Nano-reinforcement For Polymeric Nanocomposites*. in *SAMPE 2003 Dayton Conference Proceedings Materials and Processing - Enabling Flight, Our Legacy and Our Future*. 2003. Dayton, OH, United States: Soc. for the Advancement of Material and Process Engineering.

66. Lafdi, K., W. Fox, M. Matzek, and E. Yildiz, *Effect of Carbon Nanofiber - Matrix Adhesion on Polymeric Nanocomposites Properties-Part II.* Journal of Nanomaterials, 2008. **2008**: p. 310126 1-8.

67. Ahn, S.-N., H.-J. Lee, B.-J. Kim, L.-S. Tan, and J.-B. Baek, *Epoxy/amine-functionalized short-length vapor-grown carbon nanofiber composites.* Journal of Polymer Science, Part A: Polymer Chemistry, 2008. **46**(22): p. 7473-7482.

68. Prasse, T., J.-Y. Cavaillé, and W. Bauhofer, *Electric anisotropy of carbon nanofibre/epoxy resin composites due to electric field induced alignment.* Composites Science and Technology, 2003. **63**(13): p. 1835-1841.

69. Gojny, F.H., M.H.G. Wichmann, B. Fiedler, W. Bauhofer, and K. Schulte, *Influence of nano-modification on the mechanical and electrical properties of conventional fibre-reinforced composites.* Composites Part A: Applied Science and Manufacturing, 2005. **36**(11): p. 1525-1535.

70. Garcia, E.J., B.L. Wardle, and A. John Hart, *Joining prepreg composite interfaces with aligned carbon nanotubes.* Composites Part A: Applied Science and Manufacturing, 2008. **39**(6): p. 1065-1070.

71. Rojas, G., B. Maruyama, and E. Barrera, *CNT/VGCF reinforced epoxy/cf composites: The role of nanofibers*, in *Society for the Advancement of Material and Process Engineering*2006: Dallas, TX.

72. Qian, H., A. Bismarck, E.S. Greenhalgh, and M.S.P. Shaffer, *Carbon nanotube grafted silica fibres: Characterising the interface at the single fibre level.* Composites Science and Technology, 2010. **70**(2): p. 393-399.

73. Zhang, Q., W. Qian, R. Xiang, Z. Yang, G. Luo, Y. Wang, and F. Wei, *In situ growth of carbon nanotubes on inorganic fibers with different surface properties.* Materials Chemistry and Physics, 2008. **107**(2–3): p. 317-321.

74. Thostenson, E.T., W.Z. Li, D.Z. Wang, Z.F. Ren, and T.W. Chou, *Carbon nanotube/carbon fiber hybrid multiscale composites.* Journal of Applied Physics, 2002. **91**(9): p. 6034-6037.

75. Sager, R.J., P.J. Klein, D.C. Lagoudas, Q. Zhang, J. Liu, L. Dai, and J.W. Baur, *Effect of carbon nanotubes on the interfacial shear strength of T650 carbon fiber in an epoxy matrix.* Composites Science and Technology, 2009. **69**(7–8): p. 898-904.

76. Qian, H., A. Bismarck, E.S. Greenhalgh, and M.S.P. Shaffer, *Carbon nanotube grafted carbon fibres: A study of wetting and fibre fragmentation.* Composites Part A: Applied Science and Manufacturing, 2010. **41**(9): p. 1107-1114.

77. Gong, Q.-J., H.-J. Li, X. Wang, Q.-G. Fu, Z.-w. Wang, and K.-Z. Li, *In situ catalytic growth of carbon nanotubes on the surface of carbon cloth.* Composites Science and Technology, 2007. **67**(14): p. 2986-2989.

78. Kepple, K.L., G.P. Sanborn, P.A. Lacasse, K.M. Gruenberg, and W.J. Ready, *Improved fracture toughness of carbon fiber composite functionalized with multi walled carbon nanotubes.* Carbon, 2008. **46**(15): p. 2026-2033.

79. Bekyarova, E., E.T. Thostenson, A. Yu, H. Kim, J. Gao, J. Tang, et al., *Multiscale Carbon Nanotube−Carbon Fiber Reinforcement for Advanced Epoxy Composites.* Langmuir, 2007. **23**(7): p. 3970-3974.

80. Zhang, J., R. Zhuang, J. Liu, E. Mäder, G. Heinrich, and S. Gao, *Functional interphases with multi-walled carbon nanotubes in glass fibre/epoxy composites.* Carbon, 2010. **48**(8): p. 2273-2281.

81. Godara, A., L. Gorbatikh, G. Kalinka, A. Warrier, O. Rochez, L. Mezzo, et al., *Interfacial shear strength of a glass fiber/epoxy bonding in composites modified with carbon nanotubes.* Composites Science and Technology, 2010. **70**(9): p. 1346-1352.

82. Martin, C.A., J.K.W. Sandler, A.H. Windle, M.K. Schwarz, W. Bauhofer, K. Schulte, and M.S.P. Shaffer, *Electric field-induced aligned multi-wall carbon nanotube networks in epoxy composites.* Polymer, 2005. **46**: p. 877-86.

83. Chen, X.Q., T. Saito, H. Yamada, and K. Matsushige, *Aligning single-wall carbon nanotubes with an alternating-current electric field.* Applied Physics Letters, 2001. **78**(23): p. 3714-16.

84. Cheol, P., J. Wilkinson, S. Banda, Z. Ounaies, K.E. Wise, G. Sauti, et al., *Aligned single-wall carbon nanotube polymer composites using an electric field.* Journal of Polymer Science, Part B (Polymer Physics), 2006. **44**(12): p. 1751-62.

85. Mahfuz, H., S. Zainuddin, V.K. Rangari, S. Jeelani, M.R. Parker, and T. Al-Saadi. *Infusion of carbon nanotubes and carbon nanofibers into SC-15 epoxy; An investigation of the influence of high magnetic fields*. in *50th International SAMPE Symposium and Exhibition, May 1, 2005 - May 5, 2005*. 2005. Long Beach, CA, United states: Soc. for the Advancement of Material and Process Engineering.

86. Garmestani, H., M.S. Al-Haik, K. Dahmen, R. Tannenbaum, D. Li, S.S. Sablin, and M.Y. Hussaini, *Polymer-Mediated Alignment of Carbon Nanotubes under High Magnetic Fields.* Advanced Materials, 2003. **15**(22): p. 1918-1921.

87. Camponeschi, E., B. Florkowski, R. Vance, G. Garrett, H. Garmestani, and R. Tannenbaum, *Uniform directional alignment of single-walled carbon nanotubes in viscous polymer flow.* Langmuir, 2006. **22**(4): p. 1858-1862.

88. Abbasi, S., P.J. Carreau, and A. Derdouri, *Flow induced orientation of multiwalled carbon nanotubes in polycarbonate nanocomposites: Rheology, conductivity and mechanical properties.* Polymer, 2010. **51**(4): p. 922-935.

89. Ci, L., J. Suhr, V. Pushparaj, X. Zhang, and P.M. Ajayan, *Continuous carbon nanotube reinforced composites.* Nano Letters, 2008. **8**(9): p. 2762-6.

90. Cheng, Q.F., J.P. Wang, J.J. Wen, C.H. Liu, K.L. Jiang, Q.Q. Li, and S.S. Fan, *Carbon nanotube/epoxy composites fabricated by resin transfer molding.* Carbon, 2010. **48**(1): p. 260-6.

91. Qing, W., D. Jianfeng, L. Weixue, W. Zhiqiang, and J. Jinlong, *The effects of CNT alignment on electrical conductivity and mechanical properties of SWNT/epoxy nanocomposites.* Composites Science and Technology, 2008. **68**(7-8): p. 1644-8.

92. Rodriguez, A., M. Guzman, C. Lim, and B. Minaie. *Electrophoretic deposition of CNF onto carbon fiber layers for manufacturing of fiber-reinforced polymer nanocomposites*. in *SAMPE '09 Spring Symposium Conference Proceedings, May 18, 2009 - May 21, 2009*. 2009. Baltimore, MD, United states: Soc. for the Advancement of Material and Process Engineering.

93. Rodriguez, A., M. Guzman, C. Lim, and B. Minaie. *Hybrid Carbon Nanofiber-Carbon Fiber Layers For Manufacturing of Fiber-Reinforced Polymer Nanocomposites*. in *SAMPE '09 Spring Symposium Conference Proceedings, May 17, 2010 - May 20, 2010*. 2010. Seattle, WA, United States: Soc. for the Advancement of Material and Process Engineering.

94. Rodriguez, A.J., *Processing and characterization of carbon nanoparticle/fiber-reinforced polymer composites*, in *Department of Mechanical* Engineering, 2010, Wichita State University: Wichita, KS. p. 132.

95. Lim, C.-S., M.E. Guzman, and B. Minaie, *Joining glass fiber layers using a functionalized carbon nanofiber entangled network.* Carbon, 2013. **54**(0): p. 489-492.

APPENDICES

APPENDIX A

FOURIER TRANSFORM INFRARED (FTIR) SPECTRUM AND THERMOGRAVIMETRIC ANALYSIS (TGA) OF AR-CNF AND OCNF FUNCTIONALIZED FOR TWO HOURS

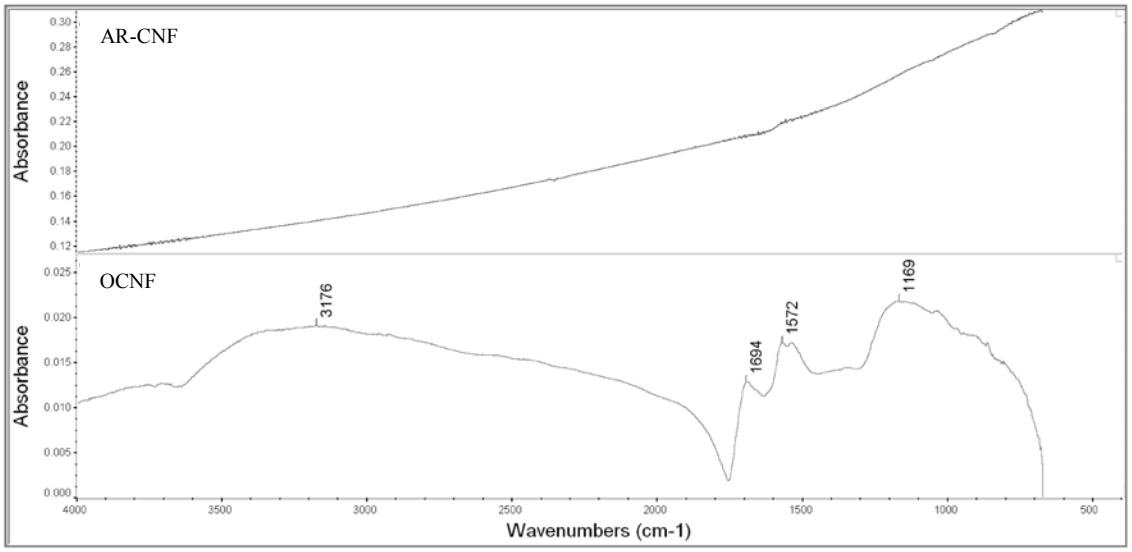

Figure A.1. FTIR spectrum of AR-CNF and OCNF.

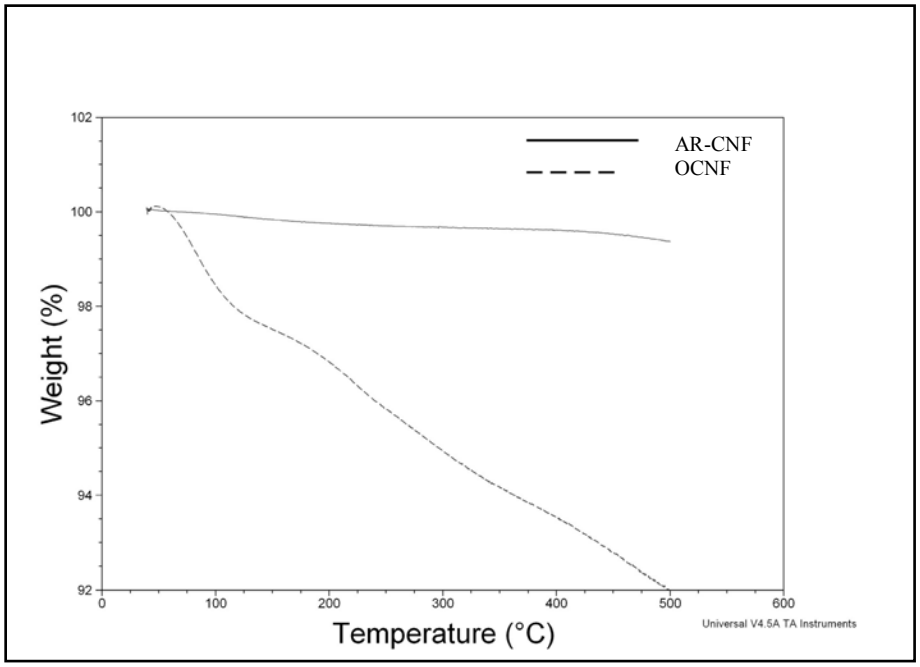

Figure A.2. TGA plots of AR-CNF and OCNF.

APPENDIX B

ACTUAL PHOTOGRAPH SHOWING THE PEEL TEST OF OCNF/GLASS FIBER ASSEMBLY USING A TENSILE STAGE

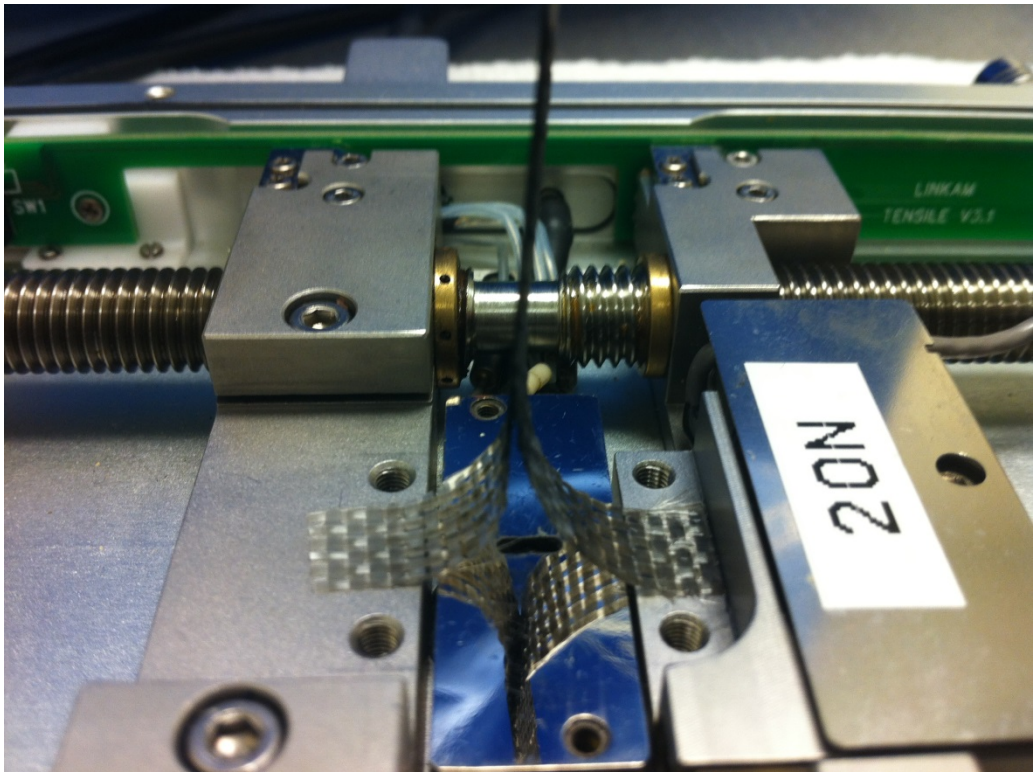

Figure B.1. Peel test of OCNF/glass fiber assembly.